

**Microcompartmentation
of cell wall integrity sensors in
*Saccharomyces cerevisiae***

Dissertation

zur Erlangung des akademischen Grades

Doctor rerum naturalium

(Dr. rer. nat.)

Fachbereich Biologie/Chemie der Universität Osnabrück

vorgelegt von:

Christian Kock

Osnabrück, Mai 2016

*“There is a theory which states that if ever
anyone discovers exactly what the Universe is
for and why it is here, it will instantly
disappear and be replaced by something even
more bizarre and inexplicable.”*

*“There is another theory which states that this
has already happened.”*

– Douglas Adams

Supervisors:

Prof. Dr. Jürgen J. Heinisch (University of Osnabrück)

Prof. Dr. Achim Paululat (University of Osnabrück)

Table of contents

1. Introduction	1
1.1 The yeast cell wall integrity (CWI) pathway	2
1.1.1 The yeast cell wall is a complex structure and involves numerous components	2
1.1.2 The cell wall integrity pathway is important during cell wall remodeling conditions	4
1.1.3 Five cell surface sensors contribute to cell wall integrity signaling	8
1.1.4 Wsc1 is a highly dynamic sensor which forms clusters in the plasma membrane ...	10
1.2 Microcompartmentation of plasma membranes	13
1.2.1 Microcompartments are functional units at a suborganellar level	13
1.2.2 The plasma membrane is a dynamic bilayer and segregates into microdomains	14
1.2.3 Several microcompartments are found in the yeast plasma membrane	15
1.3 Amyloid proteins	19
1.3.1 Wsc1 sensors have putative amyloid sequences	19
1.4 Aims of this thesis	21
2. Materials and methods	22
2.1 Materials	22
2.1.1 Equipment	22
2.1.2 Chemicals and consumables	23
2.1.3 Kits	24
2.1.4 Enzymes	24
2.1.5 Antibodies	24
2.1.6 Electrophoresis ladders	25
2.1.7 Media	25
2.1.7.1 Media for the growth of <i>E. coli</i>	25
2.1.7.2 Media for growth of <i>S. cerevisiae</i>	25
2.1.8 Oligonucleotides	26
2.1.9 Strains	27
2.1.9.1 <i>E. coli</i> strains	27
2.1.9.1.1 Incubation and storage of <i>E. coli</i> strains	27
2.1.9.2 <i>S. cerevisiae</i> strains	28
2.1.9.2.2 Incubation and storage of <i>S. cerevisiae</i> strains	32
2.1.10 Vectors and plasmids	32
2.2 Methods	36

2.2.1 Transformation protocols	36
2.2.1.1 Transformation of <i>E. coli</i> (Hanahan, 1985)	36
2.2.1.2 Transformation of <i>S. cerevisiae</i> with the lithium acetate method (Gietz <i>et al.</i> , 1992).....	36
2.2.1.2 Transformation of <i>S. cerevisiae</i> with the “freeze method” (Klebe <i>et al.</i> , 1983)	37
2.2.1.3 Transformation of <i>S. cerevisiae</i> with the spheroblast method.....	37
2.2.2 Yeast genetics.....	38
2.2.2.1 Yeast strain construction by homologous recombination	38
2.2.2.2 Crossing of yeast strains	39
2.2.2.3 Sporulation, tetrad analysis and mating type identification.....	39
2.2.2.4 Analyses of growth and sensitivities towards stress agents	41
2.2.3 DNA analysis.....	42
2.2.3.1 Genomic DNA extraction from <i>S. cerevisiae</i> by microwave treatment	42
2.2.3.2 Genomic DNA preparation from <i>S. cerevisiae</i> (phenol chloroform).....	42
2.2.3.3 Polymerase chain reaction (PCR)	42
2.2.3.4 Separation of DNA fragments by agarose gel electrophoresis	43
2.2.3.5 Purification of PCR products.....	44
2.2.3.6 Isolation of DNA fragments from agarose gels	44
2.2.3.7 Restriction and ligation of DNA	44
2.2.3.8 Purification of plasmid DNA	44
2.2.3.9 Plasmid preparation from <i>S. cerevisiae</i>	45
2.2.3.10 DNA sequencing	45
2.2.3.11 Gene synthesis.....	45
2.2.4 Protein analysis	45
2.2.4.1 Preparation of extracts for immunodetection (“Roedel”)	45
2.2.4.2 Protein separation by SDS polyacrylamide gel electrophoresis (SDS-PAGE)	46
2.2.4.3 Western Blot analysis	47
2.2.4.4 Preparation of crude extracts for the biotinylation interaction assay (Roux <i>et al.</i> , 2012).....	48
2.2.4.5 Purification of biotin-tagged proteins	48
2.2.4.6 Determination of protein concentrations	49
2.2.4.7 Mass spectrometry.....	49
2.2.5 Life cell fluorescence microscopy	50

2.2.5.1 Microscope setups.....	50
2.2.5.2 Fluorescence microscopy	50
2.2.5.3 Bimolecular fluorescence complementation (BiFC).....	51
2.2.5.4 Quantification of colocalization	51
2.2.5.5 Integrated morphometrics analysis	52
3. Results	53
3.1 Effects of a quintuple CWI sensor gene deletion	53
3.1.2 Wsc1 and Mid2 can rescue cell death in a strain lacking all five sensors	53
3.2 Distribution of cell wall integrity sensors in plasma membrane domains	56
3.2.1 Wsc1 and Mid2 reside in different plasma membrane domains.....	56
3.2.2 The transmembrane domains of Wsc1 and Mid2 do not determine their plasma membrane domain distribution	57
3.2.3 Wsc1 occupies a plasma membrane domain that is distinct from the MCC, MCP and MCT domains.....	59
3.3 The role of the cysteine-rich domain (CRD) in microcompartmentation of Wsc1.....	66
3.3.1 The cysteine-rich domain is important for Wsc1-Wsc1 sensor interaction at the cell surface.....	66
3.3.2 Blocking the turnover of Wsc1 CRD mutants at the plasma membrane in <i>end3</i> deletions shows pleiotropic signaling effects	69
3.3.3 Mutating the endocytosis signal in Wsc1 CRD mutants restores its sensor function and changes its localization within the plasma membrane.....	72
3.3.4 Wsc1 clustering and signaling can be abolished by mutating an amyloid like sequence within the CRD	76
3.4 Identification of Wsc1 interaction partners	81
3.4.1 A large-scale search for Wsc1 interaction partners using BioID reveals numerous potential interaction partners.....	81
4. Discussion	84
4.1 At least one cell wall integrity sensor is needed for cell viability	84
4.2 Wsc1 may interact with a number of intracellular proteins.....	86
4.3 The Wsc1 cell wall integrity sensor forms a distinct plasma membrane domain	90
4.4 Wsc1 sensor clustering may be important for protection from endocytosis but not for signaling.....	94
4.7 Outlook.....	103
5. References	105
6. Supplementary	120

6.1 Plasma membrane domain colocalization controls.....	120
6.2 List of potential Wsc1 interaction partners identified by BioID	121
6.3 List of abbreviations.....	131
6.3.1 Gene abbreviations	131
6.3.2 Cell wall integrity pathway-related abbreviations.....	131
6.3.3 General abbreviations	131
7. Acknowledgements / Danksagung	133
8. Statutory declaration.....	134
9. Summary.....	135
10. Zusammenfassung.....	136
11. Curriculum vitae	138
12. Publications.....	139

1. Introduction

The ability to adapt to changing environments and varying growth conditions is a common feature of all living cells, from unicellular bacteria, through fungi, to cells embedded in tissues of plants or animals. Such cellular responses can be comparatively fast, involve medium-term changes in gene expression patterns, or even allow for long-term adaptations. They are frequently mediated by signal transduction cascades, often commencing with sensors or receptors for extracellular stimuli, which relay the signal to intracellular components triggering the proper cellular responses.

Prominent examples for signal transduction in bacteria are two-component systems (TCS). In their more simple versions, they are constituted by a sensory histidine kinase, which detects the stimulus, and a response regulator, which mediates the transcriptional and/or physiological changes (Capra and Laub, 2012).

In contrast to bacteria, eukaryotic cells are usually bigger and, due to the presence of a nucleus and various organelles, much more compartmentalized. This explains why they usually require more complex signal transduction pathways involving more components. A prominent example of such complex and evolutionary highly conserved signal transduction pathways in eukaryotes are mitogen-activated protein kinase (MAPK) cascades. Although subject to variations, upstream of the central MAPK module consisting of a MAP kinase kinase kinase (MAPKKK), a MAP kinase kinase (MAPKK) and a MAP kinase (MAPK), signaling often starts with a sensor located at the cell surface, which transmit the signal through molecular switches in the form of small GTPases to the MAPK module. This involves regulators of the G-proteins, such as guanine nucleotide exchange factors (GEFs) and their counteracting GTPase-activating proteins (GAPs). Once converted into its active, GTP-bound state, the GTPase then interacts either directly with the MAPKKK of the module, or triggers its activation by one or more mediator protein kinases. The signal is then enhanced by consecutive phosphorylations within the MAPK module, until the activated MAP kinase phosphorylates its effector proteins, which may reside in the cytoplasm or more commonly are transcription factors governing gene expression in the nucleus. Famous examples of such signaling cascades in mammals are the ERK, JNK or p38 kinase pathways, which can be

activated by hormones, growth factors and cytokines, or by different stress conditions (Qi and Elion, 2005). Dysfunction in these pathways can cause severe defects in humans, including neurodegenerative diseases such as Parkinson's disease (Kim and Choi, 2010) and various forms of cancer (Dhillon *et al.*, 2007). Yet, the large number of paralogs of the pathway components in mammalian cells makes them hard to study, explaining the need for more tractable model organisms.

In this context, the unicellular ascomycetous fungus *Saccharomyces cerevisiae* possesses five different MAPK pathways, designed to react to different environmental conditions. They are characterized by their downstream MAPK. Thus, the pheromone response pathway is mediated by the Fus3 kinase, the filamentous growth pathway by Kss1, the spore wall assembly pathway by Smk1, the high osmolarity/glycerol pathway by Hog1, and the cell wall integrity pathway by Slt2/Mpk1. Many of the components within these five pathways lack paralogous proteins, but their basic architecture is similar and homologs to their counterparts in mammalian cells can be easily identified. Therefore, *S. cerevisiae* allows the application of basic research strategies on such complex eukaryotic signal transduction pathways and serves as an ideal model system (Chen and Thorner, 2007; Levin-Salomon *et al.*, 2009).

1.1 The yeast cell wall integrity (CWI) pathway

1.1.1 The yeast cell wall is a complex structure and involves numerous components

The cell wall of *S. cerevisiae* determines the cell shape and its morphology changes during the different growth phases like budding, mating, sporulation or the formation of pseudohyphae. It sustains the osmotic integrity of the cell similar to the plant's cell wall. Cell wall integrity is therefore a prerequisite for the cell's survival in normal environments. The yeast cell wall is a layered structure that consists of the polysaccharides β -1,3-glucan, β -1,6-glucan and chitin, which are crosslinked to various degrees. Furthermore it contains mannoproteins and other proteins which contribute to the overall cell wall structure (Figure 1.1, Klis, 2002; Orlean, 2012).

The cell wall has a thickness of about 100-115 nm under normal growth conditions (Dupres *et*

al., 2010; Backhaus *et al.*, 2013), but the overall thickness or thickness of different layers, the composition, degree of crosslinking or general organization can vary under different growth conditions or in mutants affecting the cell wall (Orlean, 2012).

Chitin is with 1-2 % the least abundant polysaccharide in the cell wall. It is mainly found at the primary septum in the bud neck and in bud scars and less abundant in thin layers within the lateral cell wall (Molano *et al.*, 1980; Klis, 2002). It is synthesized from N-acetyl glucosamine by the three chitin synthases Chs1 to Chs3 (Roncero, 2002). Chitin can be stained by the fluorescent dye calcofluor white, which intercalates in and binds to chitin polymers and therefore leads to cell wall stress in growing cells. Another stress reagent known to interfere with chitin is the diazo dye Congo red (Elorza *et al.*, 1983; Roncero and Duran, 1985).

The β -1,3-glucan chains constitute the backbone of the cell wall and are primarily responsible for wall strength and elasticity . They are synthesized from UDP-glucose monomers feeding two alternative isoforms of glucan synthases, characterized by their catalytic subunits Fks1 or Fks2 and their regulatory subunit Rho1 (Orlean, 2012). Glucan synthase activity is inhibited by antifungal drugs of the echinocandin family. A member of this family in clinical use is the non-competitive inhibitor caspofungin which causes severe defects in cell wall synthesis accompanied by strong growth defects (Reinoso-Martín *et al.*, 2003). β -1,6-glucan consists of shorter polysaccharide chains and forms more side-branches than β -1,3-glucan. It is therefore important for the crosslinking of different cell wall components. The biochemistry of β -1,6-glucan has not yet been completely elucidated, since many different enzymes, like the Kre-family proteins and Skn1, seem to contribute to its synthesis and crosslinking (Orlean, 2012).

The cell wall proteins or mannoproteins are highly glycosylated and can either have enzymatic functions for cell wall modulation or fulfill non-enzymatic purposes. Among the enzymes, β -1,3-glucanases and β -1,3-glucanosyltransferases play the most important roles. Structural cell wall proteins are either glycosylphosphatidylinositol (GPI)-anchored, such as flocculins and agglutinins, or do not carry a GPI anchors, like the Pir proteins, which can be directly linked to the β -1,3-glucan backbone (Kapteyn *et al.*, 1999; Orlean 2012).

1.1.2 The cell wall integrity pathway is important during cell wall remodeling conditions

As explained above, the yeast cell wall is required to survive in normal growth and under different environmental conditions. Its proper composition and stability is controlled by the cell wall integrity (CWI) pathway, which is activated during all circumstances where cell wall remodeling is needed, such as vegetative growth, pheromone-induced mating and under various stress conditions that challenge the cellular integrity. These stresses involve physical damage to the cell wall, temperature shifts, the presence of agents interfering with the cell wall and plasma membrane or fungicides, and hypo-osmotic shock (Levin 2011).

A general overview of the CWI signaling pathway is given in Figure 1.1. The outermost components involved in stress detection are the plasma membrane-spanning cell surface sensors Wsc1, Wsc2, Wsc3, Mid2 and Mtl1, which will be described in more detail in chapter 1.1.3. The activated sensors are believed to bind the mediator Rom2 which then acts as a guanine nucleotide exchange factor (GEF) for the small GTPase Rho1 (Ozaki *et al.*, 1996; Philip and Levin, 2001) and is presumably recruited to the membrane by its PH (“pleckstrin homology”) domain, which binds to phosphatidylinositol-4,5-bisphosphate (PIP₂). This way it may also be involved in Stt4-Mss4 signaling for phosphoinositide metabolism (Audhya and Emr, 2002). Two other putative GEFs for Rho1 are Rom1 and Tus1. Because *rom1* deletions lack strong cell wall related phenotypes, Rom2 seems to be the major physiological isoform (Ozaki *et al.*, 1996). Tus1 does not interact with the sensors and its PH domain does not bind to the membrane, so that it might be more closely related to cell cycle-dependent activation of Rho1 (Kono *et al.*, 2008). In addition to its role in CWI signaling, Rom2 also acts as part of the TOR1 and TOR2 complexes in mediating growth response to nutrients and cell cycle-dependent polarization of the actin cytoskeleton (Schmidt *et al.*, 1997).

The next component in the signaling cascade, Rho1, belongs to a family of small GTPases comprising Rho1-5 and Cdc42, which are generally regulating polarized growth. Rho1 has been suggested to be a master regulator of CWI signaling since it integrates cell surface and cell-cycle signals but is also involved in cell wall synthesis by the glucan synthase complex, actin organization and polarized secretion (Levin, 2011). The most important effector of Rho1 for cell wall integrity is Pkc1, which activates the downstream MAPK cascade (Heinisch *et al.*, 1999) Accordingly, Rho1, Pkc1 and the components of the MAPK cascade are localized

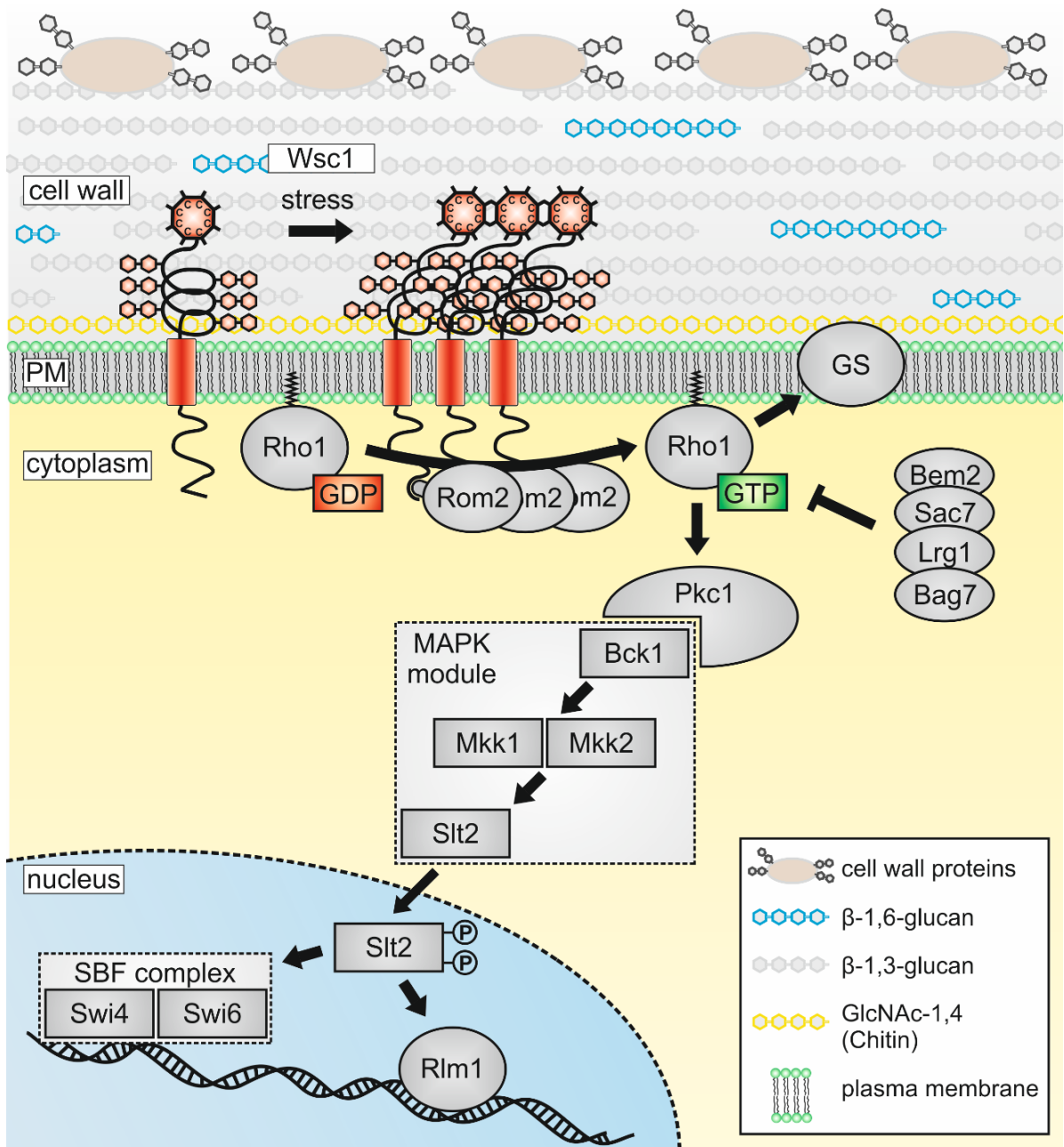


Figure 1.1: Schematic representation of cell wall integrity (CWI) signaling in *S. cerevisiae* (adapted from: Kock *et al.*, 2015). The yeast cell wall is a layered structure that consists of cell wall proteins, glucans and chitin. The cell surface sensors Wsc1-3, Mid2 and Mtl1 detect cell surface stress e.g. during growth and mating or under cell wall stress conditions and bind Rom2 upon activation (shown here for Wsc1). Rom2 acts as a guanine nucleotide exchange factor (GEF) for the small GTPase Rho1. GTP-Rho1 can be deactivated to its GDP-Rho1 form by the GTPase-activating proteins (GAP) Bem2, Sac7, Lrg1 or Bag7. The GTP-bound Rho1 is also directly able to activate the glucan-synthase complex (GS) with Fks1/Fks2 or can transfer the signal to the protein kinase C Pkc1. Pkc1 can phosphorylate the mitogen-activated protein kinase (MAPK) module with the MAPKKK Bck1, the redundant MAPKK Mkk1 and Mkk2 and the MAPK Slit2. The double-phosphorylated Slit2 is shuttled to the nucleus where it can mediate the transcriptional response by activating the transcription factors Rlm1 for cell wall related genes or the SBF complex consisting of Swi4 and Swi6 for cell cycle related gene expression.

to sites of polarized growth (Levin, 2011). Moreover, GTP-bound Rho1 is able to initiate glucan synthesis directly as it is part of the glucan synthase complex and activates the catalytic subunits Fks1 and Fks2 (Qadota *et al.*, 1996). Its role in actin nucleation has been attributed to its capacity to activate the formins Bni1 and Bnr1 (Sagot *et al.*, 2002). Polarized secretion for cell-surface extension is regulated by Rho1 upon interaction with the exocyst complex component Sec3 (Guo *et al.*, 2001). Furthermore, Rho1 has been shown to associate with the response regulator and transcription factor Skn7, a downstream target of a degenerated two-component signal transduction system with Sln1 that takes part in osmoregulation and Ca^{2+} signaling (Alberts *et al.*, 1998). During cytokinesis, Rho1 appears within the actomyosinring assembly, where it is inhibited by the cytokinesis regulator Cyk3 (Onishi *et al.*, 2013). As the activation of Rho1 involves guanine nucleotide exchange factors (GEFs), its inactivation is mediated by GTPase-activating proteins (GAPs). Out of eleven GAP proteins in yeast, Bem2, Sac7, Bag7 and Lrg1 have been shown to be able to inactivate GTP-bound Rho1 *in vitro*, with Lrg1 and Sac7 probably being of prime physiological importance (Watanabe *et al.*, 2001; Lorberg *et al.*, 2001).

The GTP-Rho1 effector Pkc1 is the only yeast homolog of the mammalian family of protein kinase C isoforms (Schmitz *et al.*, 2002; Schmitz and Heinisch, 2003). Yeast Pkc1 localizes to sites of polarized growth like the pre-bud site and the bud tip in G1 and S phase of the cell cycle, i.e. similar to Rho1, and relocalizes to the bud-neck during cytokinesis (Andrews and Stark, 2000). Pkc1 is an effector of the Pkh1 and Pkh2 kinases, that serve in an overlapping function during cell integrity and their Pkc1 activation is necessary for its full function (Inagaki *et al.*, 1999). Pkc1 can trigger chitin synthesis by phosphorylating the chitin synthase Chs3 and releasing it from chitosomes (Valdivia and Schekman, 2003). Phosphorylated Pkc1 is believed to activate the cell wall integrity MAPK cascade by phosphorylating Bck1 (Heinisch *et al.*, 1999).

The uppermost component of the MAPK cascade module is *BCK1*, which is the MAPKKK (MAP kinase kinase kinase) of the redundant pair of MAP kinase kinases (MAPKK), Mkk1 and Mkk2. All three encoding genes were identified as multicopy suppressors of *PKC1* (Lee and Levin, 1992; Irie *et al.*, 1993). Mkk2 and Mkk2 then phosphorylate the MAPK (MAP kinase) Sit2 (also known as Mpk1), a functional homolog of the human ERK kinases (Torres *et al.*, 1991).

Deletion of any of the genes encoding these MAP kinases results in lysis at high temperatures and sensitivity to cell wall stress (Levin 2011). Slt2 is dually phosphorylated by Mkk1 and Mkk2 in a Threonin-X-Tyrosin motif, which is recognized by a heterologous mammalian antibody (p42/44) raised against ERK1/ERK2, owing to its similar structure to the mammalian Thr202/Tyr204 motif (de Nobel *et al.*, 2000). Slt2 is predominantly found in the nucleus, but relocalizes to the cytoplasm upon cell wall stress (Kamada *et al.*, 1995) while a smaller fraction is also found at sites of polarized growth (Van Drogen and Peter, 2002) and at mitochondria under oxidative stress (Schmitz *et al.*, 2015). Mlp1 is a pseudokinase paralog of Slt2 which only possesses the tyrosil-residue of the phosphorylation motif and has a non-catalytic function in transcription together with its paralog (Kim, Truman, and Levin, 2008). Slt2 can be inactivated by four protein phosphatases, of which Ptp2 and Ptp3 are tyrosine-specific and the paralogs Sdp1 and Msg5 show dual-specificity towards tyrosine and serine/threonine in different target proteins (Martín *et al.*, 2005). Likely targets of Slt2 are Mkk1/2 to create a feedback loop and inactivate them. Other targets in the nucleus during cell wall integrity signaling would be the transcription factors Rlm1 and the SBF complex (Levin, 2011). Furthermore, when Slt2 becomes activated by CWI signaling, it can phosphorylate several components of the yeast eisosome complex (a plasma membrane funnel explained in detail in section 1.2.3) such as Pil1/Lsp1, Seg1 and Eis1 (Mascaraque *et al.*, 2013). It is also involved in vacuolar fusion during oxidative stress and in the degradation of peroxisomes and mitochondria during autophagy (Mao *et al.*, 2011; Pujol-Carrion *et al.*, 2013). Moreover, Slt2 was found to mediate the nuclear-cytoplasmic transport of cyclin C, which triggers yeast apoptosis (Jin *et al.*, 2013).

With respect to CWI signaling, the transcription factor Rlm1 is a primary nuclear target of Slt2 and was first isolated as a mutant suppressing the deleterious effects of overexpression of a constitutive *MKK1* allele (Watanabe *et al.*, 1997). Its DNA-binding domain shares characteristics of the MADS (MCM1, "agamous deficiens, serum response factor") box family of transcriptional regulators (Dodou and Treisman, 1997). Genome-wide surveys identified at least 25 genes whose expression is regulated by Rlm1. They mostly encode cell wall related proteins, for example mannoproteins like the Pir proteins (e.g. Pir1-3), GPI-anchored proteins (e.g. Pst1, Cwp1), and proteins involved in cell wall biogenesis like Slt2, Fks1, Fks2 and Chs3

(Jung and Levin, 1999). Slr2 also phosphorylates a subunit of the SBF transcription factor complex. SBF is composed of Swi4 and Swi6 and mediates the G1-specific transcriptional response in cell-cycle-dependent gene expression (Breedon, 2003).

In summary, although the components of the cell wall integrity pathway as shown in Figure 1.1 primarily trigger the proper cellular response to cell surface stress, many of them, e.g. Rom2, Rho1, Pkc1 and Slr2, have further roles and serve as mediators between different pathways to coordinate different stress responses and other cellular functions.

1.1.3 Five cell surface sensors contribute to cell wall integrity signaling

Five cell surface sensors have been described for the Rho1-Pkc1 dependent CWI pathway and are therefore commonly referred to as “CWI sensors”. They constitute two small protein families with a high degree of structural similarities: (i) the Wsc-type sensors include Wsc1, Wsc2 and Wsc3 (Verna *et al.*, 1997; Jacoby *et al.*, 1998) and the Mid-type sensors including Mid2 and Mtl1 (Ketela, Green, and Bussey 1999; Rajavel *et al.* 1999).

Despite showing differences in peptide length and amino acid sequence, they all share a common domain structure (Figure 1.2, Rodicio and Heinisch, 2010). This includes a short signal peptide that mediates their transport to the plasma membrane. The carboxyterminal region varies in size and structure, is located towards the cytoplasm and contains regulatory domains prone to covalent modifications, as well as putative Rom2-binding regions (Vay *et al.*, 2004) The authors suggested that Y303 and a LXVXNXD motif (amino acids 369-375 in Wsc1) mediate binding of Rom2, whereas phosphorylations at S319, S320, S322 and S323 inhibit this binding. The intracellular regions also contain signals for turnover of the sensors, for example the endocytosis signal NPFDD in Wsc1 (Piao *et al.*, 2007) and a putative residue for ubiquitination (K495) in Wsc2 (Wilk *et al.*, 2010).

A single transmembrane domain (TMD) anchors the sensors in the plasma membrane and connects the intracellular part with the extracellular part (Lodder *et al.*, 1999). The extracellular part of the sensors contains a serine/threonine-rich region (STR) with different lengths (Figure 1.2) so that the computed extension into the cell wall can vary from 61-106 nm (reviewed in Kock *et al.*, 2015). The serine/threonine-rich region is highly mannosylated during passage through the endoplasmic reticulum and the Golgi apparatus by the protein-O-

mannosyltransferases Pmt2 and Pmt4. The mannosylation stabilizes the rod-like, extracellular domain and is important for sensor function (Philip and Levin, 2001; Lommel *et al.*, 2004). The STR shows the physical properties of a nanospring depending on the degree of its mannosylation (Dupres *et al.*, 2009).

The two sensor families are mainly distinguished by their amino-terminal head groups. Thus, the Wsc-type sensors contain a cysteine-rich domain (CRD) with a size of about 10 kDa. This region contains eight conserved cysteine-residues and is involved in the clustering of the sensors (Heinisch *et al.*, 2010, see chapter 1.1.4/Figure 1.4 for further information). The asparagine N35 in Mid2 was found to be N-glycosylated and important for the sensor function and the N42 in Mtl1 presumably fulfills a similar function (Hutzler *et al.*, 2008; Rodicio and Heinisch, 2010).

It is now generally believed that the sensors act as mechanosensors. This notion is supported for example by the observation that the sensor concentration at the cell surface increases when cell wall glucans are degraded by zymolyase (Wittland, 2012). It has been proposed that the TMD anchors a sensor in the plasma membrane and the head group connects it to the cell wall polysaccharides (Heinisch *et al.*, 2010) The STR would then be expanded due to its nanospring properties as a result of displacement of the plasma membrane relative to the cell wall. This then could cause a conformational change in the intracellular part of the sensor and which allows it to interact with Rom2. In addition, the different extensions of the STR in the different sensors may detect stress in different layers of the cell wall and explain their specificities towards different stress agents (Bermejo *et al.*, 2010; Rodicio and Heinisch, 2010; Kock *et al.*, 2015).

Localization studies of fluorescently tagged variants, transcriptome and phenotypic analyses of different sensor mutants suggested partially overlapping but also specific functions in stress response (Rodicio and Heinisch, 2010). Thus, Wsc1 is predominately found at sites of polarized growth like the bud-neck of the daughter cell right after cytokinesis and at tips of emerging buds, but it also shows a punctate distribution in the plasma membrane (Straede and Heinisch, 2007; Wilk *et al.*, 2010). A *wsc1Δ* strain is hypersensitive to a variety of stress conditions such as a shift to higher or lower temperatures (Jacoby *et al.*, 1998; Córcoles-Sáez *et al.*, 2012) or the addition of compounds such as calcofluor white, congo red, caspofungin

or tea tree oil (Verna *et al.*, 1997; Straede *et al.*, 2007; Straede and Heinisch, 2007; Rodicio and Heinisch, 2010). These observed growth defects are further enhanced by additional deletion of *WSC2* and *WSC3* (Verna *et al.*, 1997), which show similar cellular distributions as *Wsc1* (Wilk *et al.*, 2010). In addition, *WSC3* is upregulated in response to organic solvents (Nishida *et al.*, 2014).

Mid2 on the other hand shows a more uniform distribution in the plasma membrane and seems to play more important roles in general stress response and during mating (Ono *et al.*, 1994; Straede and Heinisch, 2007). In contrast to *wsc1Δ*, *mid2Δ* is hyper-resistant to calcofluor white and tea tree oil (Ketela *et al.*, 1999; Straede *et al.*, 2007) and is sensitive to mating pheromone (Ono *et al.*, 1994). Double deletions of *WSC1* and *MID2* show a severe cell wall-related lysis phenotype and are highly sensitive to cell surface stress like high temperature or presence of calcofluor white, caspofungin, tea tree oil and SDS (Rajavel *et al.*, 1999; Straede and Heinisch, 2007). They were therefore suggested to be the physiologically more important members of the CWI sensor family in vegetatively growing cells (Levin, 2005). Deletion mutants of *MTL1* show a synthetic temperature-sensitivity in combination with *mid2Δ* (Rajavel *et al.*, 1999). *Mtl1* was suggested to be involved in the cellular response to glucose starvation and oxidative stress (Petkova *et al.* 2010; Petkova *et al.*, 2012). In addition, *Mtl1* has been described to generate the signal for translocation of Cyclin C to the cytoplasm and apoptosis, a function for which either *Wsc1* or *Mid2* need to be functional (Jin *et al.*, 2013).

Although only *Mid2* has been described to be important for mating, all five CWI sensors were found to relocate to the shmoo upon treatment with the yeast mating alpha factor (Hutzler *et al.*, 2008; Wittland, 2012).

1.1.4 *Wsc1* is a highly dynamic sensor which forms clusters in the plasma membrane

The *Wsc1* localization at sites of polarized growth and in membrane patches described above is a highly dynamic process, which is probably mediated by endocytosis. A central component of endocytosis is *End3*, which participates in internalization of vesicles at an early stage, when it interacts with *Sla1* (Bénédetti *et al.*, 1994; Tang *et al.*, 1997). Endocytosis can also be

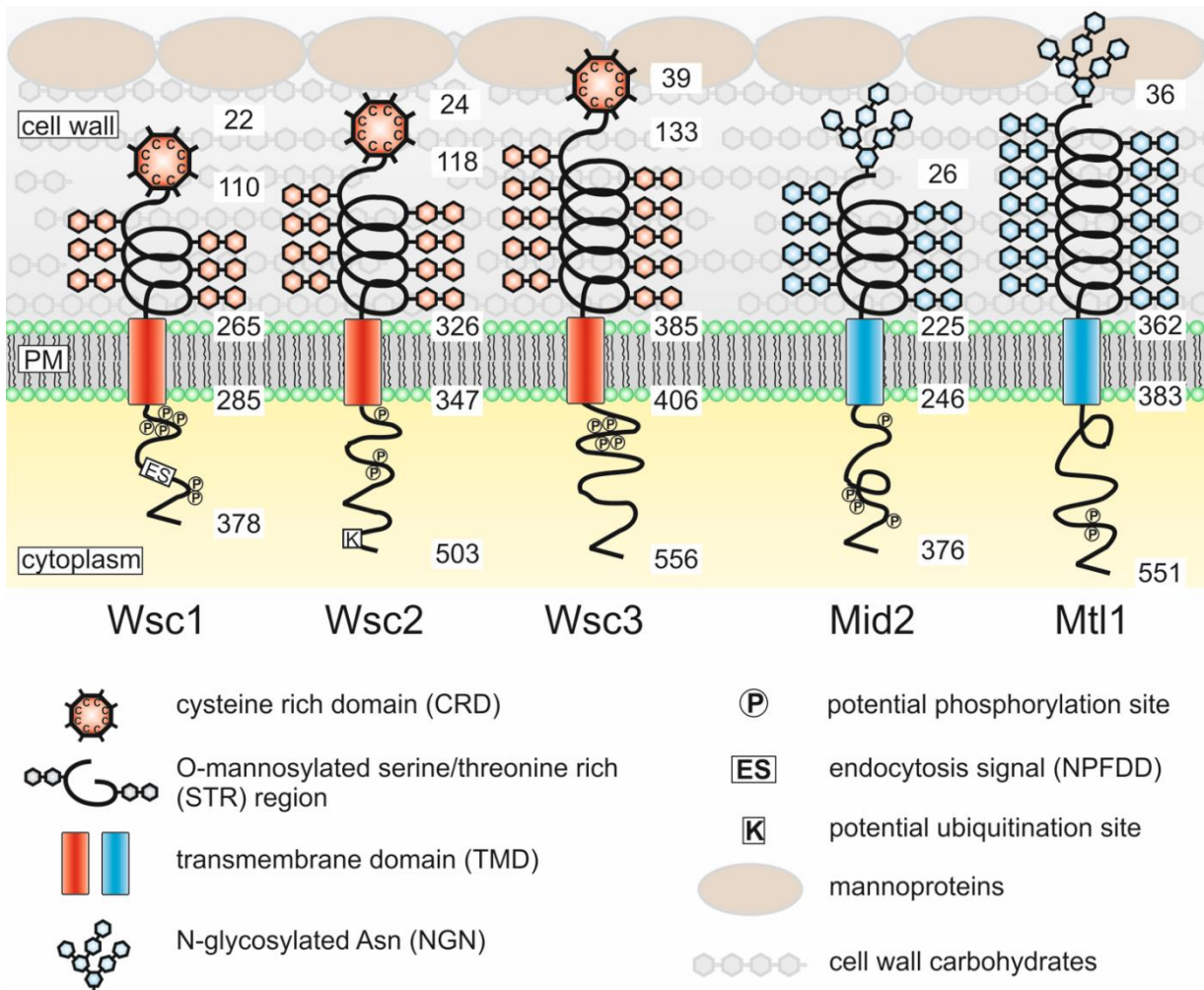


Figure 1.2: Overview of the protein structure of the five CWI sensors in *S. cerevisiae* (adapted from Kock *et al.*, 2015). Five sensors in two proteins families are known to contribute to cell wall integrity signaling. The first are the Wsc-type sensors with Wsc1-3 (red) and the other are the Mid-type sensors with Mid2 and Mtl1 (blue). All sensors show a similar protein domain structure with a cytoplasmic tail, a single transmembrane-domain (TMD) and an extracellular serine/threonine-rich region (STR) which is highly mannosylated. The major differences are the cysteine-rich domain (CRD) headgroup of the Wsc-type sensors with a proposed function in clustering and the N-glycosylation of an asparagine-residue in the Mid-type sensors. Furthermore, the length of the intracellular domain and the extracellular domain vary in the different sensors leading to different extensions into the cell wall.

blocked by deletion of the *DOA4* gene, which encodes a deubiquitinating enzyme involved in vacuolar sorting in late endocytosis (Amerik *et al.*, 2000). Deletions in either of the genes encoding End3 or Doa4 leads to an even distribution of Wsc1 in the plasma membrane, so that its polarized localization is lost. Furthermore, the sensor cannot be detected in

endosomes or in the vacuoles and its half-life upon blocking translation by cycloheximide increases dramatically, indicating that it is protein degradation, rather than changes in gene expression, which regulates its surface concentration (Wilk *et al.*, 2010). Wsc1 endocytosis is mediated by the amino acids 344-348, the intracellular recognition motif NPFDD, which interacts with Sla1 in the early endocytosis machinery (Piao *et al.*, 2007). As observed in an *end3Δ* mutant, mutation of the NPFDD motif causes a loss of polarized Wsc1 localization and blocks its endocytosis. When this motif was inserted into the intracellular domain of a chimeric Mid2 sensor it showed a Wsc1-like distribution. These data in combination with swapping the entire intracellular domains between Wsc1 and Mid2 suggested that it is the cytoplasmic C-terminal part of the sensors which determine their intracellular dynamics and localization (Piao *et al.*, 2007; Straede and Heinisch, 2007). For Wsc1, endocytosis has been proposed to prevent it from lateral diffusion in the plasma membrane and thus cause its accumulation at sites of polarized growth (Wilk *et al.*, 2010).

In addition to its highly polar localization, Wsc1 also shows a spot-like distribution in the lateral membrane (Straede and Heinisch, 2007). By AFM measurements, the size of the patches was approximately 230 nm in diameter, which increased up to 440 nm under stress conditions (Heinisch *et al.*, 2010). The formation of these clusters highly depends on the head group of the sensors which is known as the "Wsc1 domain" or "cysteine-rich domain" (CRD). It contains eight highly conserved cysteine residues (Figure 1.4), which are not only found within the Wsc-protein family of different yeast species, but also in homologous domains of other proteins, like in the β -1-3 exoglucanase (ThCRD2) of the fungus *Trichoderma harzianum* or in the disease-related human polycystin HsPKD1. Mutation of cysteine residues within the domain leads to loss of clustering in the plasma membrane, which in the wild-type can be mimicked by addition of dithiothreitol to the medium (Heinisch *et al.*, 2010; Dupres *et al.*, 2011). Clustering is thus likely to depend on the formation of disulfide bridges either between individual sensor molecules, or heterotypic bridge-formation with other cell wall proteins. Mutation of the CRD also leads to increased sensitivities towards cell wall stress agents, which are comparable to those of a *wsc1Δ* strain (Heinisch *et al.*, 2010). The modified Wsc1 sensors employed in this study accumulated in the vacuole and the sensors displayed a reduced signaling capacity, as judged by the relative concentration of dually phosphorylated

MAP kinase Slt2 (Wilk, 2010). Since Wsc1 is expected to recruit Rom2 and other downstream components of the CWI cascade, clustering has been suggested to cause the formation of a signaling complex called “Wsc1 sensosome”, which may enhance the function of individual sensors similar to sensing mechanisms in bacterial chemotaxis (Heinisch *et al.*, 2010; Tu, 2013).

With respect to its interactions with other proteins, bimolecular fluorescence complementation assays showed that it is found in close proximity to other Wsc1 sensor molecules, as well as to those of Wsc2, the GEF Rom2, and the endocytic adapter Sla1 (Piao *et al.*, 2007; Wittland, 2012). A genome-wide screen suggests an interaction with the Cdc28 subunit of the cyclin-dependent kinase, the yeast homolog of Cdk1 (Wong *et al.*, 2007).

1.2 Microcompartmentation of plasma membranes

1.2.1 Microcompartments are functional units at a suborganellar level

One major difference in the evolution of prokaryotes and eukaryotes is the compartmentation of different cellular functions within membrane-enclosed organelles in the latter, such as ATP production in mitochondria, protein transport within the endoplasmic reticulum (ER) and the *cis/trans*-Golgi network, protein degradation in lysosomes/vacuoles, and especially the maintenance and expression of nucleic acids in the nucleus (Shibata *et al.*, 2009; Wilson and Dawson, 2011; Merzendorfer and Heinisch, 2013).

These cellular compartments or organelles provide distinct environments for specialized tasks which are then protected from influences such as certain chemicals or conditions like the pH interfering with these processes. It also allows the cell to tightly regulate these processes and to save energy by providing only the necessary amount of components involved in this process. On the other hand, they also limit the availability of reaction partners, which have to be transported through the lipid bilayer barrier. Furthermore, the diffusion-dependent availability of reaction partners can be a limiting factor for cellular functions for example in the recruitment of cytoplasmic components to the plasma membrane or interaction partners within the plasma membrane (Ziółkowska *et al.*, 2012). To overcome these limitations, strategies have evolved to form suborganellar and highly

dynamic functional units, which allow a quick adaptation of cellular processes to changing conditions. These units are much smaller in size and more dynamic than organelles and have been defined as microcompartments (Merzendorfer and Heinisch, 2013). Prominent examples for microcompartments are the respiratory super complexes in the inner mitochondrial membrane (Vartak *et al.*, 2013) or the formation of endocytic sites during clathrin-dependent endocytosis (Kaksonen, 2008)

1.2.2 The plasma membrane is a dynamic bilayer and segregates into microdomains

The basic structure of biological membranes is a bilayer of amphipathic lipids into which proteins and other molecules such as sterols are incorporated. The fluid mosaic model of cell membranes proposes that this bilayer is a two-dimensional fluid in which molecules can move only in the lateral direction (Singer and Nicolson, 1972). Nowadays it is generally accepted that components within this bilayer do not distribute homogeneously and do not freely diffuse. Several mechanisms have been described to limit the random distribution of components within the bilayer which lead to the formation of membrane microcompartments. Among these mechanisms, the preferential association of proteins with lipids, protein-protein interactions, protein scaffolding that leads to membrane curvature, and the formation of “picket fences” by the actin cytoskeleton linked to the membrane, have been described to lead to the formation of domains large enough for microscopic detection (Kusumi *et al.*, 2005; Olivera-Couto and Aguilar, 2012). Such plasma membrane domains have been found both in pro- and in eukaryotes (de Bony *et al.*, 1989; Fishov and Woldringh, 1999).

One widely discussed concept of membrane domain formation is the “lipid raft” hypothesis. It is based on an unequal distribution of the three main classes of lipids found in biological membranes, i.e. the phospholipids, sphingolipids and sterols. Most abundant are the (glycero)phospholipids, with phosphatidylcholine typically contributing almost 50%. In contrast, sphingolipids and sterols are only incorporated in small amounts into the bilayer (Sonnino and Prinetti, 2013). The different lipids can segregate into liquid-disordered (L_d) and liquid-ordered (L_o) domains within the fluid membrane. The latter domains are enriched in sphingolipids and sterols, such as cholesterol or ergosterol (Baumgart *et al.*, 2003). These

lipid domains - or “rafts” - can form preferential environments for some proteins, which then form distinct domains. The formation and lifespan of these domains is highly dynamic and they typically only exist for 10-20 ms (Eggeling *et al.*, 2009). Lipid rafts have been proposed to govern different cellular processes, for example signaling in the immune system (Simons and Sampaio, 2011; Iwabuchi *et al.*, 2012; Garcia-Garcia *et al.*, 2012).

Other confined membrane domains which have been intensively studied are the caveolae found in vertebrate cells. These are plasma membrane invaginations associated with scaffolding proteins called caveolins. These domains also accumulate sphingolipids, cholesterol, and specific proteins (Sowa, 2012) and have been ascribed a variety of functions, e.g. in a clathrin-independent endocytic pathway, in cellular Ca^{2+} signaling, in lipid and cholesterol metabolism, or in cellular stress response (Bastiani and Parton, 2010). Interestingly, in the latter context they are assumed to serve as a membrane reservoir for mechanosensors employed under conditions of rapid membrane extension.

1.2.3 Several microcompartments are found in the yeast plasma membrane

Referring to the lipid raft hypothesis, Malínská and coworkers described different domains in the yeast plasma membrane. Thus, the plasma membrane proteins Can1 and Pma1 separate into two distinct domains and show raft-like properties (“RMC C” and “RMC P” for raft-based membrane compartment of Can1 or Pma1, respectively; Malinska *et al.*, 2003; Malinska, 2004). In light of the controversies associated with the lipid raft theory, these domains are now more generally referred to as “membrane compartment occupied by Can1” (MCC) and “membrane compartment occupied by Pma1” (MCP). Whereas the MCC displays a spot-like distribution in the plasma membrane, the MCP forms a non-overlapping network-like pattern (Grossmann *et al.*, 2007). A third highly dynamic compartment not overlapping with MCC or MCP harbors the TOR complex 2, named “membrane compartment containing TORC2” (MCT), was discovered later on (Berchtold and Walther, 2009). With the advance of more sensitive imaging techniques, the majority of proteins were shown to reside in subcompartments within the yeast plasma membrane, providing a range from spot-like to more network-like distributions, with very few being evenly distributed. Although some of these microcompartments overlap significantly with either Can1/Sur7 or Pma1, most

colocalizations appear to be random and very transiently (Spira *et al.*, 2012, see Figure 1.3). Despite these imaging approaches, the physiological function of these microdomains remains largely unclear. Yet, the inherent enzymatic activities have been elucidated: Pma1 is a membrane ATPase that regulates intracellular pH and plasma membrane potential, and apparently requires its association with lipid rafts to reach the yeast cell surface (Bagnat *et al.*, 2000). The TORC2 complex mediates a variety of processes, which includes actin organization (Aronova *et al.*, 2007), efficient endocytosis (de Hart *et al.*, 2002) and cell polarization during normal growth (Schmidt *et al.*, 1997) and it participates in ceramide maintenance (Aronova *et al.*, 2008). A functional connection to its presence in microdomain has not yet been shown.

The H⁺-driven arginine permease Can1 within the MCC has been shown to colocalize with several other permeases (Fur4, Tat2) and proteins of the Sur7 and of the Nce102 family (Young *et al.*, 2002; Malinska *et al.*, 2003; Malinska, 2004; Grossmann *et al.*, 2007; Grossmann *et al.*, 2008). These patches correspond to furrow like invaginations in the plasma membrane with a length of 250-300 nm, 50 nm width and 150-250 nm depth (Stradalova *et al.*, 2009). The stable invaginations are formed and maintained by a protein complex under the plasma membrane called eisosome. The core components of this complex are the paralogous BAR-domain proteins Pil1 and Lsp1 which associate with the negatively charged phospholipids of the plasma membrane through their positively charged residues and induce its curvature and invagination (Olivera-Couto *et al.*, 2011; Karotki *et al.*, 2011). Pil1 is necessary for the formation, as eisosomes do not form properly in *pil1Δ* mutants, except for a very small number of eisosomes called “remnants” while almost no remnants are found in *pil1Δ lsp1Δ* double mutants (Walther *et al.*, 2006). Several proteins have been shown to regulate eisosome formation and to be involved their proper organization. These include the two paralogous F-BAR proteins Slm1 and Slm2 (Kamble *et al.*, 2011; Olivera-Couto *et al.*, 2011) and the two necessary regulators Seg1 (Moreira *et al.*, 2012) and Eis1 (Aguilar *et al.*, 2010). Furthermore, Pil1 and Lsp1 are phosphorylated in a Slt2-dependent manner after activation of Pkc1 (Mascaraque *et al.*, 2013). This function is redundant with that of the two Pkh1 and Pkh2 kinases, which function in cellular integrity parallel to the CWI pathway (Walther *et al.*, 2007; Luo *et al.*, 2008).

Eisosome structures and genes have been identified in numerous fungi species, e.g. *Ashbya gossypii* (Seger *et al.*, 2011), *Candida albicans* (Douglas *et al.*, 2012), *Schizosaccharomyces pombe* (Kabeche *et al.*, 2011) or *Aspergillus nidulans* (Vangelatos *et al.*, 2010), so that they are most likely conserved in all fungi species.

Membranes associated with eisosomes are enriched in PI(4,5)P₂, sphingolipids and ergosterol, a composition suggested to confer raft-like properties in providing a special lipid environment to accommodate proteins. One of the proteins which diffuses between the MCC compartment and its surrounding area is Nce102. It becomes enriched in areas of high sphingolipid content and has thus been proposed to serve as a sensor for membrane composition (Grossmann *et al.*, 2007; Karotki *et al.*, 2011). Nce102 inhibits Pkh1 and Pkh2 and thereby promotes eisosome formation (Frohlich *et al.*, 2009).

Besides that, numerous differing functions for this domain have been discussed so far. In contrast to the first function proposed as specific sites for endocytosis, it seems now clear that a primary role of eisosomes is just the opposite, i.e. they serve as "safe harbors" for membrane proteins to prevent them from internalization and degradation (Walther *et al.*, 2006; Grossmann *et al.*, 2008). Further potential functions include maintaining sphingolipid homeostasis, forming scaffolding proteins involved in response to stress and organizing proton flux (Douglas and Konopka, 2014).

Similar to the caveolae membrane invaginations in vertebrate cells eisosomes also serve as membrane reservoirs under conditions when the membrane surface area rapidly increases, for example due to mechanical or hypoosmotic stresses (Bastiani and Parton, 2010; Kabeche *et al.*, 2015). *Vice versa*, hyperosmotic conditions cause yeast cells to shrink and have been found to increase the number of eisosomes (Douglas and Konopka, 2014). In the pathogenic fungus *Candida albicans* eisosomes play also an important role in membrane organization and cell wall growth, as a deletion of *SUR7* showed strong effects on septin and actin localization and lead to large plasma membrane invaginations with abnormal cell wall growth due to increased chitin synthase activity - a similar phenotype as in β -glucan synthase defective cells (Alvarez *et al.*, 2008).

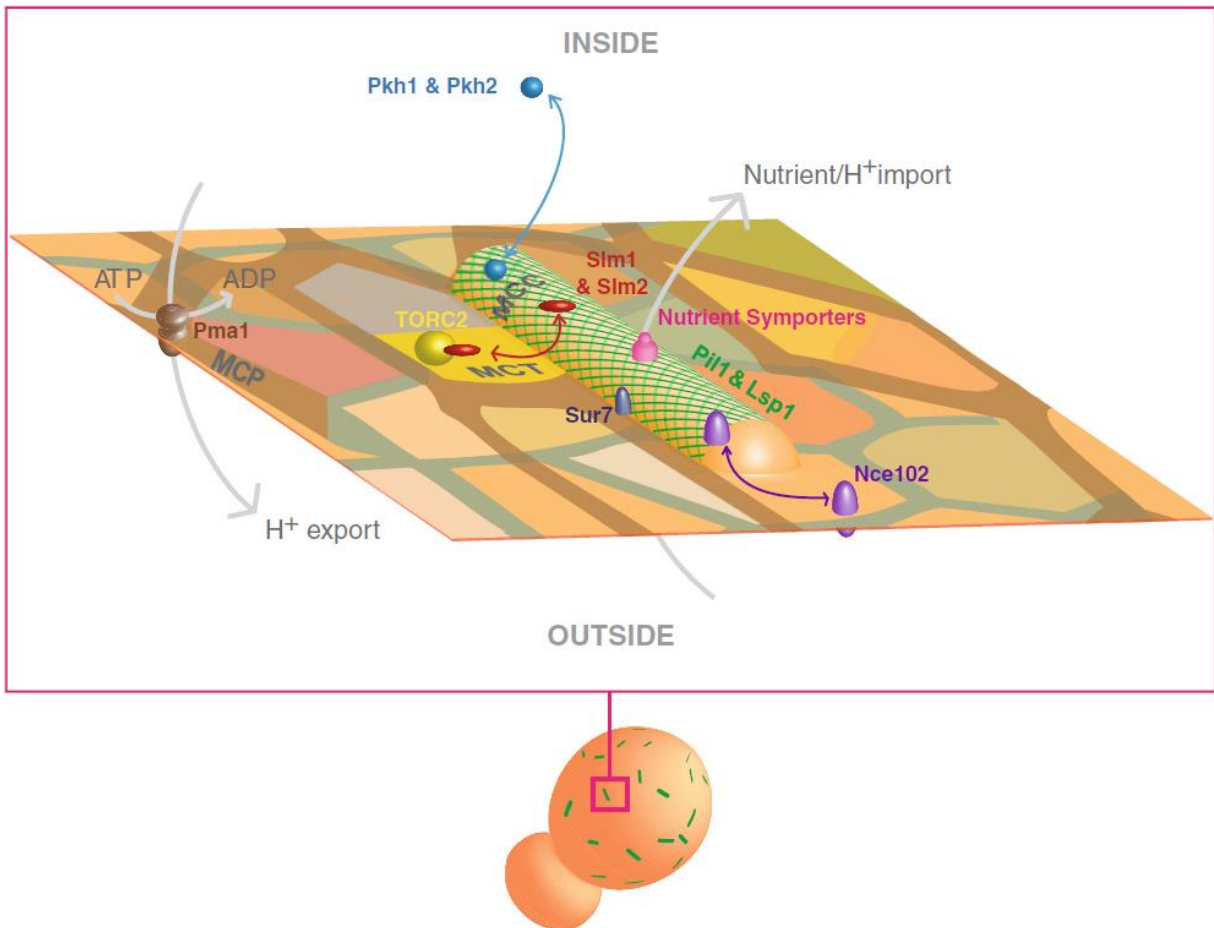


Figure 1.3: Plasma membrane organization in *S. cerevisiae* (from: Olivera-Couto and Aguilar, 2012). Yeast plasma membrane proteins show localization patterns varying from spot-like to network-like which coexist in a patchwork of partially overlapping domains (indicated by brown/orange/red/blue/green patterns). The plasma membrane ATPase Pma1 localizes in a network-like domain known as the “membrane compartment occupied by Pma1” (MCP). The “membrane compartment occupied by Can1” (MCC) forms distinct furrow-like invaginations in a spot-like pattern dependent on the eisosome proteins Pil1 and Lsp1. The formation is regulated by Slm1/ Slm2 and the Pkh1/Pkh2 kinases. Several nutrient symporters or proteins of the Sur7 family localize in this domain. Nce102 serves as a sphingolipid sensor and shuttles between the two domains. The Tor2 complex also forms a distinct, spot-like domain named as “membrane compartment containing TORC2” (MCT).

1.3 Amyloid proteins

1.3.1 Wsc1 sensors have putative amyloid sequences

Amyloids are large insoluble homotypic protein aggregates and many different proteins have been found to share this capacity. The name “amyloid” derives from the mistaken assumption by Rudolf Virchow that the aggregates consist of starch, as they can be stained by iodine similar to cellulose-like substances (Westermarck *et al.*, 2005). Unbranched protein fibrils of the amyloid type have been associated with a number of severe diseases in humans and animals, such as for example Alzheimer’s disease, AL amyloidosis, Parkinson’s disease, or type 2 diabetes (Jahn *et al.*, 2010; Lipke *et al.*, 2012; Garcia-Sherman *et al.*, 2014). The most prominent and well-studied example of an amyloid protein are indeed prions, the causing agents of the mad cow disease (vCJD; Bendheim *et al.*, 1985). Until 2005, 25 diseases were listed as amyloidosis, defined by the extracellular deposition of protein aggregates and their staining by Congo red. It should be noted that although the Congo red absorbance and Thioflavin T emission are markers for amyloid proteins, higher concentrations of these dyes can also inhibit their aggregation (Garcia *et al.*, 2011). Additional properties of amyloids include an elongated protein morphology, cooperative, nucleation-dependent aggregate formation, and a cross-beta X-Ray diffraction pattern (Sawaya *et al.*, 2007).

Apart from the disease-related features, many amyloid proteins have been found to serve important physiological functions in various organisms. Thus, the silk of the garden spider *Araneus diadematus* has amyloid-like properties (Slotta *et al.*, 2007) and mammalian cells use amyloids as template for melanin deposition in melanosomes (Hu *et al.*, 2011). Moreover, amyloid proteins play important roles in surface adhesion and biofilm formation in fungal cells as shown for the human pathogenic fungus *Candida albicans* (Garcia *et al.*, 2011).

The protein aggregation in amyloids is mediated by short amino acid sequences which fold into β -sheets. No consensus sequence could be identified for amyloid motifs because the featuring peptides vary from highly polar, glutamine-rich (e.g. GNNQQNY) to highly apolar (e.g. MVGGVV) and from amino acids with small side chains (e.g. SSTSAA) to those with large and aromatic side chains (e.g. FYLLYY). One shared feature of all these motifs is that long side

chains intercalate within the peptide bond of the adjacent motif. This way the β -sheets form zippers (Sawaya *et al.*, 2007). Amyloid forming sequences can be predicted using the TANGO algorithm, which calculates the tendency to form hydrophobic β -sheet aggregates based on the inter- and intramolecular interaction energies of unfolded protein chains (Fernandez-Escamilla *et al.*, 2004). Such regions correlate well with the amino acids that have been identified as the aggregation domains in many amyloid proteins (Otoo *et al.*, 2008).

A TANGO analysis revealed that the three Wsc-type CWI sensors contain sequences potentially forming amyloids in a conserved region within the CRD, between the third and fourth cysteine residue. In Wsc1 this would be the amino acids 58-65 (ASYFALYN), in Wsc2 the amino acids 64-70 and in Wsc3 the amino acids 78-84 (both AVVALFN, Figure 1.4). In Wsc1 the software predicted 40% aggregation potential of this motif which could be reduced to 2.63% by exchange of the tyrosine at position 60 for a serine (Edupaganti and Lipke, personal communication). This indicates that amyloids may be important for the clustering of Wsc1 in the plasma membrane described above.

			C1			C2	C3	Amyloid sequence	
Wsc1	22	--YEYVNC	FSSLP---	SDFSKADS	----	YNWQSSSH	CNSECS	SAK	GASYFALYNH
Wsc1 Y60S	22	--YEYVNC	FSSLP---	SDFSKADS	----	YNWQSSSH	CNSECS	SAK	GASSFALYNH
Wsc2	24	DQFTYKAC	CYSA----	SDIRKLGL	TYKGVY	EYQSVSY	CQNEC	--PGQ	AVVALFNG
Wsc3	39	D-FNYEGC	CYSAADI	QSAGLS	SLKNS	----	YIYQSVSY	CQNQC	PE--SAVVALFNG
									▲
		C4	C5		C6	C7	C8		
Wsc1	67	SECYCG	DTNP---	SGSESTSS	SCNTYCF	FGYSSEM	CGGEDAYS	VYQLD-	110
Wsc1 Y60S	67	SECYCG	DTNP---	SGSESTSS	SCNTYCF	FGYSSEM	CGGEDAYS	VYQLD-	110
Wsc2	72	TGCYCG	GSAQLQ	SLTQVD	SSKCDV	SCAGWPY	QNCGGSS	AMNVY	INN-
Wsc3	86	SDCYCG	NSVFLT	SLTKST	DSNCG	GTKCSG	WPYQMC	GGSSYM	NVYVNAE

Figure 1.4: Sequence alignment of the CRD domains of the Wsc-type CWI sensors. The cysteine-rich domain of the sensors contains eight conserved cysteine residues (marked in red). A potential amyloid-forming sequence was found in all three sensors between C3 and C4 using the TANGO algorithm (marked in yellow). The Wsc1 ASYFALYN motif was calculated to have a potential of 40% for aggregation. An Y60S substitution (red arrow) was predicted to reduce the aggregation tendency to 2.63% (Edupaganti and Lipke, personal communication).

1.4 Aims of this thesis

The five cell wall integrity sensors Wsc1, Wsc2, Wsc3, Mid2 and Mtl1 are the uppermost components of a signal cascade detecting cell surface stress in *S. cerevisiae*. Since the CWI signaling cascade is essentially conserved throughout the fungal kingdom and required for cell survival, it is a potential target for antifungal drugs. The conservation of the MAPK cascade in all eukaryotes also makes yeast a perfect model system to study such signal transduction pathways, with implications in cancer therapy. Although the CWI sensors Wsc1 and Mid2 have been intensively studied, the role of the other three sensors largely remains obscure. Another field to be explored is the exact distribution of the sensors in yeast plasma membrane microcompartments and their physiological role.

In this context, the following questions were addressed in this thesis:

1. What is the role of individual sensors in response to cell wall stress? - For this purpose the construction of a quintuple mutant should be attempted, in order to introduce single sensor genes and study their effect on cell wall integrity.
2. Do the yeast CWI sensors reside in different microdomains within the plasma membrane and, if so, do they overlap with known domains? - In order to address these questions, different fluorescent tags were attached to the sensors and employed for live-cell microscopic colocalization studies, including quantification.
3. How is the Wsc1 sensor delivered and maintained in its microdomain and what effect has a perturbation of this localization on signal transduction? - To study the physiological relevance of microcompartmentation, *wsc1* mutants encoding mislocalized sensors were obtained, their membrane distribution was determined, as was their capacity to activate the CWI pathway.
4. Are there any interaction partners of Wsc1 within its microdomain which have not yet been described? - An approach of labeling transiently associated proteins by a fusion of Wsc1 with a biotinylation activity and their identification by mass spectrometry after purification was tested in this context.

2. Materials and methods

2.1 Materials

2.1.1 Equipment

The equipment used in this work is listed in Table 2.1.

Table 2.1: Equipment used in this work.

Function	Product	Supplier
Autoclaves	3870 EL	Systec GmbH, Linden, Germany
	Fedegari autoclave	ibs tecnomara GmbH
Cameras (microscopes)	ORCA-Flash4.0 LT	Hamamatsu Photonics Deutschland GmbH, Herrsching am Ammersee, Germany
	sCMOS	PCO, Kelheim, Germany
Centrifuges	Micro centrifuge	Carl Roth, Karlsruhe, Germany
	Heraeus Pico 17	Thermo Scientific, Waltham, Massachusetts, USA
	EBA 8S	Andreas Hettich GmbH & Co.KG, Tuttlingen, Germany
	Heraeus Megafuge 1.0	Thermo Scientific, Waltham, Massachusetts, USA
	Mikro 22R	Andreas Hettich GmbH & Co.KG, Tuttlingen, Germany
	Allegra X-22R	Beckman Coulter GmbH, Krefeld, Germany
Incubator		BINDER GmbH, Tuttlingen, Germany
Infrared imager	Odyssey infrared imaging system	LI-COR Biotechnology, Lincoln, New York, United States
Light engine (microscope)	SPECTRA light engine	Lumencor, Beaverton, Oregon, USA
Magnetic stirrer	MAG RH	IKA-Werke GmbH & CO. KG, Staufen, Germany
Micromanipulator	MSM system series 300	Singer Instrument Company Limited, Roadwater, Watchet, Somerset, United kingdom
Microscopes	Axio Imager Z1	Carl Zeiss AG, Oberkochen, Germany
	DeltaVision Elite	Applied Precision, Issaquah, Washington, USA
pH meter	Labor pH meter 766	Knick Elektronische Messgeräte GmbH & Co. KG, Berlin, Germany
Photometer	Amersham Biosciences Ultrospec 2100 pro	GE Healthcare Europe GmbH, Freiburg, Germany
Power supplies	Standard Power Pack P25	Biometra GmbH, Göttingen, Germany
	2197 Power supply	LKB Bromma, Sollentuna, Sweden

Scanner	Scanjet 3500c	HP Inc., Palo Alto, California
Shakers	Duomax 1030	Heidolph Instruments GmbH & Co.KG, Schwabach, Germany
	Innova 2300 platform shaker	Eppendorf AG, Hamburg, Germany
	TC-7 roller drum	Eppendorf AG, Hamburg, Germany
	Vibrax VXR basic	IKA-Werke GmbH & CO. KG, Staufen, Germany
	Vortex-Genie 2	Scientific Industries, Inc., Bohemia, New York, USA
SDS-Gel system	Mini-PROTEAN 3 Cell	Bio-Rad, Hercules, California, USA
Semi-dry blotter	Trans-Blot SD Semi-Dry Transfer Cell	Bio-Rad, Hercules, California, USA
Thermoblock	ThermoStat plus	Eppendorf AG, Hamburg, Germany
Thermocyclers	Tpersonal	Biometra GmbH, Göttingen, Germany
	Tgradient	Biometra GmbH, Göttingen, Germany
UV Documentation	GelDoc-It Imaging system	UVP, LLC, Upland, California, USA
UV transilluminators	Ultraviolet Transilluminator	UVP, LLC, Upland, California, USA
	BiImaging Systems	
	Vilber Lourmat 302 nm	Bachofer Laboratoriumsgeräte, Reutlingen, Germany

2.1.2 Chemicals and consumables

Chemicals and consumables used in this work were supplied by the following companies: Applichem (Darmstadt, Germany), BD (Franklin Lakes, USA), Bio-Rad (Munich, Germany), Biozym (Hessisch Oldendorf, Germany), Boehringer Ingelheim (Ingelheim, Germany), Brand (Gießen, Germany), Difco (Heidelberg, Germany), Eppendorf (Hamburg, Germany), Fluka (Steinheim, Germany), Formedium (Hunstanton, UK), GE Healthcare (Freiburg, Germany), Greiner BioOne (Solingen, Germany), Invitrogen (Darmstadt, Germany), Li-Cor (Bad Homburg, Germany), Merck (Darmstadt, Germany), MP Biomedicals (Illkirch, France), Neolab (Heidelberg, Germany), Omnilab (Bremen, Germany), Riedel-de Haën (Seelze, Germany), Roche (Mannheim, Germany), Roth (Karlsruhe, Germany), Sarstedt (Nümbrecht, Germany), Schott (Mainz, Germany), Serva (Heidelberg, Germany), Sigma (Steinheim, Germany), Süd-Laborbedarf (Gauting, Germany), Thermo Scientific (Waltham, USA) and Trefflab (Degersheim, Switzerland)

2.1.3 Kits

Kits used in this work are listed in Table 2.2. Changes from the protocol are described, otherwise the steps were done as described in the supplier's manual.

Table 2.2: Kits used in this work

Kit	Supplier
GeneJET Plasmid Miniprep Kit	Thermo Scientific, Waltham, Massachusetts, USA
GeneJET PCR Purification Kit	Thermo Scientific, Waltham, Massachusetts, USA
μMACS Streptavidin Kit	Miltenyi Biotec, Bergisch Gladbach, Germany
maxXbond MB007 DNA binding column regeneration kit	AppliChem GmbH, Darmstadt, Germany

2.1.4 Enzymes

“FastDigest” endonucleases (restriction enzymes) for DNA restriction, “DreamTaq” and “Phusion HiFi” polymerases, T4 ligase, “FastAP” alkaline phosphatase and TPCK-trypsin were supplied by Thermo Scientific (Waltham, Massachusetts, USA). The glucanase preparation Zymolyase-20T for digestion of ascus and cell walls was supplied by MP Biomedicals (LLC, Santa Ana, California, USA).

2.1.5 Antibodies

The antibodies used in this work were provided by the companies listed in Table 2.3.

Table 2.3: Antibodies used for Western Blotting in this work

antigene	organism	dilution	supplier
anti-Phospho-p44/42 MAP kinase (Thr202/Tyr204) Lot. 23 (monoclonal)	rabbit	1:100 in TBST + 1 % milk powder	Cell Signaling Technology, Inc., Danvers, Massachusetts, USA
anti-Mpk1 (yC-20) (polyclonal)	goat	1:7000 in TBST + 1 % milk powder	Santa Cruz Biotechnology, Inc., Santa Cruz, California, USA
anti-rabbit-IgG IRDye700 (polyclonal)	donkey	1:5000 in TBST + 1 % milk powder	Rockland Immunochemicals Inc., Limerick, Philadelphia, USA
anti-goat-IgG (polyclonal)	donkey	1:5000 in TBST + 1 % milk powder	Rockland Immunochemicals Inc., Limerick, Philadelphia, USA

2.1.6 Electrophoresis ladders

The ladders used for size comparison in gel electrophoreses were “GeneRuler 1 kb DNA ladder” or “GeneRuler 100 bp Plus DNA Ladder” in DNA agarose gel electrophoresis and the “PageRuler Prestained Plus” standard for proteins in SDS polyacrylamide gel electrophoresis (SDS-PAGE). All standards were provided by Thermo Scientific (Waltham, Massachusetts, USA).

2.1.7 Media

2.1.7.1 Media for the growth of *E. coli*

Rich medium (LB):

- 0.5 % (w/v) yeast extract
- 1 % (w/v) Trypton
- 0.5 % NaCl

1.5 % (w/v) agar was added for plates (solid medium) before autoclaving.

For selection medium ampicillin or kanamycin were added in a concentration of 100 µg/ml.

2.1.7.2 Media for growth of *S. cerevisiae*

Rich medium (YEP):

- 1 % (w/v) yeast extract
- 2 % (w/v) pepton
- 2 % (w/v) sugar (glucose for YEPD or galactose for YEPGal)

Synthetic complete medium (SC):

- 0.67 (w/v) % yeast nitrogen base w/o amino acids (YNB)
- 2 % (w/v) sugar (glucose for SCD or galactose for SCG)
- 0.06 % (w/v) CSM-HIS-LEU-TRP-URA

amino acids and uracil were added for preparation of dropout media, as required, in the following concentrations:

- 20 mg/l uracil
- 20 mg/l L-histine
- 20 mg/l tryptophan

100 mg/l leucine

pH was adjusted to 6.2

Synthetic minimal medium (SMD): 0.67 % (w/v) yeast nitrogen base w/o amino acids (YNB)

2 % (w/v) glucose

pH was adjusted to 6.2

Sporulation medium: 1 % (w/v) potassium acetate

For preparation of plates, 1.5 % (w/v) agar was added to YEP, SC and SM media, and 3 % (w/v) agar to sporulation medium, before autoclaving. 1 M sorbitol was added to plates when osmotic stabilization was necessary. For kanMX selection, 200 µg/ml geneticin sulfate (G418) was added to the medium after autoclaving. The chemicals for stress medium (caffeine, calcofluor white, caspofungin or congo red) were added to the medium at the concentrations indicated.

2.1.8 Oligonucleotides

The oligonucleotides used in this work were supplied by Metabion International AG (Martinsried, Germany) and are listed in Table 2.4.

Table 2.4: Oligonucleotides used in this work. Plasmid binding sequences are printed in bold and restriction sites are underlined.

Number	Name	Sequence (5'-3')
03.50	SLG1gfp5'	ACCAGGAGGGAAAAACAACGTTTTAACAGTGGTCAATCCAGACGAAG CTGAT CGGATCCCCGGGTTAATTAA
03.51	SLG1gfp3'	GGAGATGATTTGGCAAATGAAATCGGAAAAAGAAAAATTAATGG GAAG GAATTCGAGCTCGTTTAAAC
03.52	MID2gfp5'	GAAGAAAAATTCTATGATGAACAAGGTAACGAATTATCACCACGAAA TTAT CGGATCCCCGGGTTAATTAA
03.53	MID2gfp3'	GTCCACCTACTCAATATCAGAAATATAATTAAGATGGTCAATTTACAA TAATT GAATTCGAGCTCGTTTAAAC
03.59	SLG1rein3'	GATGATTTGGCAAATGAAATCGG
04.119	GFPraus	GGACAGGGCCATCGCCAATTGG
04.94	vorSLGSall	GCGC <u>GTCGACC</u> GAGGCACTAACATTACAG
05.150	SLG1außerrück	GGTTGAGCTCGCCAGGACTTGAACCTGGAATC
06.176	SpHIS5-5'out	GCAGTATCTTCTGCAGTGTG

06.31	Mtl1rev	GCTACCCCTTAGGAACAGGAACC
07.174	WSC3EcoRI	CCGGGAATTCCGGGCTATCCATATTACATCTGAAC
07.175	WSC3BamHI	CGCCGGATCCCATCTACATAGTGGCACTCACTACG
07.259	WSC3-R3	GTCCAGCAGAACCAGTTGATTACCATTAATGTTGAGAGTTTATGCGAG TTTTTCGATGAATTCGAGCTCG
07.82	PMA1zurück	GTATCTTGAGTGTCTGTATGGGCGC
08.138	WSC1-ATGvor	ATGAGACCGAACAACAAGTCTGC
08.255	WSC2vor	CGAGACAATTGGCACTGTAGT
08.256	WSC2rück	TTTGCGACCGATTACGGTTG
10.225	TEFprom-5'out	CCTCAGTGGCAAATCCTAAC
11.113	MTL1-raus	CCAACCTCCATAACAGAGGC
11.300	WSC3-S3	CCTGATAATCCTGAATTATCTAGTACCGTATCTCATAATCGAGCCCTTC GTACGCTGCAGGTCGAC
12.144	PIL1vorEco	GCGCGAATTCATTAGTAGTGTACTCAAACG
12.158	ScPil1mChF5	AAGTCGGACACCAGCAAAGTGAGTCTCTTCCCAACAACAACAGCT GGTGACGGTGCTGGTTA
12.159	ScPil1mChR1	ATTTTTTCAGAGTGAGGGAACAGAAATGATTATCTGTCCACGCATAG GCCACTAGTGGATCTG
12.601	MID2rein5'	AGTTACGAGTACAGTGGACC
13.082	WSC1revTMDXho	CCGCCTCGAGTGCCCTACATTGGCTTTC
13.083	WSC1forTMDXho	CCGCCTCGAGCAGACACATTAATATGAAGC
13.084	MID2revTMDXho	CCGCCTCGAGTTTCTATTTTTTTTAGAAAGACCC
13.085	MID2forTMDXho	CCGCCTCGAGTTTTGTATCCAATCATCAAGGAC
13.186	dsRedraus5	GGCCGTTAACAGTACCTTCC
13.261	MTL1vor_PstI	GCGCGGACTGCAGAAAAACCAAGCGGACACC

2.1.9 Strains

2.1.9.1 *E. coli* strains

The *Escherichia coli* strain used in this work for plasmid amplification was DH5 α (Thermo Scientific, Waltham, Massachusetts, USA). Genotype:

F⁻ Φ 80*lacZ* Δ M15 Δ (*lacZYA-argF*) U169 *recA1 endA1 hsdR17* (rK⁻, mK⁺) *phoA supE44* λ -*thi-1 gyrA96 relA1*

2.1.9.1.1 Incubation and storage of *E. coli* strains

E. coli strains were grown at 37 °C overnight under aerobic conditions. Plates and cultures were stored at 4 °C for a maximal time of two months.

2.1.9.2 *S. cerevisiae* strains

Already existing *Saccharomyces cerevisiae* strains used in this work are listed in Table 2.5. Strains created for this work by *in-vivo* recombination or obtained by crossing and tetrad analyses are listed in Table 2.6.

Table 2.5: Existing *S. cerevisiae* strains used in this work.

Name	Genotype	background strain	Reference
DHD5	<i>MATa/alpha ura3-52/ura3-52 leu2-3,112/leu2-3,112 his3-11,15/his3-11,15 MAL3/MAL3 SUC2/SUC2 GAL/GAL</i>	-	Kirchrath <i>et al.</i> , 2000
HD56-5A	<i>MATalpha ura3-52 leu2-3,112 his3-11,15 MAL3 SUC2 GAL</i>	-	Arvanitidis and Heinisch, 1994
HAJ150-A	<i>MATa ura3-52 leu2-3,112 his3-11,15 BIT61-mCherry-CaURA3 MAL SUC GAL</i>	HD56-5A	Arne Jendretzki, pers. communication
HAS17-3C	<i>MATa ura3-52 leu2-3,112 his3-11,15 wsc1::SpHIS3 MAL SUC GAL</i>	HD56-5A	Straede and Heinisch, 2007
HAS35-13D	<i>MATalpha WSC1-GFP-kanMX ura3-52 leu2-3,112 his3-11,15 MAL SUC GAL</i>	HD56-5A	Straede and Heinisch, 2007
HJW116-B	<i>MATalpha WSC3-3myEGFP-SpHIS5; ura3-52 leu2-3,112 his3-11,15 MAL SUC GAL</i>	HD56-5A	Janina Jendretzki, pers. communication
HJW25-A	<i>MATa end3::KIURA3 ura3-52 leu2-3,112 his3-11,15 MAL SUC GAL</i>	HD56-5A	Wilk <i>et al.</i> , 2010
HJW25-B	<i>MATalpha end3::KIURA3 ura3-52 leu2-3,112 his3-11,15 MAL SUC GAL</i>	HD56-5A	Wilk <i>et al.</i> , 2010
HOD134-1C	<i>MATalpha ura3-52 his3-11,15 leu2-3,112 trp1N::loxP</i>	HD56-5A	Jürgen Heinisch, pers. communication
HOD137-3A	<i>MATa ura3-52 his3-11,15 leu2-3,112 trp1N::loxP wsc1::KIURA3</i>	HD56-5A	Jürgen Heinisch, pers. communication
HOD137-3C	<i>MATalpha ura3-52 his3-11,15 leu2-3,112 trp1N::loxP wsc1::KIURA3</i>	HD56-5A	Jürgen Heinisch, pers. communication
HOD145-1D	<i>MATalpha ura3-52 his3-11,15 leu2-3,112 trp1::loxP wsc1::KIURA3 mid2::KILEU2</i>	HD56-5A	Jürgen Heinisch, pers. communication
HOD145-5B	<i>MATa ura3-52 his3-11,15 leu2-3,112 trp1::loxP wsc1::KIURA3 wsc2::KITRP1 wsc3::kanMX mtl1::SkHIS3</i>	HD56-5A	Jürgen Heinisch, pers. communication
HOD165-3C	<i>MATalpha ura3-52 his3-11,15 leu2-3,112 trp1N::loxP mid2::KILEU2</i>	HD56-5A	Jürgen Heinisch, pers. communication
HOD188-7D	<i>MATalpha ura3-52 his3-11,15 leu2-3,112</i>	HD56-5A	Jürgen Heinisch,

	<i>trp1N::loxP wsc1::KIURA3 wsc3::kanMX mtl1::SkHIS3 KIURA3-GAL1p::WSC2 KIURA3- GAL1p::MID2</i>		pers. communication
HSK11-2C	<i>MATalpha WSC1-GFP-kanMX end3::KIURA3 ura3-52 leu2-3,112 his3-11,15 MAL SUC GAL</i>	HD56-5A	Wilk <i>et al.</i> , 2010
HSK15-1D	<i>MATalpha ura3-52 leu2-3,112 his3-11,15 PMA1-GFP-kanMX MAL SUC GAL</i>	HD56-5A	Sabrina Wilk, pers. communication
HSK17-1C	<i>MATalpha ura3-52 leu2-3,112 his3-11,15 mid2::loxP slg1 ::SpHIS3 MAL SUC GAL</i>	HD56-5A	Straede and Heinisch, 2007
HSK28	<i>MATalpha ura3-52 leu2-3,112 his3-11,15 MID2-EGFP-SpHIS5 MAL SUC GAL</i>	HD56-5A	Straede and Heinisch, 2007
HSK29	<i>MATalpha ura3-52 leu2-3,112 his3-11,15 WSC1-EGFP-SpHIS5 MAL SUC GAL</i>	HD56-5A	Straede and Heinisch, 2007
HSK38-3A	<i>MATalpha wsc1 ::WSC1_{C1A}-kanMX ura3-52 leu2-3,112 his3-11,15 MAL SUC GAL</i>	HD56-5A	Sabrina Wilk, pers. communication
HSK39-3B	<i>MATalpha wsc1 ::WSC1_{C2,3A}-kanMX ura3-52 leu2-3,112 his3-11,15 MAL SUC GAL</i>	HD56-5A	Sabrina Wilk, pers. communication
HSK40-1C	<i>MATalpha wsc1 ::WSC1_{C4,5A}-kanMX ura3-52 leu2-3,112 his3-11,15 MAL SUC GAL</i>	HD56-5A	Sabrina Wilk, pers. communication
HSK41-2A	<i>MATalpha wsc1 ::WSC1_{C6,7A}-kanMX ura3-52 leu2-3,112 his3-11,15 MAL SUC GAL</i>	HD56-5A	Sabrina Wilk, pers. communication
HSK42-3C	<i>MATalpha wsc1 ::WSC1_{C8A}-kanMX ura3-52 leu2-3,112 his3-11,15 MAL SUC GAL</i>	HD56-5A	Sabrina Wilk, pers. communication
HSK69-1B	<i>MATalpha ura3-52 leu2-3,112 his3-11,15 WSC2-EGFP-kanMX MAL SUC GAL</i>	HD56-5A	Sabrina Wilk, pers. communication
HSK76	<i>MATalpha ura3-52 leu2-3,112 his3-11,15 PMA1-dsred-kanMX MID2-EGFP-SpHIS5 MAL SUC GAL</i>	HD56-5A	Sabrina Wilk, pers. communication
HSK82-1A	<i>MATa ura3-52 leu2-3,112 his3-11,15 PMA1- dsred-kanMX MAL SUC GAL</i>	HD56-5A	Sabrina Wilk, pers. communication
HSK83-9D	<i>MATa ura3-52 leu2-3,112 his3-11,15 WSC1- GFP-kanMX PMA1-dsred-kanMX MAL SUC GAL</i>	HD56-5A	Sabrina Wilk, pers. communication
HSK92-8C	<i>MATa ura3-52 leu2-3,112 his3-11,15 WSC2- EGFP-kanMX PMA1-dsRED-kanMX MAL SUC GAL</i>	HD56-5A	Sabrina Wilk, pers. communication

Table 2.6: *S. cerevisiae* strains that were constructed for this work by *in vivo* recombination or crossing and tetrad dissection. All diploid strains (beginning with a “D”) are based on DHD5 and all haploid strains (beginning with an “H”) are based on HD56-5A or the isogenic *MATa* strain. The genotypes are additions or variations of the normal DHD5/HD56-5A genotype (see Table 2.5). Oligos=oligonucleotides.

Name	Mating type	Genotype	Construction
DCK18	<i>MATa/alpha</i>	<i>PIL1-yEGFP-SpHIS5/PIL1</i>	PCR-product of pKT128 and oligos 12.158+12.159 introduced into DHD5 and checked with oligos 12.144+06.176
HCK18-3C	<i>MATalpha</i>	<i>PIL1-yEGFP-SpHIS5</i>	Sporulation and tetrad dissection of DCK18
DCK27	<i>MATa/alpha</i>	<i>WSC1-tdTomato-SkHIS3/WSC1</i>	PCR-product of pOCK006 and oligos 03.50+03.51 introduced into DHD5 and checked with oligos 08.138+10.225
HCK27-2C	<i>MATa</i>	<i>WSC1-tdTomato-SkHIS3</i>	Sporulation and tetrad dissection of DCK27
DCK28	<i>MATa/alpha</i>	<i>MID2-tdTomato-SkHIS3/MID2</i>	PCR-product of pOCK006 and oligos 03.52+03.53 introduced into DHD5 and checked with oligos 12.601+10.225
HCK28-3A	<i>MATa</i>	<i>MID2-tdTomato-SkHIS3</i>	Sporulation and tetrad dissection of DCK28
DCK36	<i>MATa/alpha</i>	<i>WSC1-ScBirA*-SkHIS3/WSC1</i>	PCR-product of pJJH1617 and oligos 03.50+03.51 introduced into DHD5 and checked with oligos 08.138+03.59
HCK36-1B	<i>MATalpha</i>	<i>WSC1-ScBirA*-SkHIS3</i>	Sporulation and tetrad dissection of DCK36
HCK36-9B	<i>MATa</i>	<i>WSC1-ScBirA*-SkHIS3</i>	Sporulation and tetrad dissection of DCK36
DCK37	<i>MATa/alpha</i>	<i>PIL1-yEGFP-SpHIS5/PIL1 PMA1-dsRed-kanMX/PMA1</i>	Crossing of HCK18-3C and HSK82-1A
HCK37-5C	<i>MATalpha</i>	<i>PIL1-yEGFP-SpHIS5 PMA1-dsRed-kanMX</i>	Sporulation and tetrad dissection of DCK37
DCK38	<i>MATa/alpha</i>	<i>WSC3-3myEGFP-SkHIS3/WSC3 PMA1-dsRed-kanMX/PMA1</i>	Crossing of HJW116-B and HSK82-1A
HCK38-4C	<i>MATalpha</i>	<i>WSC3-3myEGFP-SkHIS3 PMA1-dsRed-kanMX</i>	Sporulation and tetrad dissection of DCK38
DCK39	<i>MATa/alpha</i>	<i>WSC1-GFP-kanMX/WSC1 MID2-tdTomato-SkHIS3/MID2</i>	Crossing of HCK28-3A and HAS35-13D
HCK39-2C	<i>MATalpha</i>	<i>WSC1-GFP-kanMX MID2-tdTomato-SkHIS3</i>	Sporulation and tetrad dissection of DCK39
DCK40-2	<i>MATa/alpha</i>	<i>PMA1-GFP-kanMX/PMA1-dsRed-kanMX</i>	Zygotes of HSK15-1D crossed with HSK82-1A and checked with oligos 07.82+13.186 and 07.81+04.119

DCK49	<i>MATa/alpha</i>	<i>WSC1-EGFP-SpHIS5/WSC1 BIT61-mCherry- CaURA3/BIT61</i>	Crossing of HSK29 and HAJ150-A
HCK49-7C	<i>MATalpha</i>	<i>WSC1-EGFP-SpHIS5 BIT61- mCherry-CaURA3</i>	Sporulation and tetrad dissection of DCK49
DCK50	<i>MATa/alpha</i>	<i>MID2-EGFP-SpHIS5/MID2 BIT61-mCherry- CaURA3/BIT61</i>	Crossing of HSK28 and HAJ150-A
HCK50-3C	<i>MATalpha</i>	<i>MID2-EGFP-SpHIS5 BIT61- mCherry-CaURA3</i>	Sporulation and tetrad dissection of DCK50
DCK51	<i>MATa/alpha</i>	<i>WSC3-3myEGFP- SpHIS5/WSC3 BIT61- mCherry-CaURA3/BIT61</i>	Crossing of HJW116-B and HAJ150-A
HCK51-1B	<i>MATalpha</i>	<i>WSC3-3myEGFP-SpHIS5 BIT61-mCherry-CaURA3</i>	Sporulation and tetrad dissection of DCK51
DCK56	<i>MATa/alpha</i>	<i>WSC1-tdTomato- SkHIS3/WSC1 WSC2-GFP- kanMX/WSC2</i>	Crossing of HCK27-2C and HSK69-1B
HCK56-4A	<i>MATalpha</i>	<i>WSC1-tdTomato-SkHIS3 WSC2-GFP-kanMX</i>	Sporulation and tetrad dissection of DCK56
HCK58-1	<i>MATalpha</i>	<i>WSC1_{C2/3A}-EGFP-SpHIS5</i>	pOCK025 restriction with <i>Sna</i> BI and <i>Xho</i> I and transformation in HCK39-3B and checked with 08.138+03+59
HCK59-3	<i>MATalpha</i>	<i>WSC1_{C4/5A}-EGFP-SpHIS5</i>	pOCK025 restriction with <i>Sna</i> BI and <i>Xho</i> I and transformation in HCK40-1C and checked with 08.138+03+59
HCK60-4	<i>MATalpha</i>	<i>WSC1_{C6/7A}-EGFP-SpHIS5</i>	pOCK025 restriction with <i>Sna</i> BI and <i>Xho</i> I and transformation in HCK41-2A and checked with 08.138+03+59
HCK61-1	<i>MATalpha</i>	<i>WSC1_{C8A}-EGFP-SpHIS5</i>	pOCK025 restriction with <i>Sna</i> BI and <i>Xho</i> I and transformation in HCK42-3C and checked with 08.138+03+59
DCK62	<i>MATa/alpha</i>	<i>MTL1-3myEGFP- SpHIS5/MTL1</i>	PCR-product of pAJ060 and oligos 07.259+11.300 introduced into DHD5 and checked with oligos 11.113+06.31
HCK62-1A	<i>MATalpha</i>	<i>MTL1-3myEGFP-SpHIS5</i>	Sporulation and tetrad dissection of DCK62
DCK66	<i>MATa/alpha</i>	<i>WSC1_{C2/3A}-EGFP- SpHIS5/WSC1 end3::KIURA3/END3</i>	Crossing of HCK58-1 and HJW25-A
HCK66-2D	<i>MATalpha</i>	<i>WSC1_{C2/3A}-EGFP-SpHIS5 end3::KIURA3</i>	Sporulation and tetrad dissection of DCK66
DCK67	<i>MATa/alpha</i>	<i>WSC1_{C4/5A}-EGFP- SpHIS5/WSC1 end3::KIURA3/END3</i>	Crossing of HCK59-3 and HJW25-A
HCK67-1D	<i>MATalpha</i>	<i>WSC1_{C4/5A}-EGFP-SpHIS5 end3::KIURA3</i>	Sporulation and tetrad dissection of DCK67

DCK68	<i>MATa/alpha</i>	<i>WSC1_{C6/7A}-EGFP-SpHIS5/WSC1 end3::KIURA3/END3</i>	Crossing of HCK60-4 and HJW25-A
HCK68-4C	<i>MATalpha</i>	<i>WSC1_{C6/7A}-EGFP-SpHIS5 end3::KIURA3</i>	Sporulation and tetrad dissection of DCK68
DCK69	<i>MATa/alpha</i>	<i>WSC1_{C8A}-EGFP-SpHIS5/WSC1 end3::KIURA3/END3</i>	Crossing of HCK61-1 and HJW25-A
HCK69-4A	<i>MATalpha</i>	<i>WSC1_{C8A}-EGFP-SpHIS5 end3::KIURA3</i>	Sporulation and tetrad dissection of DCK69
DCK73	<i>MATa/alpha</i>	<i>wsc1::WSC1_{C6,7A}-kanMX/WSC1 end3::KIURA3/END3</i>	Crossing of HSK41-2A and HJW25-B
HCK73-8D	<i>MATa</i>	<i>wsc1::WSC1_{C6,7A}-kanMX end3::KIURA3</i>	Sporulation and tetrad dissection of DCK73
DCK75	<i>MATa/alpha</i>	<i>wsc1::SpHIS5/WSC1 end3::KIURA3/END3</i>	Crossing of HAS17-3C and HJW25-B
HCK75-11B	<i>MATalpha</i>	<i>wsc1::SpHIS5/WSC1 end3::KIURA3/END3</i>	Sporulation and tetrad dissection of DCK75

2.1.9.2.2 Incubation and storage of *S. cerevisiae* strains

S. cerevisiae strains were incubated at 30 °C for 1 or 2 days, unless noted otherwise. After incubation cultures and plates were stored at 4 °C for several months. For permanent storage, glycerol cultures were prepared from 500 µl overnight culture added to 1 ml of sterile 33 % (v/v) glycerol. These stock cultures were kept at -80 °C.

2.1.10 Vectors and plasmids

A list of the plasmids employed in this work is presented in Table 2.7. Plasmids created in this work are listed in Table 2.8 with information about how the plasmid was constructed.

Table 2.7: Existing Plasmids and vectors used in this work.

Plasmid	Description	Reference
YCplac111	CEN4/ARS1 <i>S. cerevisiae</i> / <i>E.Coli</i> shuttle vector with LEU2 selection marker, ampicillin resistance and lacZ cloning site.	Gietz and Akio, 1988
YEplac352	2µm multicopy <i>S. cerevisiae</i> / <i>E.Coli</i> shuttle vector with LEU2 selection marker, ampicillin resistance and lacZ cloning site.	Hill <i>et al.</i> , 1986
YEplac181	2µm multicopy <i>S. cerevisiae</i> / <i>E.Coli</i> shuttle vector	Gietz and Akio, 1988

	with LEU2 selection marker, ampicillin resistance and lacZ cloning site.	
pUK1921	<i>E. coli</i> cloning vector with ampicillin resistance and lacZ cloning site.	Heinisch, 1993
pUK21	<i>E. coli</i> cloning vector with ampicillin resistance and lacZ cloning site.	Vieira and Messing, 1991
pAGT213	<i>Ashbya gossypii</i> tagging vector with tdTomato	Kaufmann, 2009
pFA6a-GFP-kanMX	Yeast tagging vector with GFP, kanMX selection marker and ampicillin resistance	Longtine <i>et al.</i> , 1998
pFA6a-GFP-SkHIS3	Yeast tagging vector with GFP, SkHIS3 selection marker and ampicillin resistance	Longtine <i>et al.</i> , 1998
pKT128	Yeast tagging vector with yeast optimized GFP, SpHIS5 selection marker and ampicillin resistance	Sheff and Thorn, 2004
pAJ060	Yeast tagging vector with yeast optimized monomeric 3xGFP, SpHIS5 selection marker and ampicillin resistance	Arne Jendretzki, pers. communication
pBH01	YCplac111 with <i>MIDWSC1</i> (<i>Wsc1</i> with <i>Mid2</i> _{STR} elongation)	Heinisch <i>et al.</i> , 2010
pJJH1123	pUK1921 with <i>WSC1</i>	Jürgen Heinisch, pers. communication
pJJH1124	pUK1921 with <i>MID2</i>	Jürgen Heinisch, pers. communication
pJJH1140	YCplac111 with <i>WSC1</i> _{NPF/AAI}	Wilk <i>et al.</i> , 2010
pJJH1169	YCplac111 with <i>MID2WSC1</i> _{C4,5A}	Heinisch <i>et al.</i> , 2010
pJJH1191	YCplac111 with <i>MID2WSC1-GFP</i>	Heinisch <i>et al.</i> , 2010
pJJH1617	pFA6A-GFP-SkHIS3 with GFP exchanged for <i>ScBirA</i> *	Jürgen Heinisch, pers. communication
pJJH1892	YCplac111 with <i>MID2WSC1</i> _{V60S}	Jürgen Heinisch, pers. communication
pJW05	YCplac111 with <i>WSC1-VN-SpHIS5</i>	Janina Jendretzki, pers. communication
pJW06	YCplac111 with <i>WSC1-VC-kanMX</i>	Janina Jendretzki, pers. communication
pJW09	YCplac111 with <i>WSC1</i> _{C4,5A} - <i>VN-SpHIS5</i>	Janina Jendretzki, pers. communication
pJW10	YCplac111 with <i>WSC1</i> _{C6,7A} - <i>VN-SpHIS5</i>	Janina Jendretzki, pers. communication
pOCK002	pRS306 with Pil1-mCherry	Olivera-Couto <i>et al.</i> , 2011
pSK27	YCplac111 with <i>WSC1</i>	Sabrina Wilk, pers. communication

pSK44	YCplac111 with <i>WSC1_{NPF/AAI}-GFP-kanMX</i>	Wilk <i>et al.</i> , 2010
YEp352-Mid2	Yep352 with <i>MID2</i>	Sabrina Wilk, pers. communication
YEp352-Wsc1	Yep352 with <i>WSC1</i>	Sabrina Wilk, pers. communication

Table 2.8: Plasmids that were constructed for this work. Oligos=oligonucleotides, ivR=*in vivo* recombination.

Plasmid	Backbone	Insert	Construction
pOCK009	pFA6a-GFP-kanMX	<i>tdTomato</i>	tdTomato from pAGT213 cut with AscI+PacI and cloned in pFA6a-GFP-kanMX
pOCK010	pJH1123	<i>WSC1_{ΔTMD}</i>	Inverse PCR with oligos 13.082+13.083 & XhoI ligation
pOCK011	pJH1124	<i>MID2_{ΔTMD}</i>	Inverse PCR with oligos 13.084+13.085 & XhoI ligation
pOCK012	Ycplac111	<i>WSC1_{ΔTMD}</i>	pOCK010 BamHI+HindIII restriction and ligation in YcpLac111
pOCK013	Ycplac111	<i>MID2_{ΔTMD}</i>	pOCK011 BamHI+HindIII restriction and ligation in YcpLac111
pOCK014	YcpLac111	<i>WSC1_{TMD-MID2}</i>	ivR of XhoI-cut pOCK012 and <i>WSC1_{TMD-MID2}</i> from gene synthesis
pOCK015	YcpLac111	<i>MID2_{TMD-WSC1}</i>	ivR of XhoI-cut pOCK013 and <i>MID2_{TMD-WSC1}</i> from gene synthesis
pOCK016	pOCK014	<i>WSC1_{TMD-MID2}-myGFP-SkHIS3</i>	ivR of pOCK014 and PCR-product of pJH1620 and oligos 03.50+03.51
pOCK017	pOCK015	<i>MID2_{TMD-WSC1}-myGFP-SkHIS3</i>	ivR of pOCK015 and PCR-product of pJH1620 and oligos 03.52+03.53
pOCK018	YEplac181	<i>WSC3</i>	PCR-product of genomic DNA (DHD5) & oligos 07.174+07.175, EcoRI+BamHI restriction and ligation in YEplac181
pOCK019	YEplac181	<i>WSC2</i>	PCR-product of genomic DNA (DHD5) & oligos 08.255+08.256, XbaI+XhoI restriction and ligation in YEplac181 (XbaI+Sall)
pOCK020	YEplac181	<i>MTL1</i>	PCR-product of genomic DNA (DHD5) & oligos 13.261+06.31, PstI+BamHI restriction and ligation in YEplac181
pOCK025	pUK21	<i>WSC1-EGFP-SpHIS5</i>	PCR-product of genomic DNA (HSK29) & oligos 04.94+05.150, Sall+XhoI restriction and ligation in pUK21

pOCK027	pJW06	<i>WSC1_{C4,5A}-VC-kanMX</i>	Insert from pJW09 <i>Sna</i> BI+ <i>Sall</i> restriction and ligation in pJW06
pOCK028	pJW10	<i>WSC1_{C6,7A}-VC-kanMX</i>	Insert from pJW06 <i>Pac</i> I+ <i>Kpn</i> I restriction and ligation in pJW10
pOCK029	pJJH1140	<i>WSC1_{C4,5A} NPF/AAI</i>	Insert from pJW09 <i>Sna</i> BI+ <i>Swa</i> I restriction and ligation in pJJH1140
pOCK030	pJJH1140	<i>WSC1_{C6,7A} NPF/AAI</i>	Insert from pJW10 <i>Apa</i> I+ <i>Swa</i> I restriction and ligation in pJJH1140
pOCK031	pOCK029	<i>WSC1_{C4,5A} NPF/AAI -GFP-SkHIS3</i>	ivR of pOCK029 and PCR-product from pFA6a-GFP-SkHIS3 and oligos 03.50+03.51
pOCK032	pOCK030	<i>WSC1_{C6,7A} NPF/AAI -GFP-SkHIS3</i>	ivR of pOCK030 and PCR-product from pFA6a-GFP-SkHIS3 and oligos 03.50+03.51
pOCK033	pJJH1892	<i>MID2_{STR}-WSC1_{Y60S}-GFP-SkHIS3</i>	ivR of pJJH1892 and PCR-product from pFA6a-GFP-SkHIS3 and oligos 03.50+03.51
pOCK035	pSK27	<i>WSC1-GFP-SkHIS3</i>	ivR of pSK27 and PCR-product from pFA6a-GFP-SkHIS3 and oligos 03.50+03.51

2.2 Methods

2.2.1 Transformation protocols

2.2.1.1 Transformation of *E. coli* (Hanahan, 1985)

Transformation of *E. coli* was performed using the rubidium chloride protocol described in Hanahan, 1985: For preparation of competent cells an overnight culture of *E. coli* was used to inoculate cells in 50 ml LB medium at an OD₆₀₀ of approximately 0.05. Cells were incubated with shaking at 37 °C until the cultures reached an OD₆₀₀ of 0.4-0.6. The culture was stored on ice for 1-2 hours and centrifuged for 10 min at 2000 rpm and 4 °C before they were resuspended in 20 ml of cold RFI buffer (100 mM RbCl, 50 mM MnCl₂, 30 mM potassium acetate, 10 mM CaCl₂, 15% v/v glycerol, adjusted to pH 5.8). After storage on ice for another two hours cells were harvested by centrifugation and resuspended in 4 ml cold RFII buffer (10 mM RbCl, 10 mM MOPS, 75 mM CaCl₂, 15% v/v glycerol, adjusted to pH 6.8). After storage on 4 °C for 15 min 100 µl aliquots of the cells were prepared in sterile Eppendorf cups and stored at -80 °C.

For transformation, competent cells were thawed on ice and 1 µl of plasmid stock or 10 µl from a ligation reaction were added and kept on ice for 30 min. Cells were then heat shocked at 42°C for 45 s. After 5 min on ice, 1 ml of LB medium was added and tubes were incubated at 37 °C for 45 min. Cells were then pelleted at 8000 rpm for 2 min, resuspended in 200 µl LB, plated onto selective LB plates and grown overnight at 37 °C. Single colonies were inoculated for plasmid preparations.

2.2.1.2 Transformation of *S. cerevisiae* with the lithium acetate method (Gietz *et al.*, 1992)

In most cases, the protocol used for genomic transformation of *S. cerevisiae* has been described in Gietz *et al.*, (1992): Cells from an overnight culture were inoculated in 12.5 ml YEPD medium with an OD₆₀₀ of 0.5 and grown at 30 °C to reach an OD₆₀₀ of 1.6-2.0. The cells were then centrifuged at 3000 rpm for 1 min and washed in 5 ml of sterile water. After another centrifugation step the cells were washed with 1 ml 100 mM sterile lithium acetate and centrifuged again. The washed cells were resuspended in 400 µl 100 mM lithium acetate and used to prepare aliquots of 100 µl in sterile Eppendorf cups.

For transformation, each aliquot was centrifuged at 3000 rpm for 1 min and the supernatant was discarded. 240 μ l of 50% PEG4000, 36 μ l of 1 M lithium acetate, 5 μ l of carrier DNA (from a stock of 10 μ g/ μ l), and 45 μ l of a PCR product (approximately xx μ g) and/or 5 μ l of plasmid DNA (approximately 1 μ g) were added. Cells resuspended in this mixture were incubated for 30 min at 30 °C, followed by a heat shock at 42 °C for 20 min. After centrifugation at 3000 rpm for 2 min cells were resuspended in 200 μ l of sterile water, plated onto selective media and incubated for 2-3 days at 30 °C. For selection on geneticin sulfate (G418) the cells were first resuspended in 1 ml water and 2 ml YEPD rich media and stored at room temperature over night. The supernatant was discarded before plating onto YEPD/G418 medium.

2.2.1.2 Transformation of *S. cerevisiae* with the “freeze method” (Klebe *et al.*, 1983)

50 ml of YEPD medium was inoculated with cells from an overnight culture to a final OD₆₀₀ of 0.25 and incubated at 30 °C with shaking to reach an OD₆₀₀ of 0.8. Cells were harvested by centrifugation (3000 rpm, 3 min) and washed in 5 ml of buffer A (1 M sorbitol, 10 mM bicine pH 8.35, 3% ethylene glycol) and resuspended in 4 ml of buffer A. 200 μ l aliquots were prepared in sterile Eppendorf cups and stored at -80 °C until further use (from 1 h up to 1 year).

For transformation, aliquots of the competent cells were placed on ice and 5 μ l of carrier DNA (herring sperm DNA at 10 μ g/ μ l) and 5 μ l of plasmid DNA (approximately 1 μ g) were added. After a heat shock at 37 °C for 5 minutes, 1 ml of buffer B (200 mM bicine pH 8.35, 40 % PEG-1000) was added. The cups were inverted several times to mix the cells and incubated at 30 °C for 1 hour, harvested by centrifugation (3000 rpm, 3 min) and washed with 1 ml 1 M sorbitol. After another centrifugation step (3000 rpm, 3 min) the cells were resuspended in 200 μ l 1 M sorbitol and streaked onto selective media. For selection of G418 resistance, cells were resuspended in 2 ml YEPD medium and incubated over night at room temperature before plating.

2.2.1.3 Transformation of *S. cerevisiae* with the spheroblast method

For transformation of strains lacking the CWI sensors, an adapted spheroblast transformation protocol described for *Torulasporea delbrueckii* by (Compagno *et al.*, 1989) was used. An

overnight culture grown in YEPD with 1 M sorbitol was used to inoculate 50 ml of fresh medium with an OD₆₀₀ of 0.25 and inoculated with shaking at 30°C to reach an OD₆₀₀ of 0.6-0.8. After centrifugation at 3000 rpm for 5 min cells were washed with 4 ml of 1.2 M sorbitol, collected again by centrifugation, resuspended in buffer 1 (1.2 M sorbitol, 0.025 M EDTA pH 8, 50 mM DTT), and incubated without shaking for 10 min at 30 °C. Cells were then harvested by centrifugation at 2500 rpm for 3 min and washed twice with 4 ml sorbitol. After suspension in buffer 2 (1.2 M sorbitol, 0.01 M EDTA pH 8, 0.1 M sodium citrate pH 5.7, 15 µg/ml zymolyase) the cells were incubated for 15 min at 30 °C for digestion of the cell wall. After this step the cells were handled with care without vigorous shaking and washed twice with 1.2 M sorbitol and pelleted at 2000 rpm for 5 min. Cells were then suspended in buffer 3 (1.2 M sorbitol, 10 mM CaCl₂ and 10 mM Tris pH 7.5) and aliquoted into ten samples of 100 µl each in sterile 15 ml Falcon tubes.

For transformation, 5 µl of carrier DNA (10 µg/µl) and 5 µl of plasmid (approximately 1 µg) were added to the spheroblast suspension and incubated for 15 min at room temperature. After addition of 1 ml buffer 4 (20% PEG-4000, 10 mM CaCl₂, 10 mM Tris pH 7.5) tubes were incubated for an additional 15 min at room temperature. After collection at 2000 rpm for 10 min the cells were resuspended in 2 ml buffer 3 and 2 ml of YEPD containing 1.2 M sorbitol was added. The cells were then allowed to regenerate their cell wall remnants for 40 min at room temperature without shaking, centrifuged at 2000 rpm for 10 min and resuspended in 0.5 ml 1.2 M sorbitol. 15 ml of top-layer agar (1.2 M sorbitol, 1% agar) cooled to 45 °C was added, mixed and quickly poured on selective plates containing 1.2 M sorbitol. These were incubated for at least three days at 25 °C.

2.2.2 Yeast genetics

2.2.2.1 Yeast strain construction by homologous recombination

Yeast strains with genomic insertions were constructed *via* homologous recombination in combination with a PCR-directed approach. The integration cassette was amplified from suitable template vectors, e.g. the ones described by Longtine *et al.*, 1998 or by Sheff and Thorn, 2004, using oligonucleotide pairs (20-25 nucleotides) that bind up- and downstream of the deletion or fusion cassette of the template vector and carry additional 40-45

nucleotides of sequences homologous to the (genomic) target at their 5'- ends. The amplified double-stranded PCR product was then introduced into a suitable recipient strain and plated to select for the respective integration markers. Clones obtained were then verified by PCR to contain the correct insertion. Two alternative PCR setups were employed: 1) primers flanking the target sequence that produce PCR products of different lengths in wild type and mutant or 2) a combination of such a flanking primer with one binding within the integrated cassette, with the PCR reaction only yielding a product if the cassette was integrated correctly. An example of strategy 1) is shown in Figure 2.1: Schematic representation of the DCK36 strain construction using homologous recombination. for the construction of the heterozygous diploid strain DCK36.

2.2.2.2 Crossing of yeast strains

Diploid yeast strains were selected by complementation of auxotrophic markers after crossing of the haploid parental strains on a YEPD plate. For this, a *MAT α* strain was streaked out with a sterile toothpick in one line and a *MAT a* strain was streaked out crossing this line in a 90 ° angle by mixing cells at the crossing point and streaking out the mixed cells for single colonies, below. This plate was incubated for overnight at 30 °C and then used to replica-plate with a sterile velvet onto selective medium for the diploids. Single clones from this plate were inoculated in YEPD for further use.

2.2.2.3 Sporulation, tetrad analysis and mating type identification

To sporulate yeast cells, a fresh overnight culture was grown in 3 ml of YEPD, centrifuged at 3000 rpm for 2 min and the supernatant was discarded. The cells were then washed in 1 ml of sterile water, resuspended in 50 μ l of sterile water and dropped on potassium acetate plates (1 % potassium acetate, 3 % agar). After three days of incubation at 30 °C, ascus formation was checked by microscopic examination. For gentle digestion of ascus walls a small amount of sporulated cells was resuspended in 200 μ l of sterile water, and 2 μ l zymolyase 20T (10 mg/ml) was added and incubated for 10 minutes at room temperature. Suspensions were then stored on ice and 800 μ l of sterile water were added. 15 μ l of this

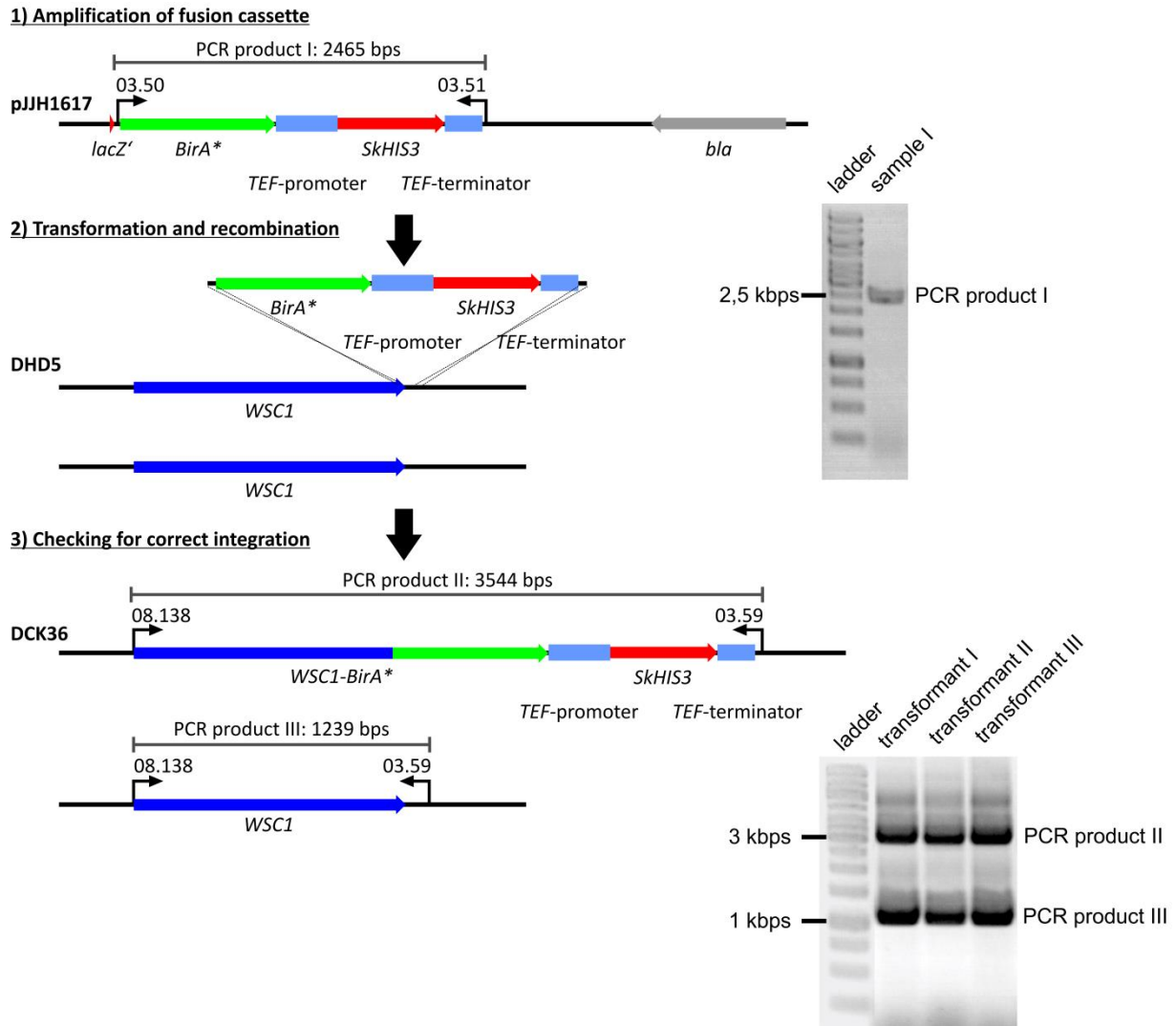


Figure 2.1: Schematic representation of the DCK36 strain construction using homologous recombination. **1)** For the fusion of *BirA**-*SkHIS3* to *WSC1* the cassette was amplified from the vector pJH1617 using the primers 03.50 (SLG1gfp5') and 03.51 (SLG1gfp3'). Besides the binding sequence for the template vector, these oligonucleotides had 45 base pairs for specific target integration attached at their 5'-ends which then produced a PCR product of the integration cassette flanked by homologous sequences to the 3'-end of the *WSC1* gene. The expected PCR product ("PCR product I") had a size of 2465 base pairs which matched with the size observed in the agarose gel electrophoresis. **2)** The PCR product was then introduced into the diploid wild-type strain DHD5 as a recipient for homologous recombination. **3)** Correct integration was checked by PCR in three transformants (I-III) with the flanking primers 08.138 (*WSC1*-ATGvor) and 03.59 (SLG1rein3') which would produce a PCR product of 3544 base pairs in case of successful integration (PCR product II) or 1239 base pairs (PCR product III) for the wild-type locus. The PCR produced both bands in all samples, confirming that only one of the two *WSC1* alleles in the diploid strain had the PCR product inserted, while the other remained wild-type. The heterozygous strain was named DCK36, sporulated and subjected to tetrad analysis to yield the haploid segregants HCK36-1B and HCK36-9B.

suspension were streaked onto a YEPD plate and tetrads were dissected by micromanipulation. Plates were then incubated at 25-30 °C for 2-3 days, a masterplate with the segregants was prepared on YEPD and again incubated for 1 day at 30 °C. For assessment of auxotrophic markers and resistances, this masterplate was replica-plated onto the respective selective media. To determine the mating type of the segregants, the yeast strains LD3R-7B and SMC-19A were spread in a lawn on plates with synthetic minimal medium (SMD) and the masterplate was replica-plated onto each. Plates were incubated for 2 days at 30 °C and checked for complementation. The common intermediate step of crossing the segregants with the tester strains on YEPD plates overnight followed by replica-plating onto selective medium was omitted.

2.2.2.4 Analyses of growth and sensitivities towards stress agents

To analyze and compare the growth and sensitivities of different yeast strains, serial drop dilution assays were performed. The plates for such assays were prepared fresh by mixing the different stress reagents in suitable concentrations 1:1 (v/v) with double-concentrated SCD selection medium. A fresh overnight culture was used to inoculate selective growth medium at an OD_{600} of 0.25 and incubated with shaking at 25 or 30 °C. After reaching an OD_{600} of 1.0, 2×10^7 cells (i.e. 1 ml of each culture) were harvested by centrifugation at 3000 rpm for 2 min. The pellet was resuspended in 100 μ l of sterile water and transferred to a 96 well plate. From this stock, consecutive 1:10 dilution steps were prepared in sterile water and 3 μ l of each dilution were dropped onto the different media. Plates were then incubated for 2-3 days at the indicated temperatures. For documentation, plates were scanned and edited using the "Photo Paint X5" program (Corel GmbH, Munich, Germany). In order to maintain comparability, adjustments of brightness and other parameters were always applied to the entire plate, but never on individual rows or spots.

2.2.3 DNA analysis

2.2.3.1 Genomic DNA extraction from *S. cerevisiae* by microwave treatment

Genomic DNA for PCR was obtained by dissolving cells from a yeast colony in 50 μ l of 20 mM NaOH in sterile Eppendorf cups. The suspension was incubated for 5 min at room temperature and then boiled for 1 min in the microwave. After 5 min of incubation at room temperature, cell debris was pelleted at 3000 rpm for 1 min and 5 μ l of the supernatant were used as a PCR template.

2.2.3.2 Genomic DNA preparation from *S. cerevisiae* (phenol chloroform)

A yeast colony was dissolved in 100 μ l extraction buffer (50 mM NaCl, 1 mM ethylenediamine tetraacetic acid [EDTA], 10 mM Tris-HCl pH 8.0, 0.5% Triton X-100) and incubated on ice for 5 min. 100 μ l of glass beads with a diameter of 0.25-0.5 mm and 100 μ l of a phenol-chloroform mixture were added and the sample was vigorously shaken for 10 min at 4°C. After centrifugation for 10 min at 14000 rpm and 4 °C 10 μ l of the aqueous upper phase were transferred to a new Eppendorf cup and 100 μ l of sterile water were added. 5 μ l of this solution were used as PCR template.

2.2.3.3 Polymerase chain reaction (PCR)

Polymerase chain reactions (PCR) were used for the amplification of desired DNA fragments. For control PCRs (e.g. for verification of genomic DNA insertions) the “DreamTaq DNA Polymerase” preparation was used according to the manufacturer’s instructions. Oligonucleotides (“primers”) were used at a final concentration of 0.4 pmol/ μ l each, in a reaction buffer containing 0.2 mM of a mixture of the four deoxy nucleoside triphosphates (dNTPs). 5 μ l of the DNA from either of the preparations described above were added as template.

For PCRs on templates requiring a decreased error rate, the “Phusion High-Fidelity DNA Polymerase” was employed. In a final volume of 100 μ l, enzyme mix and buffer were added according to the manufacturer’s instructions. Oligonucleotides and dNTPs were used in concentrations as above. 3 μ l dimethyl sulfoxide (DMSO) was added when primers were longer than 20 nucleotides. 5 μ l of genomic DNA preparation or 0.5 μ l of plasmid DNA were

added as template. Reactions mixtures and PCR programs for both polymerases are listed in Table 2.9 and Table 2.10.

Table 2.9: Conditions for PCR reactions using “DreamTaq”-Polymerase

Reaction mixture		PCR program		
Ingrident	Volume	Step	Temperature	Time
template DNA	5 µl	Initial denaturation	95 °C	5 min
forward primer	2 µl	denaturation	95 °C	45 sec
reverse primer	2 µl	annealing	52-58 °C	30 sec
polymerase buffer	5 µl	elongation	72 °C	1 min / 1 KBps
dNTPs	5 µl	(repeat for 35 cycles)		
Polymerase	0.5 µl	final elongation	72 °C	15 min
H ₂ O	30.5 µl		18 °C	pause
<hr/>				
	50 µL			

Table 2.10: Conditions for PCR reactions using “Phusion HiFi”-Polymerase..

Reaction mixture		PCR program		
Ingrident	Volume	Step	Temperature	Time
template DNA	5 µl gen. DNA or 0.5 µl plasmid	Initial denaturation	98 °C	3 min
forward primer	3 µl	denaturation	98 °C	30 sec
reverse primer	3 µl	annealing	52-58 °C	30 sec
polymerase buffer	20 µl	elongation	72 °C	30 sec / 1 KBps
dNTPs	10 µl	(repeat for 35 cycles)		
DMSO	3 µl	final elongation	72 °C	8 min
Polymerase	1 µl		18 °C	pause
H ₂ O	55 / 59.5 µl			
<hr/>				
	100 µL			

2.2.3.4 Separation of DNA fragments by agarose gel electrophoresis

DNA fragments were separated by agarose gel electrophoresis using a concentration of 1 % agarose in TAE buffer (20 mM acetic acid, 1 mM EDTA, 40 mM Tris-HCl, pH 8.3). 6x DNA loading dye was added to samples from PCR reactions and 10x FastDigest Green Buffer was

used for restriction fragments. Size standards have been described above (2.1.6).

The gels submerged in TAE buffer and 90 V were applied for separation of DNA fragments for 45-55 minutes. DNA was visualized by incubation for 15-20 minutes in a ethidium bromide solution (3.33 µg/ml) and inspected and documented after UV-light excitation ($\lambda = 366 \text{ nm}$).

2.2.3.5 Purification of PCR products

PCR products were purified using the “GeneJET PCR Purification Kit” (Thermo Scientific, Waltham, Massachusetts, USA) according to the protocol provided by the manufacturer.

2.2.3.6 Isolation of DNA fragments from agarose gels

To isolate DNA fragments from agarose gels, gels were stained for 15-20 minutes with ethidium bromide as described above and desired bands were cut out after UV-excitation at 302 nm. Gel slices were placed in a sterile Eppendorf cup and suspended in 300 µl binding buffer from the “GeneJET PCR Purification Kit” by incubation for 5 min at 56 °C. After addition of 100 µl 2-propanol the sample was applied to a purification column, washed and eluted according to the manufacturer’s protocol.

2.2.3.7 Restriction and ligation of DNA

Double-stranded DNA was digested with restriction endonucleases and fragments were joined using T4 DNA ligase according to the instructions of the manufacturer.

2.2.3.8 Purification of plasmid DNA

Plasmid was prepared from *E. coli* transformants using 5 ml of fresh overnight cultures in LB medium selecting for the respective antibiotic resistance. Cells were collected by centrifugation at 8000 rpm for 3 minutes plasmids were isolated and purified using the “GeneJET Plasmid Miniprep Kit” (according to the manufacturer’s instructions). To screen larger numbers of *E. coli* transformants, an alternative method was used: For this, used columns from the “GeneJET Plasmid Miniprep Kit” were regenerated using the “maxXbond MB007” DNA binding column regeneration kit according to the manufacturer’s instructions. The plasmid preparation was then done with 5 ml of a fresh over night *E. coli* culture according to the protocol of the “GeneJET Plasmid Miniprep Kit” with the following

self-made buffers: Resuspension buffer (50 mM Tris-HCl, 10 mM EDTA, pH 8), lysis buffer (200 mM NaOH, 1 % SDS), neutralization buffer (4 M guanidine hydrochloride, 0.5 M potassium acetate, pH 4.2) and washing buffer (20 mM NaCl, 2 mM Tris-HCl, 70 % ethanol). The elution was done in 50 μ l H₂O.

2.2.3.9 Plasmid preparation from *S. cerevisiae*

For preparation of plasmids from *S. cerevisiae* a fresh over night culture was grown in 5 ml SCD selection medium and centrifuged at 3000 rpm for 3 min. The cells were resuspended in 250 μ l “Resuspension solution” from the “GeneJET Plasmid Miniprep Kit” (Thermo Scientific, Waltham, Massachusetts, USA). 100 μ l glass beads were added and the sample was shaken for 20 min on a “Vibrax VXR basic” at 4 °C. After that, 250 μ l of “Lysis solution” was added and the plasmid preparation was done according to the manufacturer’s instructions from the “GeneJET Plasmid Miniprep Kit” and the plasmid was eluted in 30 μ l water.

2.2.3.10 DNA sequencing

Custom DNA sequencing on plasmids was performed by GATC Biotech AG (Konstanz, Germany), with mixtures of DNA and primers prepared according to the supplier’s instructions for the “LightRun” program. Sequences were then analyzed using “Clone Manager Professional 9” (Scientific & Educational Software, Morrisville, North Carolina, USA).

2.2.3.11 Gene synthesis

Gene constructs that were synthesized were ordered from GeneArt™ Gene synthesis (ThermoFisher Scientific, Waltham, Massachusetts, USA) as “Strings DNA Fragments and Libraries” synthesis.

2.2.4 Protein analysis

2.2.4.1 Preparation of extracts for immunodetection (“Roedel”)

Cultures were grown in selective SCD media or YEPD rich media over night and inoculated to an OD₆₀₀ of 0.05 and grown approximately 0.5. Cells were then transferred to YEPD with an OD of approximately 0.002 and harvested after reaching an OD₆₀₀ of 1.0. For this, a sample containing 2×10^7 cells (1 ml) from this culture was centrifuged at 8000 rpm for 3 min and 4

°C, the supernatant was discarded and the pellet frozen in liquid nitrogen. Cell wall stress was applied for 40 min to the remaining culture by addition of 50 ng/ml Caspofungin after which another sample of 2×10^7 cells were collected and treated as above. The frozen cells were resuspended in 500 μ l freshly prepared "Roedel mixture" (0,25 N NaOH, 100 mM PMSF, 1x Roche Complete Protease Inhibitor mix, 100 mM sodium orthovanadate, 1 % β -mercaptoethanol, 1x phosphatase inhibitor mixture (4 mM sodium fluoride [NaF], 4 mM sodium azide [NaN₃], 4 mM p-nitrophenylphosphate, 4 mM sodium pyrophosphate, 4 mM β -glycerophosphate)), stored on ice for 10 min, and 100 μ l 78 % trichloroacetic acid were added. After centrifugation (14000 rpm, 10 min, 4 °C) the supernatant was completely removed and the pellet was suspended in 1 ml of cold acetone and again centrifuged. The pellet was dried for 1 min at 55 °C and suspended in 40 μ l SDS-gel loading buffer (100 mM Tris-HCl pH 6.8, 0.2 % bromophenol blue, 20 % glycerine, 4 % SDS, 100 mM freshly added dithiothreitol). The samples were heated to 99 °C for 5 min and employed for SDS-PAGE

2.2.4.2 Protein separation by SDS polyacrylamide gel electrophoresis (SDS-PAGE)

Proteins were separated by sodium dodecyl sulfate (SDS) polyacrylamide gel electrophoresis (PAGE). Gels were prepared with a stacking phase and a resolving phase, containing 1.8 % or 10 % of an acrylamide-bisacrylamide solution (Rotiphorese Gel 30, Carl Roth GmbH + Co. KG, Karlsruhe, Germany), respectively. The stacking gel was prepared in 4x collection gel buffer (CGB: 0.5 M Tris-HCl pH 8.8, 8 mM EDTA, 0.4 % SDS), the resolving gel in 4x separation gel buffer (SGB: 0.5 M Tris-HCl pH 6.8, 8 mM EDTA, 0.4 % SDS). Ammonium persulfate (APS) and tetramethylethylenediamine (TEMED) were added to induce polymerization. Detailed informations on the gel composition are summarized in Table 2.11.

Electrophoresis was performed using SDS running buffer (192 mM Glycine, 35 mM SDS, 250 mM Tris, pH 8) and 3 μ l of the "PageRuler Plus Prestained Protein Ladder" as a molecular weight marker. For passage of samples through the stacking gel 90 V were applied and then increased to 120 V for separation.

Table 2.11: Preparation of SDS-PAGE gels

Chemical	1.8 % stacking gel	10 % resolving gel
Rotiphorese Gel 30 (30% acrylamide-bisacrylamide solution)	3 ml	6,6 ml
4x gel buffer	3 ml (CGB)	5 ml (SGB)
H ₂ O	7 ml	8,4 ml
TEMED	15 µl	10 µl
10 % APS	150 µl	200 µl

2.2.4.3 Western Blot analysis

Proteins separated by SDS-PAGE were transferred to a nitrocellulose membrane and detected by antibodies using the Western blot procedure. For protein transfer “Gel-Blotting-Papiere 3 MM” (Whatman, GE Healthcare, Freiburg, Germany) papers, the “PROTRAN Nitrocellulose Transfer Membrane” (Whatman, A. Hartenstein, Würzburg, Germany) and the SDS gel were equilibrated in blotting buffer (192 mM Glycine, 20 % (v/v) methanol, 29 mM Tris/HCl) for 30 minutes. The blotting was done using the “semi-dry” method at 20 V for 60 minutes.

After completion of the transfer, the membrane was washed for 5 min in TBST buffer (150 mM NaCl, 0.05 % (v/v) Tween 20, 50 mM Tris, pH 8.0) and blocked with TBST containing 5 % milk powder (Carl Roth GmbH + Co. KG, Karlsruhe, Germany) for 1 hour at room temperature. For detection of dually phosphorylated Slt2/Mpk1 membranes were washed with TBST buffer and incubated over night at 4 °C with a rabbit p42/44-specific antiserum diluted 1:100 in TBST containing 1 % milk powder. This was followed by 5 washing steps for 5 min with TBST and a subsequent incubation with the donkey rabbit-IgG-specific IRDye700 secondary antibody diluted 1:5000 in TBST containing 1 % milk powder. After 3-5 washing steps with TBST, the membrane was incubated with a goat Slt2-specific antiserum in a 1:8000 dilution and a donkey goat-IgG-specific IRDye800 in a 1:5000 dilution, following the procedures described above for the phosphospecific primary and secondary antisera. The signal was detected using an Odyssey infrared imaging system. The Slt2 phosphorylation signal was quantified using the Odyssey application software version 3.0.30 and normalized to the signal corresponding to total Slt2. The average of three independent Western blot quantifications was determined

2.2.4.4 Preparation of crude extracts for the biotinylation interaction assay (Roux *et al.*, 2012)

The biotinylation assay as described in Roux *et al.*, 2012 (“BioID”) was used to identify potential protein-protein interaction partners. *In vivo*, a mutated version of the *E. coli* biotinylation BirA biotinylates proteins in close proximity to the tagged bait protein, which can then be purified using the affinity of the biotin-tag towards streptavidin beads.

For this, the strain expressing Wsc1 tagged with BirA* was grown over night in YEPD medium supplemented with 50 μ M biotin and used to inoculate 500 ml of fresh medium containing 10 ng/ml Caspofungin to induce cell wall stress at an OD₆₀₀ of 0.2. The culture was grown to an OD₆₀₀ of 1-2 and centrifuged at 3000 rpm for 3 min. The cells were then washed with 10 ml of water and again with 10 ml PBST (137 mM NaCl, 2.7 mM KCl, 10 mM Na₂HPO₄, 2 mM KH₂PO₄, 0.05 % Tween 20, pH 7.4). After suspension in 3 ml PBST and samples were equally divided into two reaction tubes. To break the cells, 100 μ l of glass beads were added and tubes were shaken vigorously for 30-45 min on a “Vibrax VXR basic” shaker at 4°C. Cell debris was removed by centrifugation at 13000 rpm for 10 min at 4 °C and the supernatant was kept at -20 °C until further use

2.2.4.5 Purification of biotin-tagged proteins

To purify biotinylated proteins from crude extracts the μ MACS Streptavidin Kit was used. 100 μ l of μ MACS streptavidin beads were added to 3 ml of crude extract and incubated for 3-5 min. A column was placed in a magnetic separator and rinsed with 100 μ l protein equilibration buffer and 2x100 μ l PBST. The mixture of crude extract and streptavidin beads was applied to this column and the flow-through was collected and applied again to the column. During washing for 5-6 times with 100 μ l PBST, each, fractions were separately collected in sterile Eppendorf cups. To elute bound proteins from the streptavidin beads, the column was removed from the magnetic separator and placed over a plasticiser-free reaction cup, and 100 μ l PBST was added to eluate the sample. Afterwards 10 μ l PBST was added gradually until the brown eluate became clear. After that a second elution fraction was collected in an additional cup with 100 μ l PBST.

10 μ l of each fraction was mixed with 10 μ l gel loading buffer and applied to SDS-PAGE as

described in 2.2.4.2. The gel was then stained with Coomassie blue (0.1 % Serva Blue [w/v] (Serva, Heidelberg, Germany), 10 % acetic acid [v/v], 25 % methanol [v/v]) for 15 seconds in the microwave followed by 5 min on a rocking shaker and washed with water. The gel was then destained for 15 seconds in the microwave followed by 5 min on a rocking shaker with destaining solution (20 % methanol [v/v], 10 % acetic acid [v/v]).

2.2.4.6 Determination of protein concentrations

The “Bradford method” was used to determine the protein concentration in crude extracts. 1 µl of sample was mixed with 799 µl sterile water and 200 µl Bradford reagent (Bio-Rad, Hercules, California, USA) and incubated for 20 min at room temperature. The extinction of the sample was measured at 595 nm and the extinction of a control sample not containing any protein was subtracted. Protein concentration was then calculated using the formula

$$\text{protein concentration} \left[\frac{\text{mg}}{\text{ml}} \right] = \text{extinction}_{595} \times \text{Bradford factor}$$

The Bradford factor was determined by a bovine serum albumin (BSA) calibration curve to be 19.04.

2.2.4.7 Mass spectrometry

Mass spectrometry was used to identify proteins purified from the “BioID” assay. The purified proteins bound to the magnetic beads were harvested (centrifugation for 20 min, 13000 rpm, 4°C), the supernatant was discarded and the beads were resuspended in 100 µl reducing solution (10 mM DTT, 100 mM NH₄HCO₃). The suspension was incubated at 25 °C for 5 min followed by 50 °C for 30 min. The beads were then harvested, suspended in 250 µl acetonitrile and incubated for 15 min at room temperature. Beads were pelleted, after discarding the supernatant suspended in 100 µl alkylating solution (54 mM iodoacetamide, 100 mM NH₄HCO₃) and incubated for 15 min at room temperature in the dark. Beads were again harvested and suspended in 250 µl destaining solution (30 % acetonitrile, 100 mM NH₄HCO₃). After shaking for 10 min at room temperature the beads were harvested and suspended in 250 µl acetonitrile for 15 min with agitation at room temperature. After another harvesting step and suspension in 20 µl trypsin digestion solution (0.01 mg/ml TPCK-

trypsin, 5 % acetonitrile, 50 mM NH_4HCO_3 , 1 mM HCl, pH 8.5), they were incubated at 15-37°C for a minimum of 15 hours, after which 10 μl were transferred to a HPLC vial. The digested peptides were separated by high performance liquid chromatography (HPLC) and detected by the mass spectrometry using the ESI-ETD ion trap method. The peptides were then identified by a search employing the MASCOT algorithm. The protein list from the MASCOT search was compared to a control sample prepared from a yeast strain not carrying the biotinylation tag and proteins appearing in both samples were discarded, leaving a list of potential interaction partners.

2.2.5 Life cell fluorescence microscopy

2.2.5.1 Microscope setups

Two different setups were used for different life cell fluorescence microscopy applications. The first consisted of a Zeiss Axio Imager Z1 with a 100x/1.45 NA Oil DIC objective (Carl Zeiss AG, Oberkochen, Germany) and filter sets obtained by Chroma. A SPECTRA light engine provided by Lumencor was used for fluorescence excitation light and a Photometrics CoolSNAP HQ or a Hamamatsu ORCA-Flash4.0 LT was used for image acquisition. Metamorph 7.8.8.0 (Molecular Devices, Sunnyvale, California, USA) was used as acquisition software for the microscope.

The second setup was a DeltaVision Elite microscope from Applied Precision, Issaquah, WA with a sCMOS camera (PCO, Kelheim, Germany). SoftWoRx v6 (GE Healthcare, Freiburg, Germany) and higher versions with integrated Resolve3D were used for image acquisition.

2.2.5.2 Fluorescence microscopy

For life cell fluorescence microscopy, cells were inoculated in selective synthetic complete (SC) medium to an OD_{600} of 0.1 and grown to early logarithmic phase. Cells were then harvested by centrifugation at 3000 rpm for 2 min and applied to microscope slides. Axio Imager Z1 bright field and fluorescence images were acquired as single planes using differential-interference-contrast (DIC) and appropriate fluorescence filters. Images were deconvoluted using Huygens Essential with compute engine 3.7.0p3 64b. On the DeltaVision Elite, bright field images were acquired as single planes using polarized light microscopy

(POL) and fluorescence images were acquired as z-series with 200 nm intervals using dichroic filter sets. For the deconvolution of the images the integrated softWoRx software was used. Image processing, scaling and overlays for colocalization were done using ImageJ 1.47i and Metamorph 7.8.8.0 (Molecular Devices, Sunnyvale, California, USA).

2.2.5.3 Bimolecular fluorescence complementation (BiFC)

The bimolecular fluorescence complementation (BiFC), also known as “SplitYFP” (Hu *et al.*, 2002) was used to study spatio-temporal protein-protein interactions in life cells. Neither the C-terminal nor the N-terminal fragments of the Venus fluorophore are able to emit fluorescence autonomously. However, if these fragments are fused to proteins which come into close proximity of each other, Venus can be reconstituted (“complemented”) to form a functional fluorophore.

Different BiFC constructs were obtained on centromeric vectors in this work and co-expressed in yeast cells to determine the interaction of the encoded fusion proteins. For this, cells were then grown in double-selective media as described in 2.2.5.2 and imaged using a YFP filter.

2.2.5.4 Quantification of colocalization

For the quantification of colocalization events in the yeast plasma membrane a “count and colocalize” ImageJ plugin provided by Arlt *et al.*, 2015 was used on deconvolved images obtained with the DeltaVison Elite setup with 60x magnification. Single channel z-series of half cells and a bright field reference image were applied to the ImageJ plugin with a “Huang” thresholding method for cell segmentation. “MaxEntropy” for endosome detection and “consider vacuoles” were applied to distinguish organellar structures from membrane microcompartments. The data sets of at least 30 cells were collected and the median and standard errors for the percentage of colocalization, as well as the Pearson’s correlation coefficient and the Mander’s overlap coefficient were calculated.

2.2.5.5 Integrated morphometrics analysis

The MetaMorph Software version 7.8.0.0 (Molecular Devices, Sunnyvale, California, USA) was used for the calculation of the area parameters of fluorescent membrane patches. Maximal projections of the three top plains of z-series were set with an exclusive threshold of 1000 and the software function “Integrated morphometrics analysis” was used to calculate the area (total pixels of the object), average intensity, perimeter, shape factor (as a degree of circular shape) and length (longest possible diameter) and breadth (widest possible distance orthogonally to the length) of the patches. The arithmetic means were calculated for all spots of at least 30 cells, each.

3. Results

3.1 Effects of a quintuple CWI sensor gene deletion

There are five cell wall integrity sensors which contribute to cell wall integrity signaling in *S. cerevisiae*. Among these, *Wsc1* and *Mid2* are probably the most important ones, since deletions in their encoding genes show the most severe cell wall related phenotypes (Rajavel *et al.*, 1999). Deletions in the other three sensor genes *WSC2*, *WSC3* and *MTL1* show less severe or almost no cell wall related phenotypes so that they are thought to act as backup sensors or have different, yet undiscovered functions. To gain insight into their implication in cell wall integrity signaling, complementation analysis of single sensor genes in a quintuple deletion was investigated.

3.1.2 *Wsc1* and *Mid2* can rescue cell death in a strain lacking all five sensors

A quintuple deletion of all five CWI sensor genes is lethal and therefore cells can neither be grown nor transformed for further investigations (Jürgen Heinisch, personal communication). To overcome this problem, the strain HOD188-7D (*MAT α wsc1::KIURA3 wsc3::kanMX mtl1::SkHIS3 KIURA3-GAL1p::WSC2 KIURA3-GAL1p::MID2*) was used for complementation analyses. In this strain, *WSC2* and *MID2* are controlled by the conditional *GAL1/10* promotor so that they are expressed in high amounts when grown on galactose media. This way, the cells are viable, even though *WSC1*, *WSC3* and *MID2* are deleted. When grown on glucose media, *WSC2* and *MID2* are not expressed and the cells are inviable, thus mimicking a quintuple deletion strain.

Single sensor genes expressed from episomal multicopy plasmids were introduced into the conditional quintuple deletion strain and tested for complementation on glucose and galactose media at 30 °C, 30 °C with 1 M sorbitol for osmotic stabilization and at 37 °C for heat stress by a serial drop dilution assay and compared to a wild-type and the conditional deletion strain (Figure 3.1). On galactose media all strains grew at the three different conditions. The strain with *MTL1* showed a slight growth decrease on 30 °C while all conditional quintuple deletions except for the strain with the *WSC3* plasmid showed slightly decreased growth at 37 °C. The conditional strain expressing *WSC2* and *MID2* showed strong

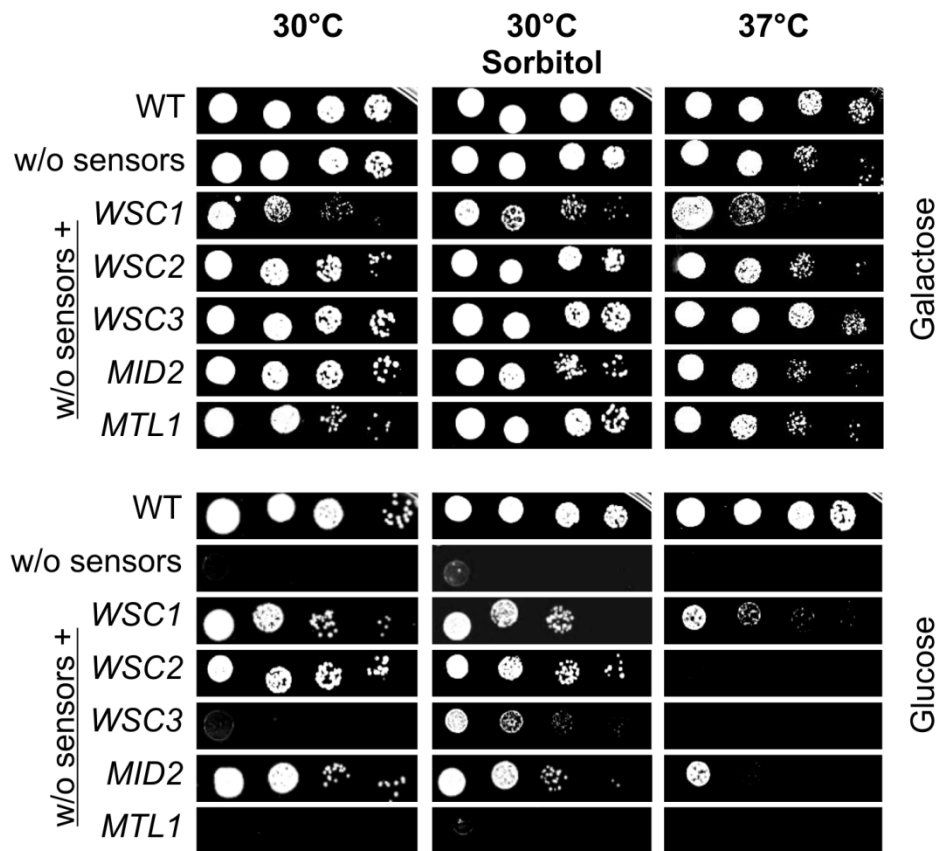


Figure 3.1: Complementation analysis of single CWI sensors in a quintuple sensor gene deletion.

The conditional quintuple deletion strain HOD188-7D (*MAT α wsc1::KIURA3 wsc3::kanMX mtl1::SKHIS3 KIURA3-GAL1p::WSC2 KIURA3-GAL1p::MID2* = “w/o sensors”) was transformed with episomal multicopy plasmids carrying single sensor genes and the empty plasmid, respectively, and growth on glucose and galactose media was compared by serial drop dilution assays at 30 °C, 30 °C with osmotic stabilization (1 M Sorbitol) and 37 °C. Note that *WSC2* and *MID2* are expressed on galactose medium in this strain while the cells do not grow on glucose media. WT: HOD134-1C + YEplac181, w/o sensors: HOD188-7D + YEplac181, *WSC1*: HOD188-7D + Yep352-Wsc1, *WSC2*: HOD188-7D + pOCK019, *WSC3*: HOD188-7D + pOCK018, *MID2*: HOD188-7D + YEP352-Mid2, *MTL1*: HOD188-7D + pOCK020.

decrease in growth at all conditions when *Wsc1* was expressed additionally. On glucose media, the conditional quintuple mutant did not grow because *WSC2* and *MID2* are not expressed, indicating that a strain lacking the five CWI sensors is not viable. Strains only expressing *WSC1*, *WSC2* and *MID2* grew normal at 30 °C and 30 °C with osmotic stabilization. *WSC3* expressing cells did not grow at 30 °C but were able to grow with osmotic stabilization, while cells expressing *MTL1* were not able to grow at all on these plates. At 37 °C, only cells

with *WSC1* and *MID2* were able to grow, although strongly decreased in comparison to wild-type cells while cells with *WSC2*, *WSC3* and *MTL1* failed to grow under these conditions. Overall, expression of *WSC1* from multi-copy vectors in a strain, that already overexpresses *WSC2* and *MID2* seems to have harmful effects on the cell while in general *WSC1* and *MID2*, also partially *WSC2* can function as the only cell wall integrity sensor.

3.2 Distribution of cell wall integrity sensors in plasma membrane domains

The formation of plasma membrane domains has been extensively studied in the last years and various cellular functions for different domains have been discussed. Several distinct plasma membrane domains have been observed in *S. cerevisiae* and as the cell wall integrity sensors are plasma membrane proteins, their distribution in these plasma membrane domains was investigated here. The results of this chapter are soon to be published in Kock *et al.*, 2016 (revision submitted).

3.2.1 Wsc1 and Mid2 reside in different plasma membrane domains

Different functions for the five cell wall integrity sensors have been proposed and different localization patterns have been shown at least for Wsc1 and Mid2. Wsc1 has been shown to localize at sites of polarized growth like the bud-neck and in punctate clusters in the plasma membrane, whereas Mid2 distributes more evenly and in an unpolarized pattern in the plasma membrane (Straede and Heinisch, 2007). Here, colocalization studies of both sensors were performed to show whether these different patterns in the plasma membrane overlap or are distinct from each other. For this, both sensors were C-terminally fused to the tetrameric fluorophore tdTomato at its native chromosomal locus to create the strains HCK27-2C (*MATa WSC1-tdTomato-SkHIS3*) and HCK28-3A (*MATa MID2-tdTomato-SkHIS3*). HCK28-3A was then crossed with HAS35-13D to get a strain coexpressing *WSC1-GFP* and *MID2-tdTomato* (HCK39-2C). This strain was used for colocalization analysis and the top section of these cells revealed that Mid2 does not distribute homogeneously in the plasma membrane, but in patchy or network-like patterns. In addition, the Wsc1 spots mostly seemed to localize in the gaps between the Mid2 network (Figure 3.2 A). The colocalization was quantified by using a “count & colocalize” software which revealed that in a total of 116 cells approximately $8.01 \pm 8.22\%$ of the Wsc1 and Mid2 patches showed at least 50% overlap. The Pearson’s correlation coefficient (PCC) as a degree for the colocalization was 0.06 ± 0.06 , indicating a very small amount of overlap between the colocalized spots. These results suggest that Wsc1 and Mid2 do not share a plasma membrane domain.

Wsc2 shows a similar localization pattern as Wsc1 and has been shown to interact with Wsc1

at sites of polarized growth, but interaction in the lateral membrane was not observed (Wittland, 2012). To investigate whether heterologous clusters in the lateral membrane occur and if Wsc1 and Wsc2 patches therefore share a plasma membrane domain, colocalization analysis of these two sensors was done. HCK27-2C (*MAT α WSC1-tdTomato-SkHIS3*) was crossed with HSK69-1B (*MAT α WSC2-EGFP-kanMX*) and subjected to tetrad analysis to get a haploid strain with both fluorophore fusions (HCK56-4A). The images revealed moderate overlap of some clusters (Figure 3.2 A) with $13.33 \pm 11.4\%$ colocalized spots and a PCC of 0.22 ± 0.12 in a total number of 130 cells.

3.2.2 The transmembrane domains of Wsc1 and Mid2 do not determine their plasma membrane domain distribution

Wsc1 and Mid2 thus show different localization patterns in the plasma membrane which do not overlap. Spira *et al.*, 2012 showed that the Mid2 transmembrane domain (TMD) distributes in a network-like pattern and therefore proposed that TMDs can determine plasma membrane domain patterns. To test if this is also the case for full-length sensors, the predicted TMDs of Wsc1 and Mid2 were exchanged here and the localization of these hybrid sensors was investigated. For this, the sequence encoding the transmembrane domain (Wsc1: amino acids 265-285, IVGGVGGVVGAVAIALCILL and Mid2: amino acids 225-246, IVIGCVGIGVPLILVILALI) was deleted in the two sensor genes by inverse PCR and the sequence encoding for the TMD of the other sensor was integrated by homologous recombination, resulting in the centromere vectors pOCK014 (*WSC1_{TMD-MID2}*) and pOCK015 (*MID2_{TMD-WSC1}*). These hybrid sensors were C-terminally tagged with GFP (*WSC1_{TMD-MID2}-GFP-SkHIS3*, pOCK016 and *MID2_{TMD-WSC1}-GFP-SkHIS3*, pOCK017) and introduced into the MID2-tdTomato strain HCK28-3A. Life cell fluorescence microscopy revealed that *Wsc1_{TMD-MID2}* hybrid sensors still localized in patches that did not colocalize with the Mid2-tdTomato network and *Mid2_{TMD-WSC1}* hybrid sensors still showed a more network-like distribution that colocalized with the Mid2-tdTomato network (Figure 3.2 B). In addition, the localization of the sensors at sites of polarized growth was investigated. *Wsc1_{TMD-MID2}-GFP* localized at the bud neck similar to *Wsc1-GFP* (HAS35-13D, Figure 3.2 C) while *Mid2_{TMD-WSC1}-GFP* did not show a polarized localization and distributed all over the plasma membrane like *Mid2-GFP*

(HSK28, Figure 3.2 C). Overall, the transmembrane domains of Wsc1 and Mid2 did not determine the polarized and plasma membrane domain distribution of the sensors.

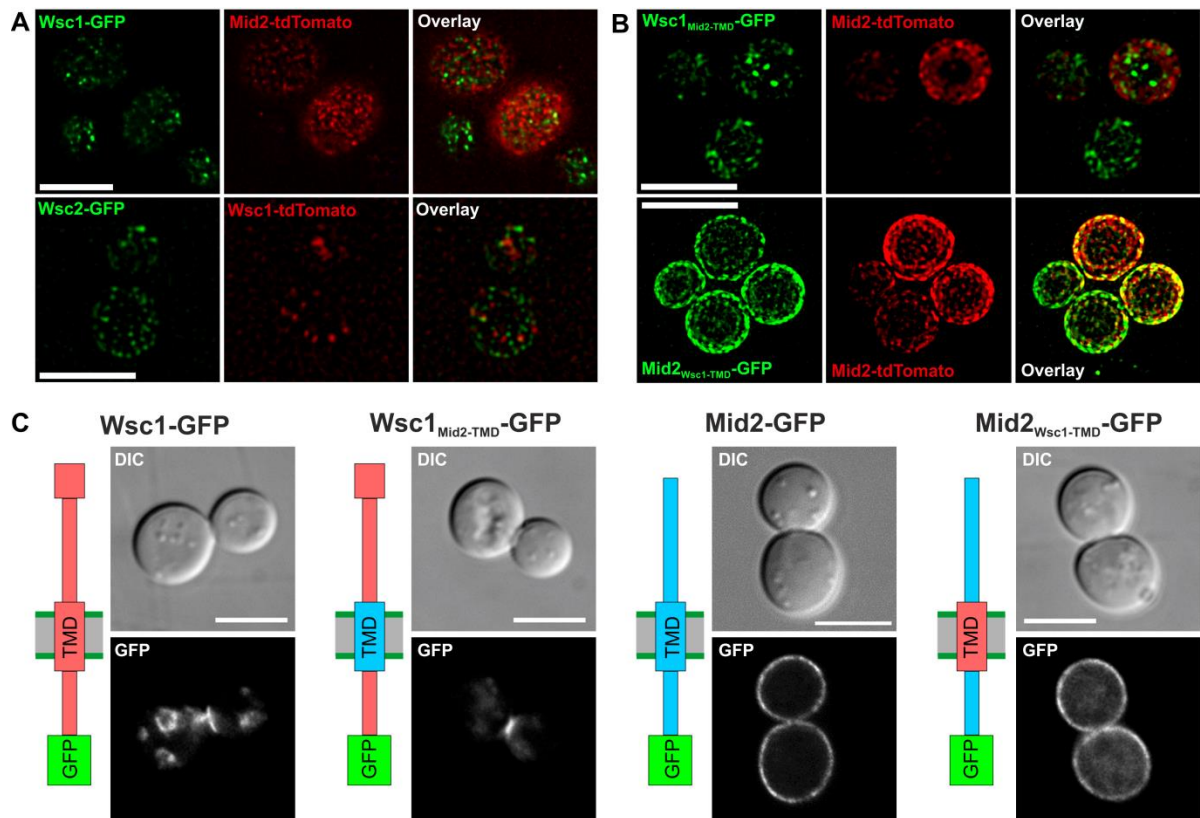


Figure 3.2: The CWI sensors Wsc1 and Mid2 reside in different plasma membrane domains (from: Kock *et al.*, 2016 (revision submitted)). Life cell fluorescence microscopy of logarithmically growing cells expressing C-terminally tagged sensors. Scale bars = 5 μ m. **A.** Colocalization analysis of maximal projections of half cells expressing Wsc1-GFP and Mid2-tdTomato (HCK39-2C, upper row) and Wsc2-GFP and Wsc1-tdTomato (HCK56-4A, lower row). The calculated percentage of colocalized spots was $8.01 \pm 8.22\%$ with a Pearson's correlation coefficient (PCC) of 0.06 ± 0.06 for Wsc1 and Mid2 ($n=116$) and $13.33 \pm 11.4\%$ with a PCC of 0.22 ± 0.12 for Wsc2 and Wsc1 ($n=130$). **B.** Colocalization analysis of hybrid sensors *Wsc1*_{TMD-MID2}-GFP (pOCK016) and *MID2*_{TMD-Wsc1}-GFP-SkHIS3 (pOCK017) in a Mid2-tdTomato strain (HCK28-3A) shown by maximal projection of half cells. The transmembrane domains of Wsc1 (amino acids 265-285, IVGGVGGVVGAVAIALCILL) and Mid2 (amino acids 225-246, IVIGCVVIGIVPLILVILALI) were exchanged for each other in these constructs **C.** Comparison of subcellular localization of wild-type and hybrid sensors with switched transmembrane domains (depicted by the coloured TMDs in the schematic representation). Constructs employed were: Wsc1-GFP (HAS35-13D), Wsc1_{Mid2-TMD}-GFP (pOCK016 introduced in HD56-5A), Mid2-GFP (HSK28) and Mid2_{Wsc1-TMD}-GFP (pOCK017 introduced in HD56-5A).

3.2.3 Wsc1 occupies a plasma membrane domain that is distinct from the MCC, MCP and MCT domains.

The data presented above showed that Wsc1 with its spot-like distribution and Mid2 with its network-like distribution have different domain patterns and that both patterns do not overlap. In yeast, different of these plasma membrane distribution patterns and domains have been described: The static punctate MCC domain, the network-like MCP domain and the dynamic spot-like MCT distribution (Malinska, 2004; Berchtold and Walther, 2009). Recently, it was shown that all plasma membrane proteins distribute in patterns varying from sport-like to network-like with different degrees of overlap (Spira *et al.*, 2012).

To investigate whether the Wsc1 and Mid2 pattern that seemed to distribute in similar patterns as the MCC and MCP can be linked to one of these classical domains, colocalization analysis of the cell wall integrity sensors fused to GFP and marker proteins of the MCC, MCP and MCT fused to red fluorophores was performed with a DeltaVision Elite microscope. In addition, the colocalization events were quantified by using a “count & colocalize” software plugin that calculates the percentages of colocalized spots (PCOL) per cell, the Pearson’s correlation (PCC) coefficient and Mander’s overlap coefficient (MOC) as measures for the degree of overlap (Arlt *et al.*, 2015). In principle, the PCOL can vary between 0% and 100%, the PCC between -1 (no colocalization) and 1 (full colocalization) and the MOC between 0 and 1 (Adler and Parmryd, 2010). To gain insight into possible values for this experimental setup, control experiments for spot-like colocalization, network-like colocalization and no colocalization were done (Supplementary Figure 6.1). The MCC/eisosome protein Pil1 was used as a spot-like colocalization control by fusing GFP c-terminally to Pil1 (HCK18-3C) and integrating Pil1-mCherry at the *URA3* locus using pOCK002. The investigation of 184 cells revealed a PCOL of 60 ± 13 % colocalized spots with a PCC of 0.79 ± 0.05 and a MOC of 0.81 ± 0.06 . The plasma membrane proteins Pil1 and Pma1 have been described in the literature to localize in distinct domains, therefore they have been used as control for no colocalization. The strains HCK18-3C (*MATalpha PIL1-GFP-SpHIS5*) and HSK82-1A (*MATa PMA1-dsRed-kanMX*) were crossed and subjected to tetrad analysis to create the strain HCK37-5C (*MATalpha PIL1-GFP-SpHIS5 PMA1-dsRed-kanMX*). 134 cells of this strain were investigated

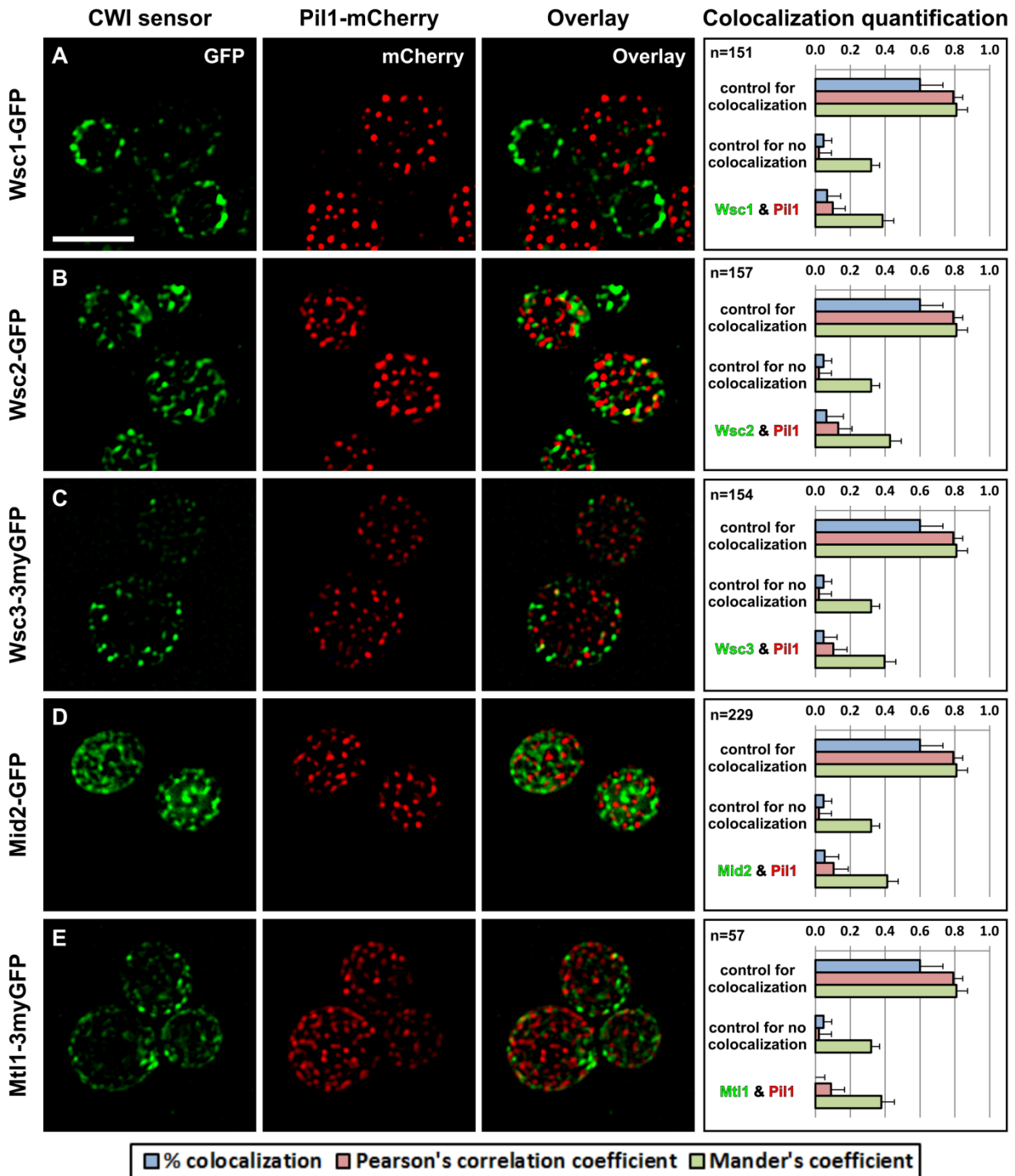


Figure 3.3: Colocalization analysis of CWI sensors with the membrane compartment occupied by Can1 (MCC). Strains with Pil1-mCherry and CWI sensors c-terminally fused to GFP were investigated by life cell epifluorescence microscopy with a DeltaVision Elite microscope and overlays of top-sections were created. The median of the percentage of colocalized spots (% colocalization, PCOL) was then determined by a “count & colocalize” software plugin together with the “Pearson’s correlation coefficient” (PCC) and the “Mander’s overlap coefficient” (MOC) to quantify the colocalization. Colocalization of Pil1-GFP and Pil1-mCherry served as ‘control for colocalization’

events and Pil1-GFP and Pma1-dsRed as ‘control for no-colocalization’ events (see Figure 6.1 for detailed information). The controls are the same in A-E. The scale bar corresponds to a size of 5 μm . **A.** Wsc1-GFP and Pil1-mCherry (HAS35-13D with pOCK002). PCOL= 6.7 ± 7.7 %, PCC= 0.1 ± 0.07 , MOC= 0.39 ± 0.07 . **B.** Wsc2-GFP and Pil1-mCherry (HSK69-1B with pOCK002). PCOL= 6.3 ± 9.8 %, PCC= 0.13 ± 0.08 , MOC= 0.428 ± 0.06 . **C.** Wsc3-3myGFP and Pil1-mCherry (HJW116-B with pOCK002). PCOL= 4.6 ± 7.8 %, PCC= 0.08 ± 0.1 , MOC= 0.39 ± 0.06 . **D.** Mid2-GFP and Pil1-mCherry (HSK28 with pOCK002). PCOL= 5.3 ± 8.1 %, PCC= 0.1 ± 0.08 , MOC= 0.412 ± 0.06 . **E.** Mtl1-3myEGFP and Pil1-mCherry (HCK62-1A with pOCK002). PCOL= 0.0 ± 5.3 %, PCC= 0.09 ± 0.08 , MOC= 0.38 ± 0.08 .

and showed a PCOL of 4.7 ± 4.7 % colocalized spots with a PCC of 0.02 ± 0.07 and a MOC of 0.32 ± 0.05 . Pma1 was used as control for network-like colocalization and the strains HSK82-1A and HSK15-1D (*MATalpha PMA1-GFP-kanMX*) were crossed to create the heterozygous diploid strain DCK40-2. The median of 138 cells revealed 17 ± 12 % colocalized spots with a PCC of 0.25 ± 0.15 and a MOC of 0.56 ± 0.1 . These data were used to compare the data obtained for the colocalization analysis of the CWI sensors with the plasma membrane domain marker proteins and to rank the data as “colocalization” or “no colocalization”.

The eisosome protein Pil1 was used as a marker protein for the membrane compartment occupied by Can1 (MCC). For the colocalization analysis of the CWI sensors with this compartment, Pil1-mCherry in a yeast integrative vector (pOCK002) was used to transform the strains HAS35-13D (*MATalpha WSC1-GFP-kanMX*), HSK69-1B (*MATalpha WSC2-GFP-kanMX*), HJW116-B (*MATalpha WSC3-3myEGFP-SpHIS5*), HSK28 (*MATalpha MID2-GFP-SpHIS5*) and HCK62-1A (*MATalpha MTL1-3myEGFP-SpHIS5*). In 151 cells tested, the Wsc1-GFP clusters and the Pil1-mCherry spots did not overlap. Quantification revealed that 6.7 ± 7.7 % of the spots colocalized and showed a Pearson’s correlation coefficient (PCC) of 0.1 ± 0.07 . The Mander’s overlap coefficient (MOC) was 0.39 ± 0.07 . In comparison to the controls these values indicate that the two proteins do not colocalize (Figure 3.3 A). Wsc2-GFP and Pil1-mCherry showed also no overlap of single spots. In a total number of 157 cells 6.3 ± 9.8 % of spots colocalized with a PCC of 0.13 ± 0.08 and a MOC of 0.428 ± 0.06 (Figure 3.3 B). Wsc3-3myEGFP didn’t show overlap with Pil1-mCherry spots as the PCOL was 4.6 ± 7.8 % with a PCC of 0.08 ± 0.1 and a MOC of 0.39 ± 0.06 . 154 cells were investigated for this analysis (Figure 3.3 C). Mid2-GFP did not show any overlap with Pil1-mCherry either and the quantification results were comparable to the non-colocalization control. The median PCOL

of 229 cells was 5.3 ± 8.1 %, the PCC was 0.1 ± 0.08 and the MOC had a value of 0.412 ± 0.06 (Figure 3.3 D). Similar results were obtained for Mtl1-3myEGFP and Pil1-mCherry, as 0.0 ± 5.3 % colocalization was observed with a PCC of 0.09 ± 0.08 and a MOC of 0.38 ± 0.08 in a total number of 57 cells (Figure 3.3 E).

The distribution of cell wall integrity sensors in the “membrane compartment occupied by Pma1” (MCP) was investigated by colocalization analysis with Pma1-dsRed. The strain HSK83-9D (*MATalpha WSC1-GFP-kanMX PMA1-dsRed-kanMX*) was used for colocalization of Wsc1 and Pma1. The Wsc1 clusters localized in the non-fluorescent area between the Pma1-dsRed network and the calculated percentage of overlapping spots was 0.0 ± 8.6 % in a total of 116 cells. The PCC for this analysis was 0.1 ± 0.07 and the MOC was 0.373 ± 0.09 which in comparison to the controls also indicates no colocalization (Figure 3.4 A). Wsc2-GFP and Pma1-dsRed were expressed in the strain HSK92-8C (*MATa WSC2-GFP-kanMX PMA1-dsRed*) and they showed a moderate amount of overlap. Some of the Wsc2 spots localized in the network of Pma1 and some in the non-fluorescent area in between. This is backed up by the quantification analysis of 125 cells which revealed 13.3 ± 10.3 % colocalization events with a PCC of 0.13 ± 0.1 and a MOC of 0.471 ± 0.07 (Figure 3.4 B). The results for Wsc3-3myEGFP and Pma1-dsRed were comparable to Wsc2. The strain HCK38-4C (*MATalpha WSC3-3myEGFP-SpHIS5 PMA1-dsRed*) was created by crossing of HJW116-B and HSK82-1A and revealed a PCOL of 11.1 ± 9.6 % in a total of 197 cells. The corresponding PCC was 0.1 ± 0.09 and the MOC was 0.44 ± 0.07 , emphasizing a moderate amount of overlap with the MCP domain (Figure 3.4 C). The colocalization between Mid2-GFP and Pma1-dsRed was investigated with the strain HSK76 (*MATalpha MID2-GFP PMA1-DsRed*). The Mid2 and Pma1 network showed a strong amount of overlap with a PCOL of 29.4 ± 10.8 spots in 204 cells, a PCC of 0.46 ± 0.14 and a MOC of 0.66 ± 0.09 (Figure 3.4 D), indicating that Mid2 shows a large overlap with the membrane compartment occupied by Pma1.

Bit61 is part of the TORC2 protein complex and was used as a marker protein for the “Membrane compartment of TORC2” (MCT). For the analysis of Wsc1 and Bit61, the strain HAJ150-A (*MATa BIT61-mCherry-CaURA3*) was crossed with HSK29 (*MATalpha WSC1-GFP-SpHIS5*) and the resulting strain was called HCK49-7C (*MATalpha WSC1-GFP-kanMX BIT61-mCherry-CaURA3*). In a total of 81 cells the overlap of Wsc1-GFP and

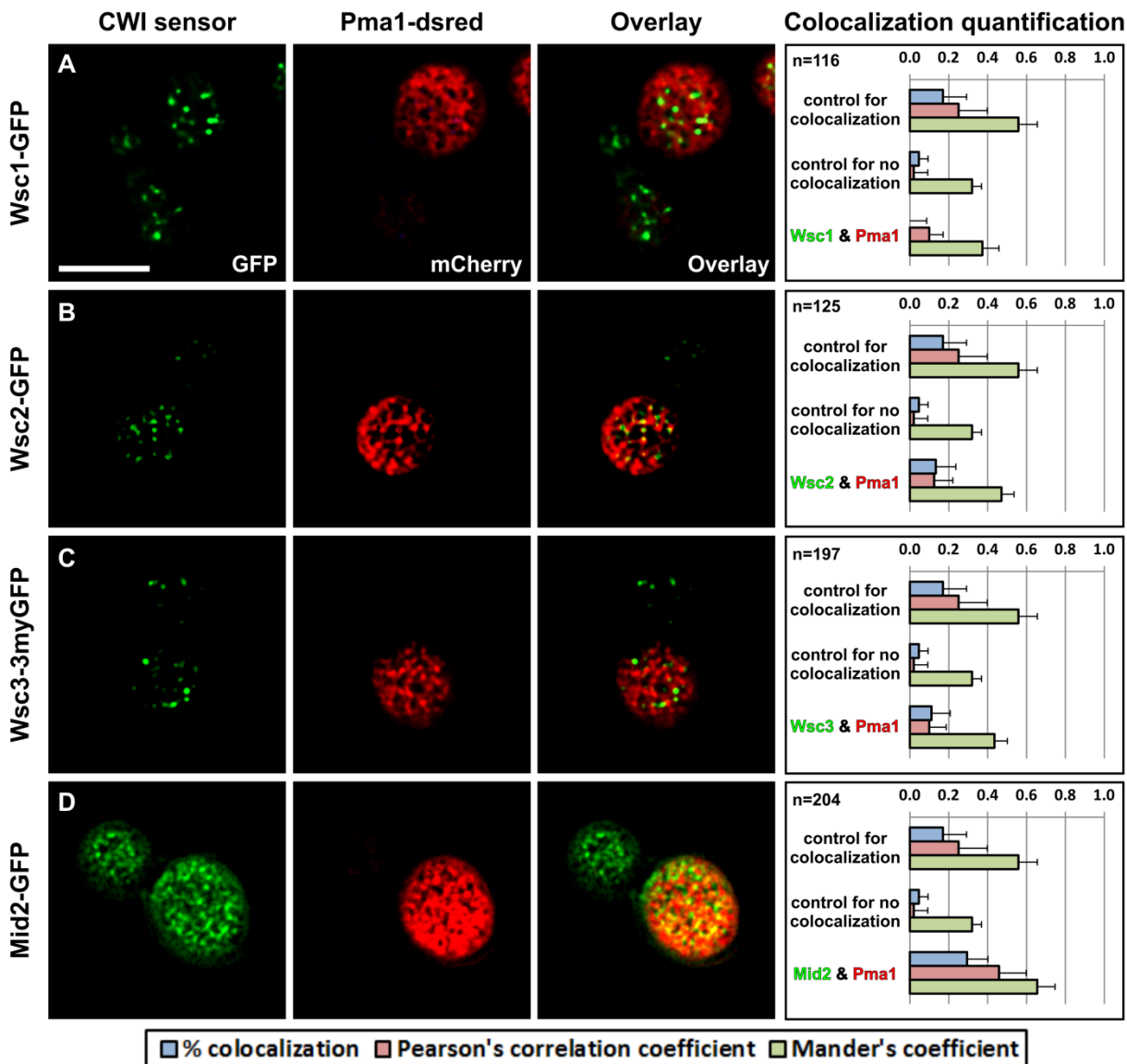


Figure 3.4: Colocalization analysis of CWI sensors with the membrane compartment occupied by Pma1 (MCP). Strains with Pma1-dsRed and CWI sensors c-terminally fused to GFP were investigated by life cell epifluorescence microscopy with a DeltaVision Elite microscope and overlays of top-sections were created. The median of the percentage of colocalized spots (% colocalization, PCOL) was then determined by a “count & colocalize” software plugin together with the “Pearson’s correlation coefficient” (PCC) and the “Mander’s overlap coefficient” (MOC) to quantify the colocalization. Colocalization of Pma1-GFP and Pma1-dsRed served as ‘control for colocalization’ events and Pil1-GFP and Pma1-dsRed as ‘control for no-colocalization’ events (see Figure 6.1 for detailed information, the two controls are the same in all diagrams from A to D). The scale bar corresponds to a size of 5 μm . **A.** Wsc1-GFP and Pma1-DsRed (HSK83-9D). PCOL=0.0 \pm 8.6 %, PCC=0.1 \pm 0.07, MOC=0.373 \pm 0.09. **B.** Wsc2-GFP and Pma1-dsred (HSK92-8C). PCOL=13.3 \pm 10.3 %, PCC=0.13 \pm 0.1, MOC=0.471 \pm 0.07. **C.** Wsc3-3myGFP and Pma1-dsRed (HCK38-4C). PCOL=11.1 \pm 9.6, PCC=0.1 \pm 0.09, MOC=0.44 \pm 0.07. **D.** Mid2-GFP and Pma1-dsRed (HSK76). PCOL=29.4 \pm 10.8, PCC=0.46 \pm 0.14, MOC=0.66 \pm 0.09.

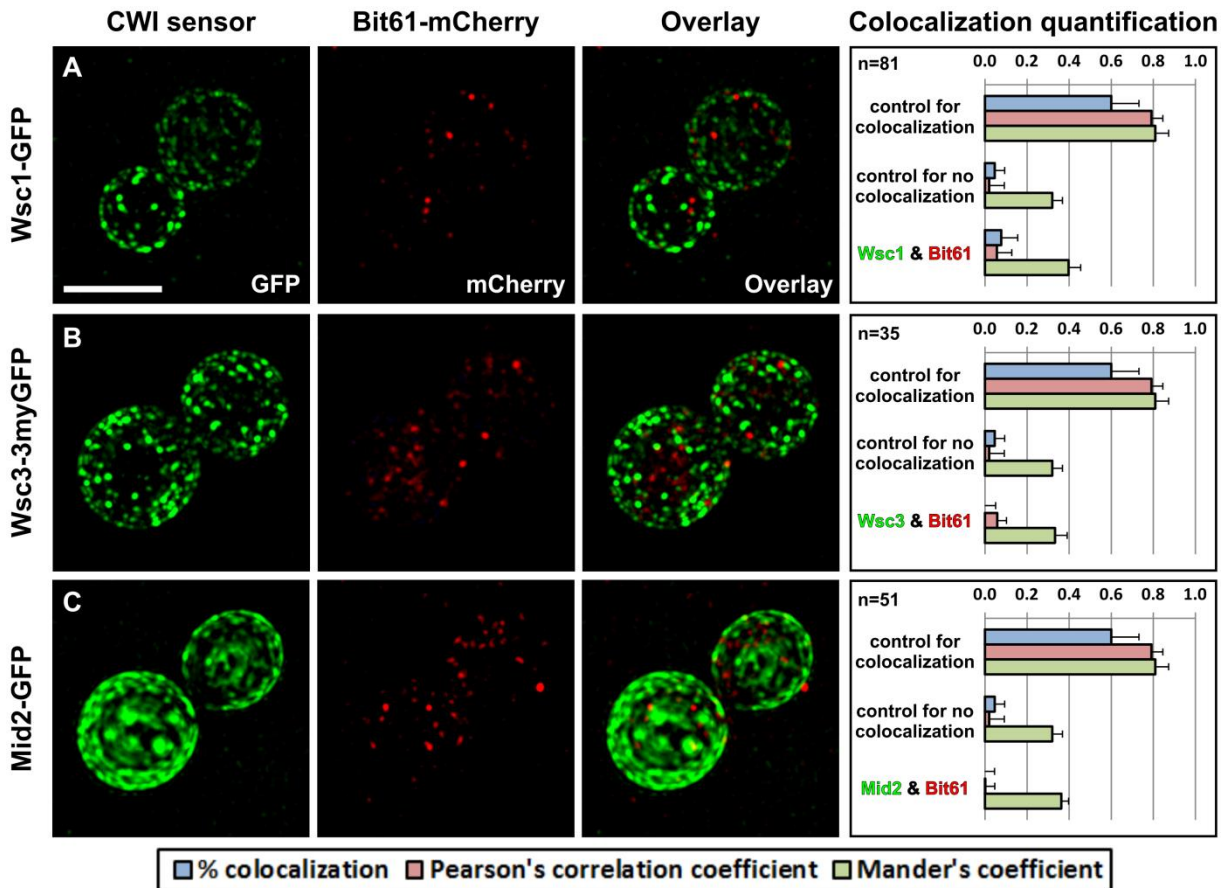


Figure 3.5: Colocalization analysis of CWI sensors with the membrane compartment of TORC2 (MCT). Strains with Bit61-mCherry and CWI sensors c-terminally fused to GFP were investigated by life cell epifluorescence microscopy with a DeltaVision Elite microscope and overlays of half-cell maximal projections were created. The median of the percentage of colocalized spots (% colocalization, PCOL) was then determined by a “count & colocalize” software plugin together with the “Pearson’s correlation coefficient” (PCC) and the “Mander’s overlap coefficient” (MOC) to quantify the colocalization. Colocalization of Pil1-GFP and Pil1-mCherry served as ‘control for colocalization’ events and Pil1-GFP and Pma1-dsRed as ‘control for no-colocalization’ events (see Figure 6.1 for detailed information, the two controls are the same in diagrams A-C). The scale bar corresponds to a size of 5 μ m. **A.** Wsc1-GFP and Bit61-mCherry (HCK49-7C). PCOL=7.7 \pm 7.9 %, PCC=0.06 \pm 0.07, MOC=0.4 \pm 0.06. **B.** Wsc3-3myGFP and Bit61-mCherry (HCK51-1B). PCOL=0.0 \pm 5.1 %, PCC=0.06 \pm 0.04, MOC=0.33 \pm 0.05. **C.** Mid2-GFP and Bit61-mCherry (HCK50-3C). PCOL=0.0 \pm 4.6%, PCC=0.00 \pm 0.05, MOC=0.36 \pm 0.03.

Bit61-mCherry was 7.7 \pm 7.9 % with a PCC of 0.06 \pm 0.07 and a MOC of 0.4 \pm 0.06, indicating a poor overall overlap (Figure 3.5 A). HJW116-B and HAJ150-A were crossed for the analysis of Wsc3 and Bit61. The resulting strain after tetrad analysis, HCK51-1B (*MAT α WSC3-myEGFP BIT61-mCherry-CaURA3*), showed no overlap which was supported by the calculated

PCOL of 0.0 ± 5.1 %, a PCC of 0.06 ± 0.04 and a MOC of 0.33 ± 0.05 of 35 cells (Figure 3.5 B). Mid2 and Bit61 were investigated by crossing of HAJ150-A and HSK28. The strain HCK50-3C (*MATalpha MID2-GFP-SpHIS5 BIT61-myCherry-CaURA3*) did also not show any overlap with the Bit61 spots (PCOL= $0.0 \pm 4.6\%$) with a PCC of 0.00 ± 0.05 and a MOC of 0.36 ± 0.03 in 51 analyzed cells (Figure 3.5 C).

Overall it can be summarized, that none of the investigated sensor fusions showed overlap with fluorescent markers for the membrane compartment occupied by Can1 (MCC) and the membrane compartment of TORC2 (MCT). Wsc2 and Wsc3 showed moderate and Mid2 strong overlap with the membrane compartment occupied by Pma1 (MCP). Alltogether, at least Wsc1 does not show overlap with any of the yet described plasma membrane domains.

3.3 The role of the cysteine-rich domain (CRD) in microcompartmentment of Wsc1

The results presented in the previous chapter indicate that the Wsc1 clusters in the lateral plasma membrane form distinct microcompartments. It has previously been shown that this clustering depends on the cysteine-rich domain (CRD) headgroup of the sensor and that mutation of the eight conserved cysteine-residues in two single and three double cysteine-mutants (C1A, C2,3A, C4,5A, C6,7A and C8A, consecutively numbered by their appearance within the CRD, see Figure 1.4) leads to loss of clustering and a phenotype comparable to a *wsc1Δ* strain (Heinisch *et al.*, 2010). Furthermore, these mutated sensors are not able to activate the CWI MAPK cascade (Wilk, 2010). The role of the cysteine-rich domain for cluster formation and for the sensor function within the signaling cascade was investigated here in more detail. The parts 3.3.1-3.3.3 in this chapter are soon to be published in Kock *et al.*, 2016 (revision submitted).

3.3.1 The cysteine-rich domain is important for Wsc1-Wsc1 sensor interaction at the cell surface

The loss of clustering upon CRD mutation was shown by atomic force microscopy (AFM) on a single molecule level and the subcellular localization of the sensors in these mutants was shown with externally extended and internally GFP-tagged sensors used for the AFM studies (Heinisch *et al.*, 2010). Therefore, the subcellular localization of Wsc1 sensors without the elongation but with the cysteine mutations was investigated by fusion proteins with a C-terminal GFP by life cell fluorescence microscopy. For this, a Wsc1-GFP fragment was cloned into a pUK21 *E. coli* multicopy vector to create pOCK025. From this vector, a *Sna*BI and *Xho*I restriction fragment was used to transform the cysteine-mutant strains HSK38-3A (*MATalpha wsc1::WSC1_{C1A}-kanMX*), HSK39-3B (*MATalpha wsc1::WSC1_{C2,3A}-kanMX*), HSK40-1C (*MATalpha wsc1::WSC1_{C4,5A}-kanMX*), HSK41-2A (*MATalpha wsc1::WSC1_{C6,7A}-kanMX*) and HSK42-3C (*MATalpha wsc1::WSC1_{C8A}-kanMX*). This resulted in the c-terminally GFP-tagged strains HCK58-1 (*MATalpha WSC1_{C2,3A}-EGFP-SpHIS5*), HCK59-3 (*MATalpha WSC1_{C4,5A}-EGFP-SpHIS5*), HCK60-4 (*MATalpha WSC1_{C6,7A}-EGFP-SpHIS5*) and HCK61-1 (*MATalpha WSC1_{C8A}-EGFP-SpHIS5*). Transformants of a *WSC1_{C1A}*-GFP fusion were not obtained. The

fusion protein strains were investigated by life-cell fluorescence microscopy for their subcellular Wsc1 localization. In comparison to the wild type, which showed distinct clusters in the plasma membrane and localization at sites of polarized growth like the bud-neck (Figure 3.6 A), the CRD mutants did not show any distinct clusters in the plasma membrane in top and mid-section images of a z-series, but a very weak homogenously distributed signal in the plasma membrane, while the majority of the GFP signal accumulated in the vacuole (Figure 3.6 A-E). The localization at sites of polarized growth like the bud-neck (Figure 3.6 B, E) and the bud-tip (Figure 3.6 D, E) was not abolished by mutation of the CRD.

To investigate if the Wsc1 clusters form by homotypic interaction mediated by the cysteine-rich domain, biomolecular fluorescence complementation (BiFC) analysis of wild-type sensors, wild-type sensors with cysteine-mutated sensors and only cysteine-mutated sensors was performed. Fluorescence complementation only occurs if C-terminal (VC) and N-terminal (VN) Venus fragments get into close proximity to form a functional fluorophore. Therefore, fusion proteins of VC or VN and investigated proteins can be used to observe interaction and its spatio-temporal pattern. Plasmids with wild-type *WSC1*-VC (pJW06) and *WSC1*-VN (pJW05) introduced into a *wsc1Δ* strain (HOD137-3C) were used as control for the interaction. These cells showed fluorescence signals at the bud-neck and at the tip of emerging buds, but punctate clusters in the plasma membrane were not observed (Figure 3.6 F). Previous studies already showed that a wild-type Wsc1-VC (pJW06) in combination with Wsc1_{C4,5A}-VN or Wsc1_{C6,7A}-VN, respectively, also show signals at these sites of polarized growth (Wittland, 2012). To quantify whether the cysteine-rich domain is required for physical interaction of Wsc1, *WSC1*_{C4,5A} and *WSC1*_{C6,7A} were cloned into VC vectors (pOCK027 and pOCK028). Then wild-type only, wild-type/mutant and mutant only combinations of VC and VN fusion constructs were introduced into a *wsc1Δ* strain (HOD137-3C) and all cells with fluorescence signal at the bud-neck or bud-tip were counted (Figure 3.6 G). Wsc1-VN (pJW05) and Wsc1-VC (pJW06) showed fluorescence signals in 19 of 95 cells (20%), which reflects the cell cycle-dependent localization of Wsc1. In cells with Wsc1-VC (pJW06) and Wsc1_{C4,5A}-VN (pJW09) or Wsc1_{C6,7A}-VN (pJW10), respectively, the number of cells showing signal was reduced about half with 6 out of 49 cells (12%) or 9 out of 81 cells (11%), respectively. *Vice versa*, Wsc1-VN (pJW05) and Wsc1_{C4,5A}-VC (pOCK027) or Wsc1_{C6,7A}-VC

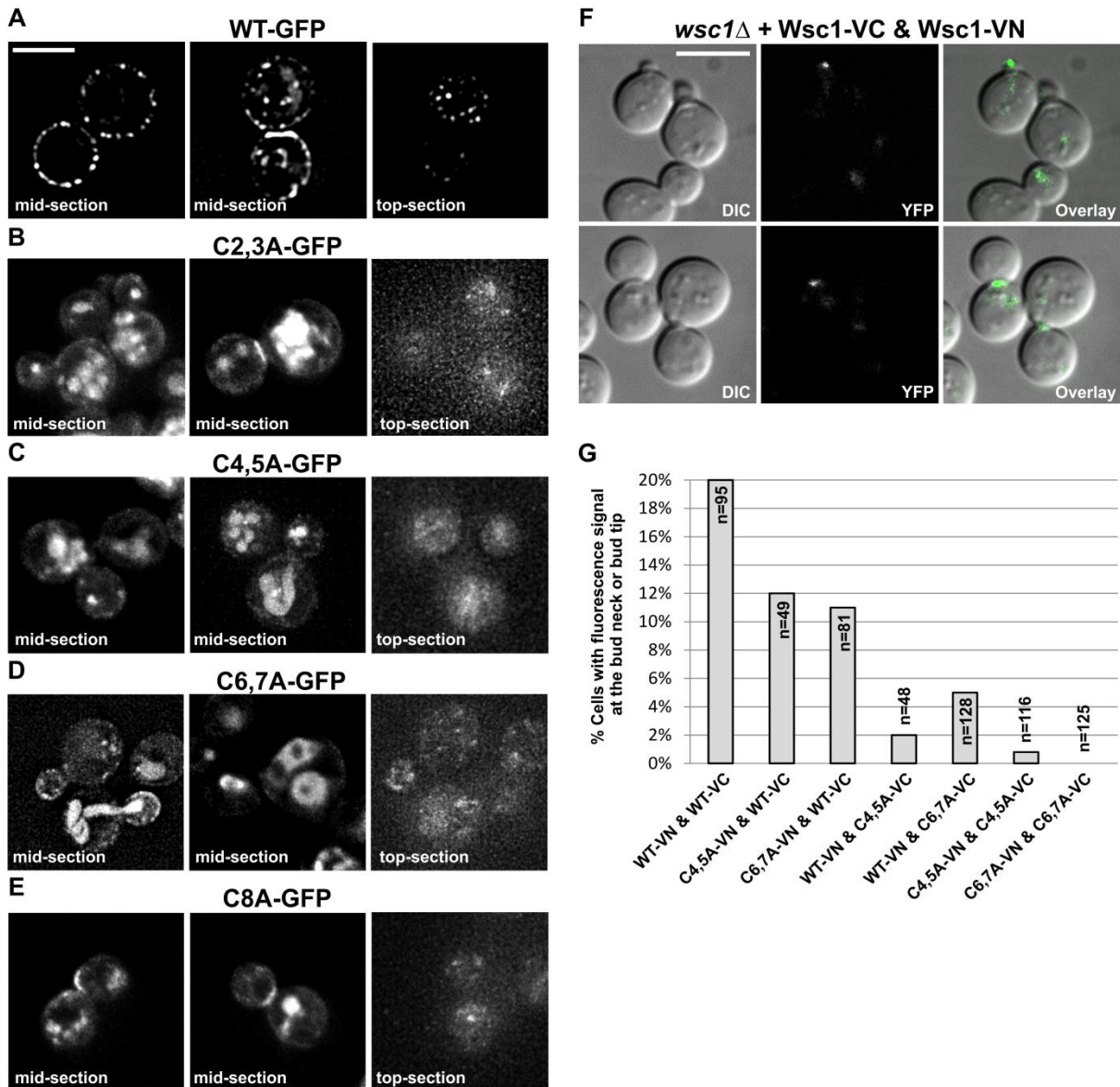


Figure 3.6: Subcellular localization of Wsc1 cysteine-rich domain (CRD) mutants. A-E. Life cell fluorescence microscopy of strains expressing wild-type or cysteine-mutated Wsc1 sensors c-terminally tagged with GFP. Mid and top-sections of z-series of different cells are shown. Scale bar=5 μ m. **A.** Wsc1-GFP (HSK29). **B.** Wsc1_{C2,3A}-GFP (HCK58-1). **C.** Wsc1_{C4,5A}-GFP (HCK59-3). **D.** Wsc1_{C6,7A}-GFP (HCK60-4). **E.** Wsc1_{C8A}-GFP (HCK61-1). **F.** Bimolecular fluorescence complementation (BiFC) analysis of Wsc1-VC (pJW05) and Wsc1-VN (pJW06) in a *wsc1*Δ strain (HOD137-3C). Scale bar=5 μ m. **G.** Quantification of BiFC analyses in *wsc1*Δ cells (HOD137-3C) with only wild-type sensors, mixed wild-type and cysteine-mutated sensors and only cysteine-mutated sensors expressed from plasmids. The number of cells with fluorescence signal at the bud-neck or bud-tip was counted. WT-VC: pJW06, Wsc1-VN: pJW05, C4,5A-VN: pJW09, C6,7A: pJW10, C4,5A-VC: pOCK027, C6,7A-VC: pOCK028.

(pOCK028) showed signal 1 out of 48 cells (2%) and 6 out of 128 cells (5%). In cells with only mutant sensors, *Wsc1_{C4,5A}-VN* (pJW09) and *Wsc1_{C4,5A}-VC* (pOCK027) showed signal in only 1 out of 116 cells (<1%), whereas *Wsc1_{C6,7A}-VN* (pJW10) and *Wsc1_{C6,7A}-VC* (pOCK028) didn't show any fluorescence signal at all in 125 cells examined.

Control experiments expressing only the VC or VN tagged versions were done in Wittland, 2012 and did not show signal, so that fluorescence signal is only present in cells with fluorescence complementation. Overall, cells with wild-type sensors show signal at sites of polarized growth which is strongly decreased in cells with one cysteine-mutated allele and one wild-type sensor allele. Cells with only mutant sensors alleles did not show physical interaction.

In conclusion, the CRD is necessary for interaction of *Wsc1* sensors and mutation of the cysteine-residues within this domain leads to loss of the normal localization pattern in the plasma membrane and accumulation of the sensor in the vacuole.

3.3.2 Blocking the turnover of *Wsc1* CRD mutants at the plasma membrane in *end3* deletions shows pleiotropic signaling effects

The results above revealed that *Wsc1* CRD mutants mostly accumulate in the vacuole, which is most likely the reason why they do not function properly in stress response (Wilk 2010; Heinisch *et al.*, 2010). To investigate whether the mutated sensors are able to function in signaling when their endocytosis is blocked or if the sensor clustering is required for functionality, the endocytosis mutant *end3Δ* was used. Studies of Wilk *et al.* 2010 showed that *Wsc1* does not undergo endocytosis in this mutant and distributes more homogeneously in the plasma membrane rather than in distinct patches. To see if this is also the case in CRD mutant GFP strains, HCK58-1 (*MATalpha WSC1_{C2,3A}-EGFP-SpHIS5*), HCK59-3 (*MATalpha WSC1_{C4,5A}-EGFP-SpHIS5*), HCK60-4 (*MATalpha WSC1_{C6,7A}-EGFP-SpHIS5*) and HCK61-1 (*MATalpha WSC1_{C8A}-EGFP-SpHIS5*) were crossed with the *END3* deleted strain HJW25-A (*MATa end3::KIURA3*). The resulting strains HCK66-2D (*MATalpha WSC1_{C2,3A}-EGFP-SpHIS5 end3::KIURA3*), HCK67-1D (*MATalpha WSC1_{C4,5A}-EGFP-SpHIS5 end3::KIURA3*), HCK68-4C (*MATalpha WSC1_{C6,7A}-EGFP-SpHIS5 end3::KIURA3*) and HCK69-4A (*MATalpha WSC1_{C8A}-EGFP-SpHIS5 end3::KIURA3*) were investigated by live cell fluorescence microscopy and compared

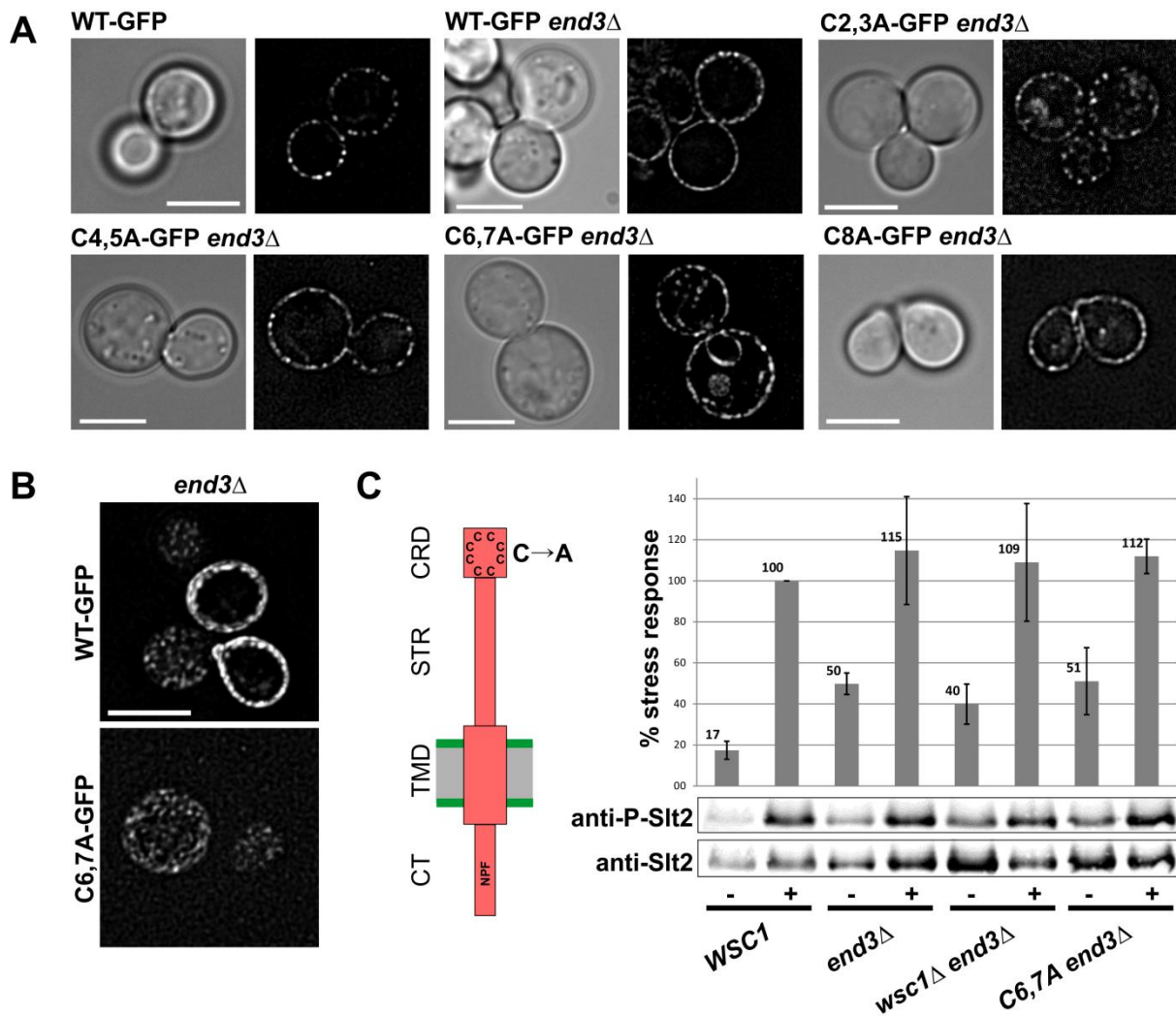


Figure 3.7: Localization and signaling of Wsc1 cysteine-rich domain mutants in an *end3Δ* endocytosis mutant (from: Kock *et al.*, 2016 (revision submitted)). A.+B. Life cell fluorescence microscopy of strains with Wsc1 CRD mutants (see scheme in C for mutated region) in an *end3Δ* deletion background in comparison to wild-type localization. Scale bars = 5 μ m. **A.** Mid-section view of the strains HSK29 (Wsc1-GFP), HSK11-2C (Wsc1-GFP *end3Δ*), HCK58-1 (Wsc1_{C2,3A}-GFP *end3Δ*), HCK59-3 (Wsc1_{C4,5A}-GFP *end3Δ*), HCK60-4 (Wsc1_{C6,7A}-GFP *end3Δ*) and HCK61-1 (Wsc1_{C8A}-GFP *end3Δ*). **B.** Top-section view of HSK11-2C (Wsc1-GFP *end3Δ*) and HCK60-4 (Wsc1_{C6,7A}-GFP *end3Δ*). **C.** Stress response of the Wsc1_{C6,7A} mutant in *end3Δ* after 40 minutes of treatment with 50 ng/ml Caspofungin. The relative amounts of double-phosphorylation of the Wsc1 target MAPK Slt2 (anti-Phospho-Slt2) were quantified and compared to the overall Slt2 levels (anti-Slt2) in untreated (-) and stress induced (+) samples. The bars correspond to the arithmetic mean and the error bars to the standard deviation of three independent blots. The induced WSC1 sample was set as 100%. The strains used were HD56-5A (WSC1), HJW25-B (*end3Δ*), HCK75-11B (*end3Δ wsc1Δ*) and HCK73-8D (*end3Δ WSC1_{C6,7A}*).

to Wsc1-GFP (HSK29) and Wsc1-GFP in *end3Δ* background (HSK11-2C). As already described in (Wilk *et al.*, 2010), Wsc1-GFP *end3Δ* did not form the distinct clusters as in a wild-type Wsc1-GFP strain and the sensor was blocked at the cell surface (Figure 3.7 A). In addition, Wsc1_{C2,3A}-GFP, Wsc1_{C4,5A}-GFP, Wsc1_{C6,7A}-GFP and Wsc1_{C8A}-GFP in the *end3Δ* mutant did not accumulate in the vacuole but showed fluorescence signals mostly in the plasma membrane also in a more homogenous pattern and not as distinct patches as in a wild-type Wsc1-GFP strain. Furthermore, looking at top-sections in z-series of images showed, that Wsc1_{C6,7A}-GFP in an *end3Δ* mutant seems to distribute in a more network-like pattern than in distinct patches compared to Wsc1-GFP in an *end3Δ* mutant (Figure 3.7 B).

After showing that Wsc1 CRD mutants localize at the cell surface and not in the vacuole in *END3* deleted strains, it was investigated whether these sensors are able to activate the cell wall integrity signaling cascade at the level of the MAP kinase Slt2. Western blot analyses using a monoclonal anti-Phospho-p44/42 MAP kinase (Thr202/Tyr204) antibody that is specific for dual-phosphorylated Slt2 and a polyclonal antibody that recognizes the overall Slt2 amount was performed to quantify the relative pathway activation. Furthermore, cell wall stress was induced using 50 ng/ml Caspofungin and compared to non-induced samples. Previous results using this experimental setup for CRD mutant strains in the non *end3Δ* background revealed, that Caspofungin induction increased the Slt2 phosphorylation in wild-type strains about fivefold and that the activation in *WSC1* deleted strains is decreased to 60 % compared to the wild type. The CRD mutants showed a comparable level of phospho-Slt2 to a *wsc1Δ* strain, meaning that *WSC1* is not functional in this strain (Wilk, 2010).

The fivefold induction upon Caspofungin treatment was also observed for the wild-type strain HD56-5A in this experiment in a series of three independent blots (Figure 3.7 C). The *end3Δ* strain HJW25-B showed a higher basic phosphorylation level (50%) than the wild type, while the induced sample varied greatly but was at least on the same level as the control strain. The *wsc1Δ end3Δ* double deletion strain HCK75-11B was created by crossing of HAS17-3C (*MATa wsc1::SpHIS3*) and HJW25-B and showed an increased level of phospho-Slt2, too. In addition, the strain showed a level of phosphorylated Slt2 similar to the wild type upon induction as well and in contrast to the single *wsc1Δ* mutant. This was also the case for the Wsc1_{C6,7A} mutant strain in the *END3* deletion background in HCK73-8D

(*MATa wsc1::WSC1_{C6,7A}-kanMX end3::KIURA3*) which was created by crossing of HSK41-2A and HJW25-B. Overall, the *end3Δ* background resulted in a higher level of basic phosphorylation and in full activation of the cascade upon Caspofungin treatment even in the *wsc1Δ* strain. Therefore, pleiotropic effects contributed to the Slr2 phosphorylation and sensor function could not be studied in this experiment.

3.3.3 Mutating the endocytosis signal in Wsc1 CRD mutants restores its sensor function and changes its localization within the plasma membrane.

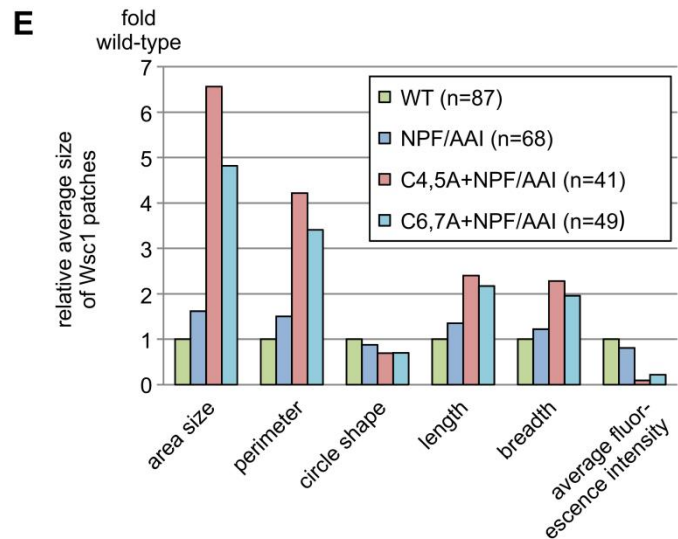
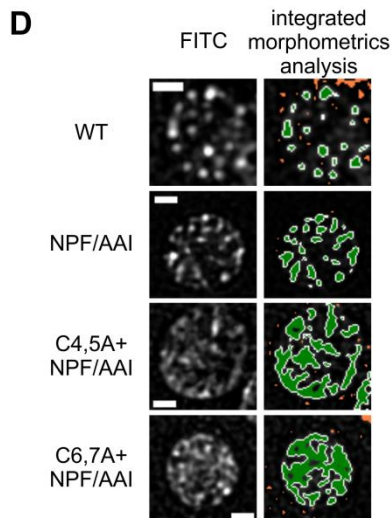
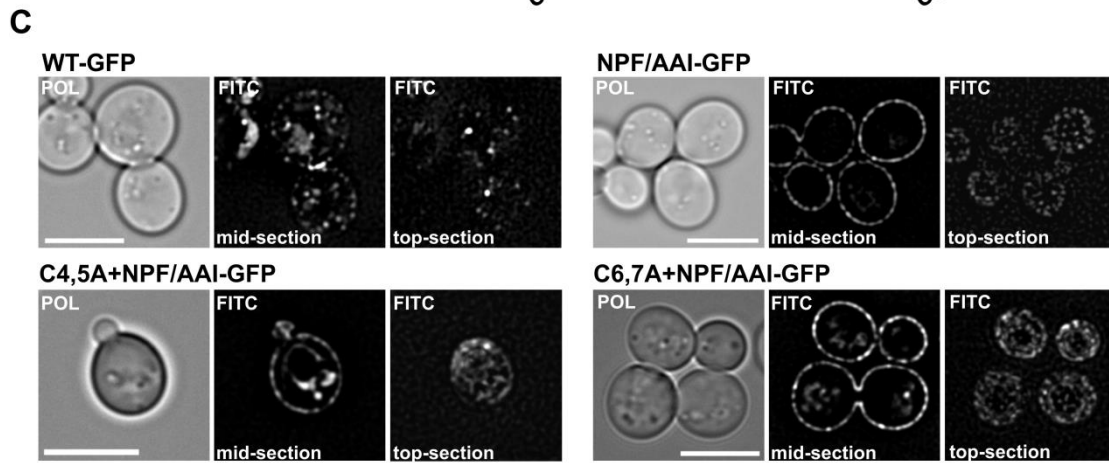
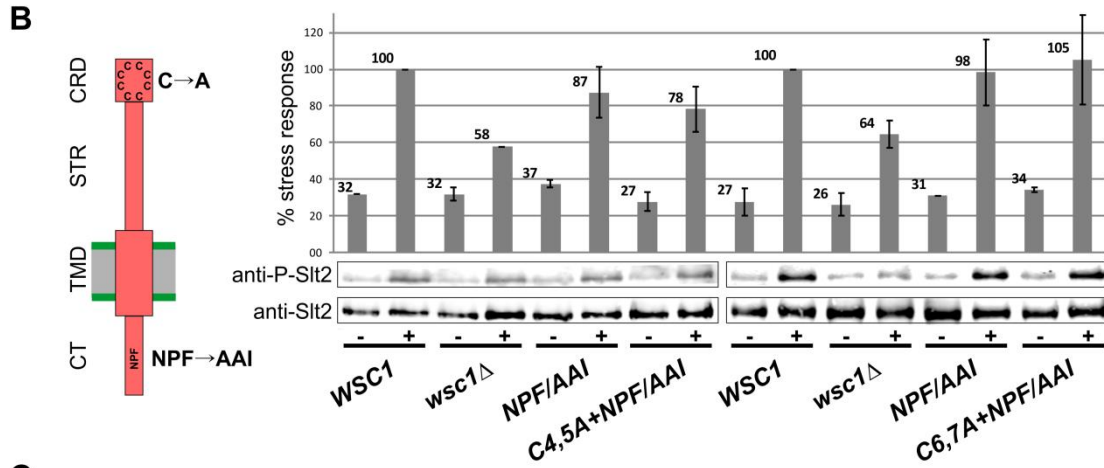
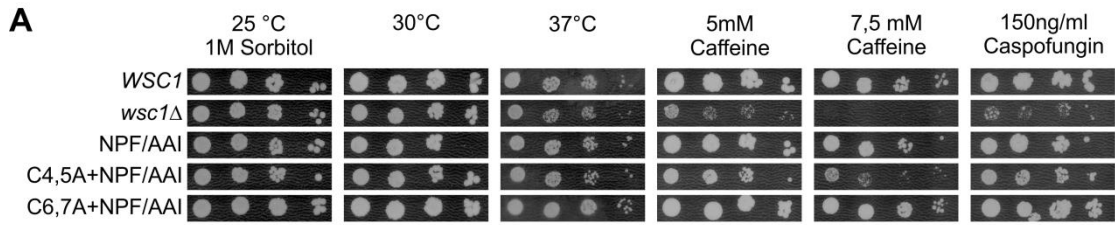
A general block of endocytosis by deleting *END3* was not suitable to study the function of Wsc1 clustering for cell wall integrity signaling, because other factors contributed to the signaling as well since this deletion is expected to have pleiotropic effects on signaling, apart from the influence on Wsc1. Piao *et al.*, 2007 could show that the amino acids 344-348 in the cytoplasmic tail of Wsc1 mediate endocytosis and that mutation of this NPFDD sequence depolarizes Wsc1 at the cell surface. Also, the effect of an NPF/AAI mutation on CWI signaling and Wsc1 localization have been intensively studied (Wilk *et al.*, 2010). Therefore, this mutation was used here to keep the Wsc1 cysteine-rich domain mutants at the cell surface in order to avoid pleiotropic effects influencing the signaling like in the *END3* deletion.

To create sensors mutated in both the CRD and the NPF motifs, the C4,5A and C6,7A mutations as examples for CRD mutants were substituted for the respective wild-type sequences in a plasmid with *WSC1_{NPF/AAI}* (pJJH1140). The resulting plasmids pOCK029 (*WSC1_{C4,5A NPF/AAI}*), pOCK030 (*WSC1_{C6,7A NPF/AAI}*), and pSK27 (*WSC1*), YCplac111 (empty vector) and pJJH1140 (*WSC1_{NPF/AAI}*) as well were introduced into a *wsc1Δ* strain (HOD137-3A). These cells were used to perform serial drop dilution assays on different stress media (Figure 3.8 A). Cells with pSK27 expressing wild-type *WSC1* grew normal on plates at 25°C with 1 M sorbitol for osmotic stabilization, on plates without sorbitol at 30°C and 37°C and on plates containing 5 mM Caffeine, 7,5 mM Caffeine and 150 ng/ml Caspofungin. Cells with the *WSC1* deletion and the empty vector showed strong growth limitation under the latter three conditions. *WSC1_{NPF/AAI}* (pJJH1140) and *WSC1_{C6,7A NPF/AAI}* (pOCK030) grew normal on all media, while *WSC1_{C4,5A NPF/AAI}* (pOCK030) showed a slight growth limitation on 7,5 mM Caffeine medium.

As the cysteine mutants didn't show any growth on the selected stress media (data not shown, Heinisch *et al.*, 2010), the CRD/NPF double mutants, in contrast, were able to grow like the wild type.

Cells with Wsc1 carrying the CRD/NPF double mutations grew normal on stress media. To further investigate the proper sensor function, the dual-phosphorylation levels of the MAPK SlT2 as a marker for pathway activation was investigated as described in chapter 3.3.2 with pSK27, YCplac111, pJJH1140, pOCK029 and pOCK030 expressed in a *wsc1Δ* strain (← Figure 3.8 B). The basal level of phosphorylation in all cells without Caspofungin treatment comparable to the cysteine mutants without NPF/AAI mutation, as the cells showed between 27% to 37% of the stress response observed in Caspofungin treated wild-type cells (HOD137-3A + pSK27). *WSC1* deleted cells (HOD137-3A + YCplac111) showed a stress response of approximately 60 % compared to wild-type cells and *WSC1_{NPF/AAI}* cells (HOD137-3A + pJJH1140) were able to activate the CWI cascade comparable to the wild type. *WSC1_{C4,5A NPF/AAI}* cells (HOD137-3A + pOCK029) showed a slight reduction in stress response which was not as severe as in *WSC1* deleted cells, while a full SlT2 phosphorylation was observed in *WSC1_{C6,7A NPF/AAI}* cells (HOD137-3A + pOCK030) cells, although showing a great variety in the amount of dual-phosphorylated SlT2.

It was published that Wsc1 with a NPF/AAI mutation localizes in a depolarized manner similar to the *END3* deleted background (Wilk *et al.*, 2010). It was investigated here if this is also the case when the cysteine-rich domain is mutated additionally. *Wsc1_{C4,5A NPF/AAI}* and *Wsc1_{C6,7A NPF/AAI}* were c-terminally tagged with GFP to create the plasmids pOCK031 (*WSC1_{C4,5A NPF/AAI}-GFP*) and pOCK032 (*WSC1_{C6,7A NPF/AAI}-GFP*). These plasmids were introduced into HOD137-3A as were the control plasmids pSK44 (*WSC1_{NPF/AAI}-GFP*) and pOCK035 (*WSC1-GFP*) and viewed by live cell fluorescence microscopy (Figure 3.8 D). Wsc1-GFP distributed in punctate clusters in the plasma membrane and at sites of polarized growth. *Wsc1_{NPF/AAI}-GFP* showed a depolarized pattern that was distributed more evenly all over the plasma membrane but the spot-like distribution of the clusters was still visible. *Wsc1_{C4,5A NPF/AAI}-GFP* and *Wsc1_{C6,7A NPF/AAI}-GFP* also showed the depolarized pattern all over the plasma membrane, but the top-section of the cells revealed a more network-like than spot-like distribution. This distribution pattern was further investigated by an integrated morphometrics analysis. By



← **Figure 3.8: Characterization of Wsc1 cysteine-rich domain (CRD) mutants with mutated NPF endocytosis signal (from: Kock *et al.*, 2016 (revision submitted)).** The mutated regions are depicted in the scheme in B. **A.** Phenotypical characterization of *wsc1Δ* cells (HOD137-3A) with different *WSC1* plasmids by serial drop dilution assays on SCD-LEU plates incubated at temperatures and containing stressors as indicated. The plates were incubated for 3 days at 30 °C if not noted otherwise. WT: *WSC1* (pSK27), *wsc1Δ*: empty vector (YCplac111), NPF/AAI : *WSC1*_{NPF/AAI} (pJH1140), C4,5A NPF/AAI : *WSC1*_{C4,5A NPF/AAI} (pOCK029), C6,7A NPF/AAI : *WSC1*_{C6,7A NPF/AAI} (pOCK030). **B.** Stress response mediated by the CWI pathway determined in Wsc1 NPF/AAI and Wsc1 NPF/AAI+CRD-mutants compared to wild-type and *WSC1* deleted cells after 40 minutes of treatment with 50 ng/ml Caspofungin. The relative double-phosphorylation of the MAPK Slt2 (anti-Phospho-Slt2) was quantified and compared to the overall Slt2 levels (anti-Slt2) in untreated (-) and stress induced (+) samples. The bars correspond to the arithmetic means and the error bars to the standard deviation of three independent blots. The induced *WSC1* sample was set as 100%. The strains and plasmids used were the same as in A. **C.** Life cell fluorescence microscopy of *wsc1Δ* cells (HOD137-3A) with pOCK035 (Wsc1-GFP), pSK44 (Wsc1_{NPF/AAI}-GFP), pOCK031 (Wsc1_{C4,5A NPF/AAI}-GFP) and pOCK032 (Wsc1_{C6,7A NPF/AAI}-GFP). Mid-section and top-sections views of the same cell. Scale bars: 5 μm. **D.** Integrated morphometrics analysis to measure Wsc1 fluorescence patches of maximal projections of the top three planes in a z-series of cells. The same strains and plasmids as in C. were used. Signal threshold 1000. Scale bars: 1 μm. **E.** Quantification of integrated morphometrics analysis. The bars represent the arithmetic mean of the calculated values of all Wsc1 fluorescence patches for one strain normalized to the patch size of wild-type Wsc1. The same strains and plasmids as in C. were used. Area size: Complete pixel area, perimeter: length of the surrounding distance, circle shape: measurement of how close an object is to a circle, length: longest possible diameter; breadth: longest possible diameter orthogonal to the length, average intensity: integrated average intensity of an area. WT: 87 cells, 242 patches, NPF/AAI: 68 cells, 919 patches, C4,5A+NPF/AAI: 41 cells, 268 patches, C6,7A+NPF/AAI: 49 cells, 438 patches.

this software, the area of a fluorescence signal is measured when a signal threshold is applied. The very three top sections of a z-series were used in a maximal projection and a signal threshold of 1000 was applied (Figure 3.8 D). The Wsc1-GFP clusters showed a very distinct, almost circular shape. In cells with Wsc1_{NPF/AAI}-GFP the number of clusters was slightly increased and they were not as circular and distinct but seemed slightly elongated. In Wsc1_{C4,5A NPF/AAI}-GFP and Wsc1_{C6,7A NPF/AAI}-GFP cells hardly any circular spots could be observed and all patches seemed to be connected to form a more network-like pattern. These patterns were also measured and the arithmetic mean of all patches was calculated and the values of Wsc1-GFP were set as 100 %. (Figure 3.8 E). This revealed that the area size of the fluorescence patches was slightly increased in the NPF/AAI mutant but up to six-fold increased in the C4,5A/C6,7A NPF/AAI double mutants. A similar increase was observed for the perimeter of the fluorescence patches which was up to four fold higher in the cysteine

mutants as compared to wild-type cells. Furthermore, the circular shape of the patches was slightly decreased in all mutants in comparison to wild-type Wsc1. Further values that were obtained by the analysis were the length (the longest possible diameter) and breadth (the longest possible diameter orthogonal to the length) of the patches, which were also found to be slightly increased in the NPF/AAI mutant, but up to twofold increased in the cysteine mutants. The average intensity of the spots varied from slightly increased in Wsc1_{NPF/AAI}-GFP cells to decreased or wild-type levels in the cysteine mutants. In all data, the observed network-like pattern was more pronounced in the C4,5A mutants than in C6,7A mutants. Overall, the NPF/AAI mutation within the cytoplasmic tail of Wsc1 introduced into CRD mutants lead to plasma membrane localization of the sensor instead of vacuolar accumulation. The plasma membrane distribution pattern was changed from spot-like in wild-type cells to network-like in the mutated cells and the growth and stress response impairments of the CRD mutants were abolished by additional NPF/AAI mutation.

3.3.4 Wsc1 clustering and signaling can be abolished by mutating an amyloid like sequence within the CRD

All the results above indicate that Wsc1 clustering depends on several cysteine-residues within the CRD, but how the clustering is achieved and what its function for signaling could be are still in question. A TANGO software analysis of the amino acid sequences of Wsc1, Wsc2 and Wsc3 revealed a conserved sequence with a 40% potential to form amyloid-like protein aggregates (Edupaganti and Lipke, personal communication). In Wsc1, this sequence is ASYFALYN and is located within the CRD between the third and fourth cysteine residue (Figure 1.4). The software also predicted a reduction of this aggregation potential from 40% to 2.63%, if the tyrosine60 was to be exchanged for a serine.

A WSC1 gene encoding the Y60S mutation within the cysteine-rich domain was introduced into a yeast centromere vector to create the plasmid pJJH1892 (Jürgen Heinisch, personal communication) and sequenced. The mutant was also used for single-molecule atomic force microscopy (AFM) and therefore the Mid2 serine/threonine-rich region elongation with a histidine-tag was used for this experiment as published in Dupres *et al.*, 2010. The elongation in the extracellular part was shown to have no impact on the Wsc1 sensor function. The

resulting plasmid was introduced into a *wsc1Δ mid2Δ* double deletion strain (HSK17-1C) for phenotypic analysis. Control plasmids for this analysis were *WSC1* without elongation (pSK27), the empty vector (YCplac111), *WSC1* with Mid2_{STR} elongation and a HIS-Tag (*MID2WSC1*, pBH01) and a *MID2WSC1*_{C4,5A} cysteine mutant (pJJH1169). These cells were used in serial drop dilution assays to investigate the phenotype of the Y60S mutant at 37 °C, at 30 °C on plates containing 5 mM caffeine, 100 ng/ml Caspofungin and 2,5 µg/ml or 5 µg/ml Congo red stress media, and at 25 °C + 1M Sorbitol and 30°C SCD-LEU plates as well (Figure 3.9 A). The results confirmed that a Mid2_{STR}-elongated Wsc1 sensor (pBH01) showed the same growth as a wild-type Wsc1 sensor (pSK27) and that the elongation does not influence the Wsc1 sensor function. Also, the Wsc1_{C4,5A} mutant (pJJH1169) behaved like cells carrying a vector without *WSC1* (YCplac111), thus confirming its lack of function. The Wsc1_{Y60S} mutant showed reduced growth at 37 °C and strongly reduced growth on 5 µg/ml Congo red, similar to the C4,5A mutant. In contrast, no growth reduction could be observed on plates containing Caffeine, Caspofungin or 2.5 µg/ml Congo red.

The serial drop dilution assay revealed a Wsc1_{Y60S} phenotype that is only partially comparable to the previously investigated cysteine mutants. To determine the degree to which signaling is impaired in the Y60S mutated Wsc1 sensor, the CWI pathway activation was investigated by measuring the double-phosphorylation levels of Slt2 as for the cysteine mutants in the previous chapters (see e.g. 3.3.2). pBH01 (*MID2WSC1*), YCplac111 (empty vector) and pJJH1892 (*MID2WSC1*_{Y60S}) were introduced into a *wsc1Δ* deletion strain (HOD137-3A). The cells were treated with 50 ng/ml Caspofungin and compared to the non-treated samples (Figure 3.9 B). In the *WSC1* control (pBH01), the Slt2 phosphorylation increased approximately five-fold under stress conditions, which was set as 100% stress response. In the empty vector control, the stress response upon induction was reduced to around 60% of the wild-type, comparable to similar experiments about Wsc1-mediated Slt2 phosphorylation. The Wsc1_{Y60S} mutant showed decreased phosphorylated Slt2 levels of about 70% of the wild-type level.

The Y60S amyloid mutant showed phenotypes and pathway activation that is basically similar to the CRD mutants investigated above, indicating that it may also be affected in clustering

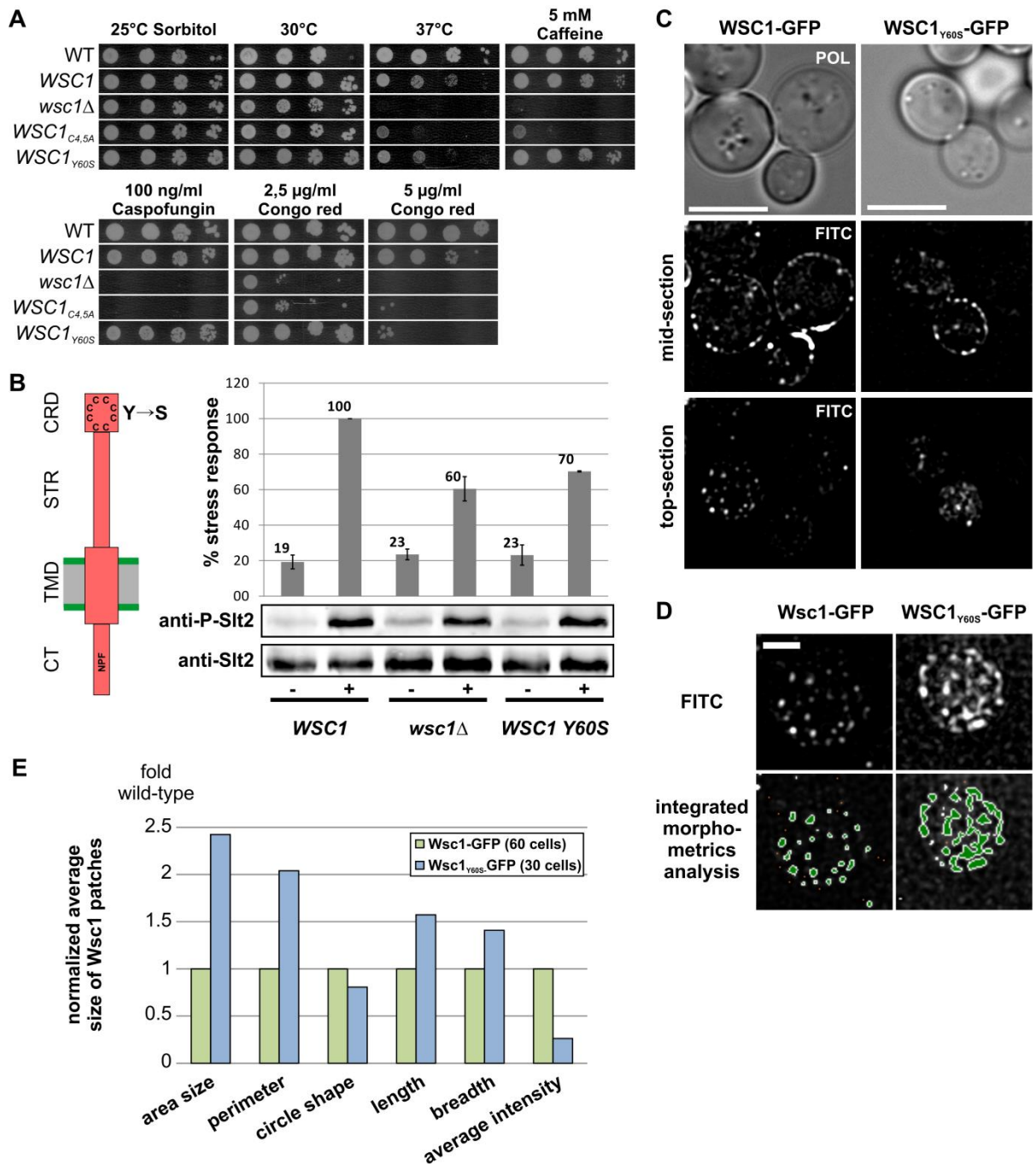


Figure 3.9: Characterization of a Wsc1 Y60S amyloid mutant. All experiments were performed with Wsc1 sensor constructs elongated with the Mid₂_{STR} as published in Dupres *et al.*, 2010 encoded on centromeric plasmids. The mutated region is depicted in the scheme in B. **A.** Phenotypical characterization of *wsc1Δ mid2Δ* cells (HSK17-1C) with different *WSC1* plasmids by serial drop dilution assays on indicated SCD-LEU stress media. The plates were incubated for 3 days at 30 °C if not noted otherwise. WT: *WSC1* without elongation (pSK27), *WSC1*: *WSC1* (pBH01), *wsc1Δ*: empty vector (YCplac111), C4,5A: *WSC1*_{C4,5A} (pJJH1169), Y60S: *WSC1*_{Y60S} (pJJH1892). **B.** Stress response mediated by the CWI pathway of the Wsc1 Y60S mutant compared to wild-type and *WSC1* deleted cells after 40 minutes of treatment with 50 ng/ml Caspofungin. The relative double-phosphorylation of the Wsc1

target MAPK SlT2 (anti-Phospho-SlT2) was quantified and compared to the overall SlT2 levels (anti-SlT2) in untreated (-) and stress induced (+) samples. The bars correspondent to the arithmetic mean and the error bars to the standard deviation of three independent blots. The induced *WSC1* sample was set as 100%. The strains and plasmids used were HOD137-3A (*wsc1Δ*) with pBH01 (*WSC1*), YCplac111 (empty vector, *wsc1Δ*) and pJJH1892 (*WSC1 Y60S*). **C.** Life cell fluorescence microscopy of *wsc1Δ* cells (HOD137-3A) with pJJH1191 (*Wsc1-GFP*), and pOCK033 (*Wsc1_{Y60S}-GFP*). Mid-section and top-sections views of the same cell are shown. Scale bars: 5 μm. **D.** Integrated morphometrics analysis to measure *Wsc1* fluorescence patches of maximal projections of the top three planes in a z-series of cells. The same strains and plasmids as in C. were used. Signal threshold 1000. Scale bar: 1 μm. **E.** Quantification of integrated morphometrics analysis. The bars represent the arithmetic mean of the calculated values of all *Wsc1* fluorescence patches for one strain normalized to the patch size of wild-type *Wsc1*. The same strains and plasmids as in C. were used. See figure 3.8 for description of parameters. *Wsc1-GFP*: 87 cells, 1078 patches, *Wsc1_{Y60S}-GFP*: 30 cells, 627 patches.

and membrane distribution. If the identified amyloid sequence is involved in the *Wsc1* clustering process, the mutant should show a loss in clustering and similar localization patterns like other CRD mutants. To investigate this, GFP was c-terminally fused to the *WSC1_{Y60S}* gene encoded on pJJH1892. The resulting plasmid pOCK033 (*MIDWSC1_{Y60S}-GFP*) was introduced into HOD137-3A and compared to the non-GFP mutant in serial drop dilution assays, where it displayed no differences (data not shown). The cells were then investigated by life-cell fluorescence microscopy and compared to those carrying a *MID2WSC1-GFP* construct without the Y60S mutation (pJJH1191). In the middle section of z-series no difference to the control strain was observed (Figure 3.9 C). The sensor localized in clusters within the plasma membrane and did not accumulate in vacuoles like the CRD mutants. In top sections of cells, the clusters were not as round and distinct as in the control strain and the patches distributed in a more network-like pattern than in distinct clusters (Figure 3.9 D). This was confirmed by quantifications as described above in chapter 3.3.3 (Figure 3.9 E). While the patches were distinct and showed a circular shape, the Y60S patches were elongated and not as distinct as in the control. The patches showed a tendency to form network-like structures. Different shape parameters for these patches were investigated by the integrated morphometric software for 87 control cells (242 fluorescence patches) and 30 Y60S mutated cells (627 fluorescence patches) like it was done in chapter 3.3.3 (Figure 3.9 E). These data revealed that the arithmetic mean of the fluorescence patch area size and that of the perimeter were more than twice of those of the control strain. The length and breadth of

these patches was on average 1.5-fold increased while their circular shape was decreased compared to the control. Interestingly, the average fluorescence intensity of the strain with the Y60S variant was decreased approximately fourfold as compared to the control strain, indicating a lower sensor concentration than in wild-type at the plasma membrane.

In conclusion, mutations of a tyrosine to serine (Y60S) within a predicted amyloid-like motif in the Wsc1 CRD lead to loss of clustering and a more network-like distribution of the sensor in the plasma membrane. The Wsc1_{Y60S} mutant showed a growth impairment and reduced stress response similar to cysteine mutants investigated in the previous chapters, although slightly less severe.

3.4 Identification of Wsc1 interaction partners

The Wsc1 sensor forms microcompartments for example at the bud-neck or as distinct clusters in the lateral membrane which have been characterized in the previous chapters. Within these microcompartments Wsc1 has been postulated to form a protein complex called the “Wsc1 sensosome”, where the Wsc1 clusters might recruit downstream signaling components like Rom2 or Rho1 (Heinisch *et al.*, 2010). Previous studies by Wittland, 2012 identified for example Wsc1, Wsc2 and Rom2 as interaction partners of Wsc1. Potential regulators or additional targets of Wsc1 have not been reported yet. Therefore, a large-scale survey to identify potential further interaction partners of Wsc1 was performed here.

3.4.1 A large-scale search for Wsc1 interaction partners using BioID reveals numerous potential interaction partners

Among the various large-scale approaches to identify interaction partners of a protein within the complete proteome of a cell, Roux *et al.*, 2012 developed a system they called “proximity-dependent biotin identification” (BioID). The method is based on the BirA biotin protein ligase of *Escherichia coli* with an R118G mutation (called BirA*) which leads to unspecific - or “promiscuous” - ligation of biotin from biotinoyl-5'-AMP to all proteins in a proximity-dependent fashion. Therefore, BirA* fused to the protein of interest leads to biotinylation of proteins in close proximity, which can be identified by biotin affinity capture and mass spectrometry. In this study, yeast optimized BirA* was fused to Wsc1 to create the strains HCK36-1B (*MATa WSC1-BirA**) and HCK36-9B (*MATalpha WSC1-BirA**) as described in Figure 2.1. Together with a wild-type control strain (HD56-5A) crude extracts of 500 ml culture grown in rich medium containing additional 50 μ M biotin were prepared, mixed with streptavidin-coated magnetic beads and applied to a magnetic column. Biotinylated proteins were purified as described in section 2.2.4.5. Figure 3.10 A presents an example of the proteins purified from a crude extract prepared from strain HCK36-1B and no protein is detected by SDS-Page after five washing steps. Furthermore, a second elution step also did not contain detectable amounts of protein. The eluted samples of all three strains contained protein detectable after staining with Coomassie blue, but a similar number of bands appeared in the negative control prepared from HD56-5A . (Figure 3.10 B).

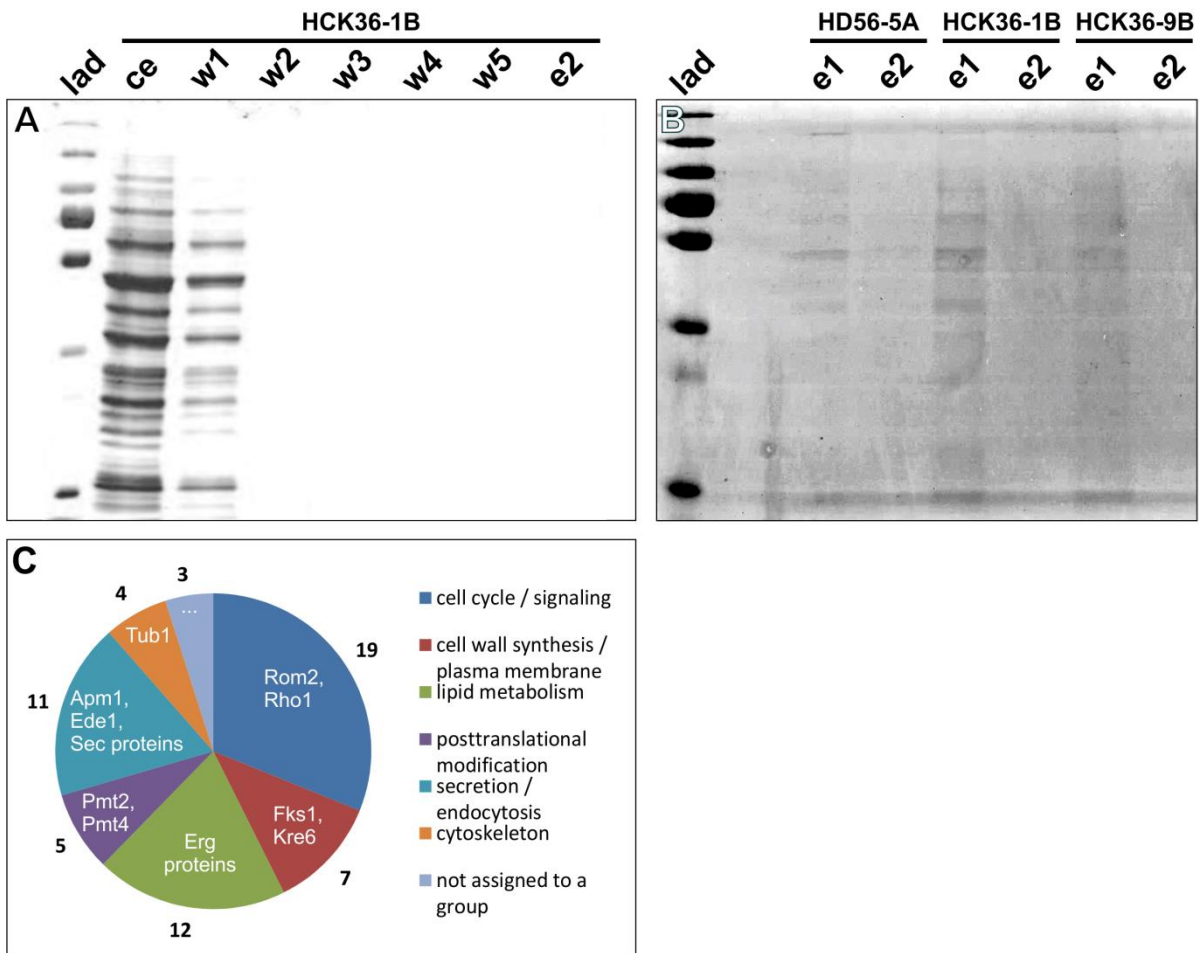


Figure 3.10: Identification of Wsc1 interaction partners by proximity-dependent biotin identification (BioID). The BirA* fusion strains HCK36-1B (*MAT α WSC1-BirA**) and HCK36-9B (*MAT α WSC1-BirA**) and the wild-type control strain HD56-5A were used in this analysis. **A.** Coomassie-stained SDS-PAGE of different protein samples during the biotin affinity capture from HCK36-1B. lad: molecular weight standard as listed in 2.1.6, ce: crude extract, w1-w5: washing steps 1-5, E2: second elution step. **B.** Coomassie-stained SDS-PAGE of protein samples after biotin/streptavidin-dependent purification. lad: prestained protein ladder plus for size comparison, e1: first elution step, e2: second elution step. **C.** Proteins identified in the BioID experiment by mass spectrometry after MASCOT search. Proteins were assigned to the functional groups as indicated and prominent examples of each group are mentioned. For a full list and information on protein functions consult chapter 6.2 in the supplementary. The results mark the summary of two independent experiments.

The protein samples of all three strains were then analyzed by mass spectrometry to identify the peptide sequences in the isolated protein samples in two independent samples, each. The detected peptides were then investigated by the MASCOT search engine to assign them to proteins in the database. The negative control HD56-5A without the BirA*-tag already

contained a large amount of different proteins. Among these were many nuclear proteins such as elongation factors, helicases, RNA/DNA polymerases, histones, histone-modifying enzymes and also ribosomal proteins. Furthermore, a lot of highly abundant proteins such as actin, glycolytic enzymes or general transport proteins were found. Most of these proteins were also found in the BirA* strains HCK36-1B and HCK36-9B and were therefore excluded from further analysis. The remaining proteins were grouped depending on their cellular functions in cell cycle/signaling, cell wall/plasma membrane, cytoskeleton, lipid metabolism, posttranslational modification, secretion/endocytosis or no assignment. A complete list of 61 identified proteins is found in the supplementary chapter 6.2. while short overview of proteins among the different categories is found in Figure 3.10 C.

Among the signaling proteins, Rom2 und Rho1 as potential parts of the Wsc1 sensosome were identified. Rom2 was already identified as an interaction partner of Wsc1 and serves as a positive control in this experiment. Further proteins in this category were for example Cdc7 and proteins related to autophagy. Among the cell wall/plasma membrane-related proteins Fks1 and Kre6 have been found as proteins involved in cell wall biosynthesis. Tub1 and the potential microtubule-associated protein (MAP) MHP1 were found among the cytoskeleton proteins and among the lipid metabolism proteins, mostly Erg proteins involved in the ergosterol biosynthesis were identified. Enzymes for the posttranslational modification of proteins that were also identified in this differential screen were Pmt2 and Pmt4, which were already shown to act as protein-O-mannosyl-transferases for Wsc1 (Lommel *et al.*, 2004; Hutzler *et al.*, 2008). Among the proteins related to secretion or endocytosis, the endocytic adaptor Apm1 which is involved in clathrin-dependent endocytosis was found. Further proteins in this category were Ede1, a scaffold protein in the formation of endocytic sites and Sar1, a GTPase of the ARF family involved in ER to Golgi transport. Furthermore, several proteins of the Sec family involved in secretion were among the list. It should be noted, that only Apm1 and Sar1 were found in both independent analyses so that further confirmation as interaction partners for all proteins on the list is necessary.

4. Discussion

4.1 At least one cell wall integrity sensor is needed for cell viability

In *Saccharomyces cerevisiae*, five plasma membrane-spanning sensors have been shown to be involved in cell wall integrity signaling. Out of these, deletions of *WSC1* and *MID2* show the most severe cell wall phenotypes (Rajavel *et al.*, 1999; Straede and Heinisch, 2007) and the three remaining sensors *Wsc2*, *Wsc3* and *Mtl1* seem to be less important. (Verna *et al.*, 1997; Ketela *et al.*, 1999). If a deletion of the two most important sensor genes is still viable and the other sensors do not show rigorous phenotypes, the question arises whether sensing cell wall stress may only be important under stress conditions or if *Wsc2*, *Wsc3* and *Mtl1* may serve as a backup and can functionally take over the stress response when *Wsc1* and *Mid2* are not present.

Unpublished results from our laboratory (Jürgen Heinisch, personal communication) showed that cells lacking all five cell wall integrity sensors are not viable and at least one sensor is needed for the cell to survive. These results indicate that activation of the cell wall integrity signaling cascade by its sensors is not only needed for stress response but also under normal growth conditions and for physiological functions. Wilk *et al.*, 2010 could show that *Wsc1* and *Wsc2* localize at the bud neck after actomyosin ring constriction starts and the colocalization studies in this work indicate that *Wsc3* concentrates at the bud neck as well (data not shown). One important function for the *Wsc*-type sensors under normal growth conditions could therefore be to guarantee proper septum formation during cytokinesis. As other components of the cascade like *Rom2*, *Rho1* and *Pkc1* are found at the bud-neck as well, they all could form a “sensosome” complex that mediates proper cell wall formation and prevents cell lysis during mitosis (Andrews and Stark, 2000; Heinisch *et al.*, 2010).

Results obtained in a bachelor thesis by Dennis Schöttelndreier may indicate, that cells expressing only *WSC2*, *WSC3* or *MTL1* are also dead or at least hardly survive. Single sensor genes were then introduced into an inducible quintuple sensor deletion strain, where *WSC2* and *MID2* are expressed under the conditional *GAL1/10* promoter (Figure 3.1) to test their ability to fulfill CWI signaling functions. Overexpression from multicopy vectors was chosen to ensure that the amount of sensors is not limiting. The results indicate again, that the cells

do not grow if none of the five sensor genes is expressed. Under normal growth conditions, *WSC1*, *WSC2* and *MID2* were able to rescue the cells, while the strain only expressing *WSC3* needed additional osmotic stabilization in order to grow. *MTL1* on the other hand was not able to rescue the lethality even though it was expressed from additional gene copies. Although the actual Mtl1 protein amounts in these cells were not investigated in this strain, these results indicate that Mtl1 may not directly sense cell wall stress like the other sensors but activate the cell wall integrity signaling cascade under different conditions. Recent studies link Mtl1 to the oxidative stress response and programmed cell death (Vilella *et al.*, 2005; Petkova *et al.*, 2012; Jin *et al.*, 2013), which also requires additional components of the CWI cascade such as Rom2 and Pkc1. Although Mtl1 has the same protein domain structure as Mid2 (Rajavel *et al.*, 1999; reviewed in Kock *et al.*, 2015), its function seems to be to sense oxidative stress under conditions that require CWI pathway activation without actually sensing cell wall damage. As several CWI pathway components have been described to be involved in various cellular responses, Mtl1 could have evolved to a more specialized function rather than being a backup sensor among the relatively high number of five similar sensors that activate the CWI cascade.

Interestingly, when *WSC2* and *MID2* are overexpressed and *WSC1* is additionally expressed from a multicopy vector, the cells show strong growth impairment in comparison to a strain that only overexpresses *WSC2* and *MID2*. Although one would maybe expect that the cells grow better when an additional sensor is reintroduced it seems as if the overexpression of *WSC1* from the additional gene copies has a harmful effect on the cells. Lodder *et al.*, 1999 revealed that cells overexpressing *WSC1* are inhibited in growth compared to wild-type expression levels. Growth inhibition was also observed with a *WSC1* truncation not containing the sequence encoding the sensors cytoplasmic tail and it was also the case if the sensor was overexpressed in a *wsc1-3Δ* triple deletion, although less severe. This underlines that *WSC1* overexpression is lethal at certain amounts and is also the reason, why *WSC1* was not used in the construction of the conditional strain here. One idea could be that additional sensors titrate other signaling factors. The growth impairment also occurs while expressing *WSC1* sensors lacking the intracellular part, that is important for signaling and endocytosis (Lodder *et al.*, 1999; Vay *et al.*, 2004; Piao *et al.*, 2007; Wilk *et al.*, 2010), so that the growth

impairment is most likely related to the extracellular part or the transmembrane domain and can't be referred for example to endocytosis. The limited o-mannosylation for other cell wall proteins by Pmt2 and Pmt4 as a result of reduced mannose or enzyme availability (*Lommel et al.*, 2004) or decreased plasma membrane diffusion may be reasons but are highly speculative since overexpression of Mid2 doesn't result in a similar phenotype (Figure 3.1). In general, the results indicate that at least one cell wall integrity sensor is necessary for the cell to survive, while Wsc1 and Mid2 are the most important ones during stress response. Mtl1 does not seem to function in sensing cell wall damage and seems to have a more specialized role for CWI cascade activation upon oxidative stress. Given that cells are able to survive with only one sensor and are dead without functional sensors, the strain HOD188-7D with *WSC2* and *MID2* expression controlled by the inducible *GAL1/10* promoter provides a useful tool to investigate functionality of single sensor constructs in the future, because the "to be or not to be"-phenotype is easier to observe than slight phenotypic differences on cell wall stress media in strains with all other sensors still present.

4.2 Wsc1 may interact with a number of intracellular proteins

The results showed that Wsc1 forms a distinct microdomain in the plasma membrane that depends on its cysteine-rich domain. But as a stress sensor its function requires the interaction with other signaling components for signal transduction and furthermore it may require stress- and cell cycle-dependent regulation. Cluster formation of Wsc1 requires interaction with other Wsc1 sensors, but bimolecular fluorescence complementation suggests that heterologous clusters with Wsc2 are also possible (Wittland, 2012). It has been shown by yeast two hybrid analysis which were confirmed by bimolecular fluorescence complementation that Wsc1 and Mid2 interact with the GEF Rom2 (Philip and Levin, 2001; Wittland, 2012). Furthermore, the endocytosis of Wsc1 is mediated by interaction with Sla1, a component of the clathrin-dependent endocytosis machinery (Piao *et al.*, 2007). Vay *et al.*, 2004 showed the existence of a phosphorylation region between S319 and S323 but did not identify kinases and phosphatases required for this regulation. A possible kinase could be the Cdc28 subunit of the cyclin-dependent kinase CDK, which was found as a Wsc1 interaction partner by Wong *et al.*, 2007 in a genome-wide screen for interaction. Using the BioID

method (Roux *et al.*, 2012) a number of proteins could be identified after differential mass-spectrometry analysis here.

First of all, the use of a negative control strain without the BirA* biotin ligase revealed that although the sample was expected to be empty, still many proteins were identified. Most of them were nuclear proteins like histones or the complete transcriptional machinery like polymerases and helicases, but also lots of housekeeping genes like glycolytic proteins were found. The initial explanation would be an intrinsic biotinylation mechanism of yeast for these proteins but such a mechanism especially for these proteins has not been described yet. Most likely, the experimental conditions are the reason for the high number of false positive proteins. It should be noted that the experimental material used was designed for protein amounts of up to 20 pmol and the equivalent of protein from 10^7 cells. In this experiment, 100 up to 500 times more protein was applied to the column because the suggested protein amount didn't produce detectable amounts of proteins for the mass spectrometry. The magnetic beads have a size of 50 nm and it may be possible that non-biotinylated proteins may clog between them with so much excess protein present. It also seems plausible that the most abundant proteins in the cell show an overrepresentation within this complex sample.

Because of this experimental design, every protein that was also identified in the negative control strain had to be sorted out. After that a relatively long list of 61 proteins remained. It seemed unlikely that all of these proteins are interaction partners of Wsc1 and as a consequence they were grouped according to their cellular function. Interaction partners that are relevant for signaling have most likely also a role in the cell cycle or signaling, for example as a kinase or phosphatase. Within this group, Rom2 and Rho1 were identified as potential interaction partners. Because the Wsc1-Rom2 interaction was already described and Rho1 may be activated by Wsc1-bound Rom2 within the sensosome protein complex (Ozaki *et al.*, 1996; Philip and Levin, 2001; Heinisch *et al.*, 2010), this may be a proof for functionality of the method and serve as positive control.

Among the possible kinases for Wsc1 regulation are Bub1 and Cdc7, while possible phosphatases could be Mih1 and Pps1. Bub1 and Cdc7 are both cell cycle-dependent kinases (Roberts *et al.*, Hoyt 1994; Sclafani and Jackson, 1994) that could possibly inactivate Wsc1 at

the bud-neck after the proper secondary septum formation is complete (Wilk *et al.*, 2010), but both are predominately active in the nucleus. The Mih1 phosphatase acts on phosphorylated Cdc28 (Sia *et al.*, 1996), a possible kinase for Wsc1. Pps1 is another phosphatase that is also involved in cell cycle regulation, but most likely also in DNA synthesis (Ernsting and Dixon, 1997). Interestingly, the two autophagy-related proteins Atg2 and Atg9 that are plasma membrane proteins involved in autophagic vesicle formation were also identified as potential interaction partners (Reggiori *et al.*, 2004). This link may show another possible role for Wsc1 in autophagy, as publications found the requirement of Wsc1 and other cell wall integrity components for this process (Mao *et al.*, 2011).

Among the proteins involved in cell wall synthesis, the glucan synthase Fks1 showed up as a possible interaction partner. Direct activation of Fks1 in areas of cell wall damage would make sense and these data indicate a close proximity of Wsc1 and Fks1 in the membrane which is not confirmed for example by colocalization data yet. This proximity may limit the response-time for synthase activation upon cell wall stress, since diffusion distance for activated Rho1 would be reduced (Qadota *et al.*, 1996). Pma1 showed up as the protein with the highest score and peptide number. An interaction between both proteins would contradict the hypothesis, that Wsc1 forms a distinct plasma membrane domain that does for example not overlap with the membrane compartment occupied by Pma1. But as Pma1 is one of the most abundant proteins in the plasma membrane (Ambesi *et al.*, 2000) it is likely that Wsc1 molecules not bound in clusters prior to and during endocytosis may get in close proximity to Pma1 molecules.

Among the remaining candidates are proteins found in the formation of endocytic patches and vesicles, as for example the early coat-phase proteins Ede1, the clathrin light chain Clc1 and the adaptor Apm1 (Weinberg and Drubin, 2012), which is the only protein in the analysis that showed up in both repeats of the experiment. It was shown that physical interaction of Wsc1 with Sla1 is necessary for its endocytosis (Piao *et al.*, 2007), but the existence of further interaction with endocytic components is highly possible. The high number of endocytic components in this screen fortify the high turnover rate of Wsc1, that was discussed before (Wilk *et al.*, 2010).

With Erg1, Erg11, Erg28, Erg3 and Erg5, five proteins of the ergosterol biosynthesis were

identified as potential interaction partners. Together with other components of the lipid metabolism, this high number would suggest direct influence of Wsc1 on the membrane composition. Interestingly, Wsc1 has been considered as a “cell surface integrity” sensor before and this would involve sensing the lipid composition as well. Several studies show an influence of CWI components on lipid metabolism, for example the Rom2-dependent phosphorylation of Elo2 regulating fatty acid metabolism providing the precursors for lipid side-chains or the involvement in phosphoinositide metabolism (Audhya and Emr, 2002; Olson *et al.*, 2015). Furthermore, Wsc1 was shown here to localize in a distinct plasma membrane domain, the MCW, with a possible unique lipid composition that would require lipid modifying enzymes, although many of the here identified lipid metabolism proteins do not localize at the plasma membrane (Mo *et al.*, 2004).

That the Wsc1-BirA* fusion protein does not have to localize at the plasma membrane to biotinylate interaction partners is shown by proteins that are involved in the posttranslational modification of Wsc1 in the ER-Golgi-network and was also described for the method in Roux *et al.*, 2012. The protein-mannosyl-transferases Pmt2 and Pmt4 have been shown to be important for adding mannose chains to the serine/threonine-rich region of the protein (Lommel *et al.*, 2004; Hutzler *et al.*, 2008) which marks another proof that interaction partners of Wsc1 are biotinylated in this experimental design. The functionality of this protein while still in secretion is most likely the reason why many proteins that are involved in secretion and lipid metabolism showed up in this screen, as posttranslational modification of secreted proteins and lipid turnover are dominated by enzymes associated with ER and Golgi. Since Wsc1 passes through these organelles, it is likely to label intrinsic proteins. Clearly, these proteins would not be directly related to cell surface signaling and the effector proteins this screen was aimed at.

In general, this large scale screen is limited by many factors. These involve for example the experimental design that was discussed above leading to a long list of false positives that have to be sorted out. From the remaining proteins only few proteins are likely to be interaction partners and have to get investigated by further protein-interaction screens like yeast two hybrid or coimmunoprecipitation. Reasonable proteins for this extensive studies among the 61 proteins found in this study would for example be Atg2/Atg9, the kinases and

phosphatases Bub1, Cdc7, Mih1 and Pps1, the glucan synthase Fks1 and the endocytic adaptor Apm1. In contrast to yeast two hybrid analyses, a problem of the BioID method is its limited capability to detect weak interactions like the “hit and run” phosphorylation of a kinase (Roux *et al.*, 2012), which should be identified in this screen. Also, potential proteins that are part of the membrane compartment occupied by Wsc1 (MCW) should be identified, but as whole cells lysates of growing cells were used, a huge fraction of the potential detected interactions occur at the bud neck, which forms a tight and crowded compartment with many proteins involved. To improve the specificity of this approach, one may want to arrest the cells in the G1 phase of the cell cycle where the budding process hasn't started in future experiments. This can be either achieved by alpha-factor synchronization or the use of thermosensitive alleles of cell division cycle mutants such as Cdc28 (Breedon, 1997; Hartwell *et al.*, 1970)

4.3 The Wsc1 cell wall integrity sensor forms a distinct plasma membrane domain

A set of studies investigated the existence of different domains in the yeast plasma membrane. Three distinct plasma membrane domains have been described in yeast named after their constituent proteins: The MCC, coinciding with membrane invaginations called eisosomes, the MCP and the MCT (Malinska, 2004; Grossmann *et al.*, 2007; Berchtold and Walther, 2009). By contrast, Spira *et al.*, 2012 showed that most membrane proteins reside in specific domains, ranging from patch-like to network-like patterns (Figure 1.3).

This study revealed that the Wsc1 patches do not overlap with Mid2 which in this investigation showed a more network-like than homogenous distribution (Figure 3.2). Their different localization patterns could correspond to the different functions of both sensors. Mid2 seems to be more important for general growth and stress response regarding to its network-like and more homogenous localization. Wsc1 is more important during polarized growth as it localizes at the bud-neck and bud-tip (Straede and Heinisch, 2007; Wilk *et al.*, 2010) and the clusters in the lateral membrane seem to form at sites of physical cell wall damage, as the fluorescence signal and patch size in the lateral membrane increases upon stress or treatment with the cell wall damaging enzyme zymolyase (Heinisch *et al.*, 2010;

Wittland, 2012). It was still unclear how these different localization patterns occur, albeit Wsc1 and Mid2 have a similar domain structure (Rajavel *et al.*, 1999; reviewed in Kock *et al.*, 2015). Spira *et al.*, 2012 proposed an influence of the transmembrane domain on lateral protein segregation caused by possible lipid-protein-interactions. The transmembrane domains of Mid2 and Fet3 tagged with fluorophores showed a network-like localization with strong overlap with the MCP protein Pmp1. For this study, the predicted transmembrane domains of Wsc1 and Mid2 were exchanged in order to see, whether their localization patterns depend on this single protein domain. The results did not reveal any change in polarized or lateral membrane localization for both hybrid sensors (Figure 3.2), indicating that other protein domains are more important for proper membrane distribution of these two sensors. Several studies on chimeric CWI-sensor localization have been done in the past years. For example, Wsc1 sensors with an elongated serine/threonine-rich region from Mid2 and *vice versa* have been used to determine the localization of single sensor molecules, revealing the spot-like/clustered distribution for Wsc1 and a more network-like distribution for Mid2 (Heinisch *et al.*, 2010; Alsteens *et al.*, 2012). As these findings are consistent with live cell fluorescence microscopy, it can be assumed, that the elongation doesn't influence the localization at all. A chimeric sensor with the extracellular part of Fus1 and the transmembrane domain and intracellular part of Mid2 (Fus1-Mid2-GFP) was used to screen for mutants affecting the trafficking from the ER to the Golgi to the plasma membrane and showed a similar localization pattern than wild-type Mid2. The authors proposed then that the intracellular domain determines localization. (Proszynski *et al.*, 2004; Proszynski *et al.*, 2005). Furthermore, Straede and Heinisch, 2007 also showed that the intracellular part determines the sensor localization by making chimeric sensor constructs of all different Wsc1 and Mid2 domains and later it was specified that the endocytosis signal in the intracellular domain is an important determining factor (Piao *et al.*, 2007; Wilk *et al.*, 2010). In addition, as discussed in chapter 4.4, the cysteine-rich domain of the Wsc-type sensors is important for the spot-like distribution because there is no cluster formation without it (Heinisch *et al.*, 2010). It should be noted, that full-length Fet3 in the studies of Spira *et al.*, 2012 did also show a different localization pattern which did not overlap with the MCP domain and that deletion of the phosphatidylserine synthase Cho1 also strongly influenced the Mid2

localization. This supports the notion that the transmembrane domain is only one of several intrinsic (e.g. different protein domains) and external (e.g. the lipid composition) factors for plasma membrane protein localization.

As described before, Spira *et al.*, 2012 found a large overlap between Mid2 and the MCP domain. In addition it was shown here that the Wsc1 patches are distinct from this Mid2 network while their size of 250nm up to 300nm (Heinisch *et al.*, 2010) matches roughly with the length of the MCC/eisosome plasma membrane invaginations of 250nm, which are also distinct from the MCP (Stradalova *et al.*, 2009). This lead to the question if one of the sensors with a spot-like distribution could be matched with eisosome patches by colocalization analysis which was not the case for any CWI sensor (Figure 3.3). As already described did Mid2 show a large overlap with the MCP domain, while Wsc2 and Wsc3 showed a mediocre overlap with Pma1 (Figure 3.4).

Despite this, the most interesting findings were that Wsc1 clusters did not show any overlap with the three classical domains MCC, MCP and MCT and therefore most likely form their own distinct plasma membrane domain. Accordingly, this microcompartment is suggested to be named “membrane compartment occupied by Wsc1” (MCW). One can speculate that this domain exists because the large and distinct Wsc1 clusters limit the free diffusion of other plasma membrane proteins in that particular area leading to a lateral segregation, although further mechanisms that lead to lateral segregation of proteins like the lipid environment were not part of this study. It is possible but not necessary that Wsc1 clusters also influence the local lipid environment by protein-lipid interaction and *vice versa* as observed for lipid raft proteins (Kusumi *et al.*, 2005).

It should be noted that the method of how the colocalization experiments were designed produces an inevitable and relatively high error margin. First of all, the fast acquisition of a full cell z-series doesn't allow to monitor dynamic movement of proteins in the plasma membrane. Although the eisosome patches are stable over time (Stradalova *et al.*, 2009; Olivera-Couto *et al.*, 2011) and Spira *et al.*, 2012 showed that the distribution patterns formed by the plasma membrane proteins are also stable, they also found constant movement within these patterns as documented by short time-lapse TIRF microscopy movies. Different proteins might randomly overlap at different time points. Preliminary

results using TIRF microscopy indicate that at least Wsc2 does indeed show dynamic movement (data not shown) which might also be the case for the other Wsc-type sensors. Furthermore, some of the fluorophores used in this work influence the counted patch number in this experiment. Especially fluorophores with a red emission range like mCherry or DsRed from corals of the *Discosoma* genus are known for their significantly longer maturation time compared to GFP (Terskikh *et al.*, 2002). This is visible in the colocalization control experiments with Pma1-GFP and Pma1-dsRed, where the GFP maturation in the bud is already completed while the red fluorescent signal is barely noticeable (Figure 6.1 A). DsRed is also known to form tetramers which then also affect the fusion protein itself by forming artificial complexes (Baird *et al.*, 2000). Pma-DsRed was used for this study because *PMA1* is an essential gene and its fusion constructs tend to be non-functional or lethal. The strain HSK82-1A used in this study only showed a slight growth impairment while fusion to other fluorophores like for example Citrine or ECFP appeared to be lethal in haploid strains.

It should be noted that in control experiments the percentage of colocalized spots for Pma1-GFP and Pma1-DsRed for example was surprisingly low (around 20%, Figure 6.1), most likely because of the problems described above. Therefore, the additional parameters of PCC and MOC were also determined and colocalization was only assumed, if the three values matched the values of the controls.

Interestingly, all three Wsc-type sensors distributed in spot-like patterns, but while Wsc1 didn't show any overlap with the MCC, MCP and MCT, Wsc2 and Wsc3 overlapped moderately with the MCP. The hypothesis for Wsc1 was, that it does not mix with other domains because of its cluster size. Because Wsc2 and Wsc3 have significantly lower expression levels than Wsc1 (Wsc2 protein levels are only 10% of Wsc1 (Wilk *et al.*, 2010) and Wsc3 fluorescence is only observable with a triple-GFP fusion), it is possible that their clusters are not as big as for Wsc1 and therefore mix with other domains. Yet, the question arises if heterologous Wsc-sensor clusters do occur and where the clusters form in general. In the colocalization analysis of this work, Wsc1 and Wsc2 patches only showed a small amount of overlap in the lateral membrane (Figure 3.2) although results of Wittland, 2012 suggested a heteromeric interaction of the two sensors at sites of polarized growth. The size of the STR in Wsc1-3 increases continuously so that their extension into the cell wall probably varies

(Figure 1.2). As discussed in Kock *et al.*, 2015 one reason for the evolution of three different Wsc-type sensors could therefore be to detect cell wall perturbances in different layers of the cell wall. Given the hypothesis that the clusters form at sites of physical cell wall expansion, heterologous clusters would therefore only occur in regions of multilayered damage in the lateral membrane and at the bud neck.

4.4 Wsc1 sensor clustering may be important for protection from endocytosis but not for signaling

The Wsc1 clusters in the lateral plasma membrane are distinct microdomains that may form at sites of physical cell wall damage. This domain formation and lateral segregation from other domains does not occur via their transmembrane domain but is most likely determined by the intracellular endocytosis signal and the headgroup known as “cysteine-rich domain” (CRD). Previous work demonstrating the importance of the CRD of Wsc1 for sensor clustering was confirmed by the mutant analyses performed herein (Heinisch *et al.*, 2010) and bimolecular-fluorescence complementation analysis in this study revealed that sensor interaction at the bud-neck is strongly decreased or lost completely in Wsc1 cysteine mutants (Figure 3.6). These results all underline that Wsc1 interaction and cluster formation is achieved by its CRD headgroup. In addition, the CRD-mutated sensors show a phenotype comparable to a *wsc1* deletion and are not able to activate the cell wall integrity signaling cascade as shown by quantification of the phosphorylation level of the downstream MAP kinase Slt2 (Heinisch *et al.*, 2010; Wilk, 2010). Fluorescence microscopy also revealed that the mutated sensors mostly accumulate in the vacuole and almost no signal is found in the plasma membrane except for sites of polarized growth (Figure 3.6). These results indicate that clustering may be important for sensor function and that the non-functional sensor is therefore targeted to the vacuole for degradation.

The internalization of the sensor was blocked by deleting the *END3* gene which is involved in the early internalization step of the endocytosis (Bénédicti *et al.*, 1994). The results showed that the mutated sensor distributed more evenly in the plasma membrane and did not accumulate in the vacuole anymore. In addition, the deletion of *END3* fully restored the pathway induction in cells with mutated Wsc1 sensors (Figure 3.7). It has already been

described in Wilk *et al.*, 2010 that Wsc1 sensors do not undergo endocytosis in this mutant and the protein amount at the surface stays the same even if the translation of new protein is abolished by cycloheximide treatment. The sensor also distributed more evenly in the plasma membrane and the concentration at sites of polarized growth was lost. The results here showed, that although the cluster number seemed to be increased in the CRD/*END3* mutants, they were not as distinct as in the wild type and showed a tendency to form networks indicating that sensor clustering is still limited in the CRD mutants even though they are located at the cell surface.

In contrast to the CRD mutants in an otherwise wild-type background, the cell wall integrity pathway was fully activated when the mutated sensors are not internalized in an *end3* deleted strain (Figure 3.7 C). In this experiment, the *end3Δ wsc1Δ* double deletion also showed a full stress response. These data and the fact that an *END3* deletion shows sensitivity to various cell wall stresses (Wilk *et al.*, 2010) suggest that pleiotropic effects contribute to the signaling process in this mutant. It doesn't seem surprising that a mutant that blocks the complete endocytosis in a cell perturbs its metabolism and ability to react to stress conditions. Thus, the density of other CWI sensors, for example Wsc2 and Wsc3, at the cell surface is probably also increased in such mutants, causing a higher level of pathway activation. Pleiotropic effects may also have a more indirect consequence such as perturbing the crosstalk between CWI and other signaling pathways, which affect Slit2 phosphorylation (Rodriguez-Pena *et al.*, 2010). Rom2 for example is also involved in phosphoinositide metabolism and is also activated by the membrane bound TOR2 kinase complex in response to nutrients and cell cycle-dependent polarization of the actin cytoskeleton (Schmidt *et al.*, 1997; Audhya and Emr, 2002). Rho1 on the other hand is also involved in polarized secretion for cell surface extension (Guo *et al.*, 2001) which may be influenced in endocytosis mutants as well. Pkc1 serves as an effector for the Pkh1 and Pkh2 kinases that have an overlapping function for cell integrity and are involved in eisosome regulation (Inagaki *et al.*, 1999; Walther *et al.*, 2007; Luo *et al.*, 2008). One of the postulated functions of the eisosomes is to act as a membrane reservoir for rapid membrane extension under surface stress conditions (Kabeche *et al.*, 2015) and one can speculate that the correct membrane composition and amount of phospholipids in the membrane is most likely also strongly disturbed in cell lacking

endocytosis. Several of these factors may contribute to pleiotropic Slt2 activation in the *end3* mutant but as many signaling components may be involved, it is hard to eliminate all the artificial contributing influences. In conclusion, given these pleiotropic effects an *end3* deletion clearly is not the best choice to test the effects of the concentration of a specific sensor in the plasma membrane on its signaling capacity.

To eliminate the pleiotropic effects, the best approach would be to specifically only block the Wsc1 endocytosis. Piao *et al.*, 2007 showed that the Wsc1 amino acids 244-348 (NPFDD) are necessary for Sla1 binding and that the Wsc1 endocytosis is blocked when the motif is mutated. The sensor then distributes more homogeneously in the plasma membrane and is not concentrated at sites of polarized growth anymore (Piao *et al.*, 2007; Wilk *et al.*, 2010). An NPF to AAI mutation was introduced here into the cysteine-rich domain mutants of Wsc1 to block only Wsc1 at the cell surface and to investigate the role of the clustering for sensor function. As expected, the sensor then seemed to distribute more evenly in the plasma membrane similar to mutants with only the NPF/AAI mutation. But looking at the top section of cells revealed that the distribution of Wsc1 was not spot-like anymore but tended to show a more network-like distribution (Figure 3.8 C). To quantify this, a software plugin that is able to calculate shape and area of a fluorescence patch was used to perform an integrated morphometrics analysis. This analysis showed that the overall size of Wsc1 patches in the CRD-mutants was strongly increased and their shape changed from almost circular to oblong and branched structures (Figure 3.8 D+E). This indicates that that localization pattern switched indeed from spot-like to network-like and confirms again, that the formation of the spot-like clusters requires the cysteine-rich domain. It still needs to be elucidated whether this clustering is necessary for the signaling or not. Serial drop dilution assays and quantification of pathway activation by measuring Slt2 phosphorylation levels revealed that the CRD-mutant sensors with NPF/AAI mutation in contrast to sensors with only CRD mutation almost grow like wild-type cells and are fully able to activate the cell wall integrity pathway (Figure 3.8, Heinisch *et al.*, 2010; Wilk, 2010). The original hypothesis on sensor clustering postulates, that the sensor clustering is needed for concentration of signaling components to amplify the stress response signal by forming a “sensosome” similar to sensing and signal amplification in bacterial chemotaxis (Heinisch *et al.*, 2010; Tu, 2013). As

suggested by the fluorescent images, it would be possible that the amount of sensors at the cell surface is increased when its internalization is blocked. The increased amount of sensors per area could partially mimic the clustering and abrogate the phenotype shown by CRD mutant sensors. But the fluorescence intensity per area was not significantly increased in the CRD/NPF mutants as shown by the integrated morphometrics analysis (Figure 3.8 E). Although these data surely need further confirmation it seems as if not the clustering but the general amount of sensors at the cell surface determines the cells capability to respond to stress conditions.

If the level of stress response is limited by the sensor amount at the surface and not by the sensor's capability to form clusters (Figure 4.1 upper row), the question arises why sensor clustering is needed for the cell. The cysteine-rich domain mutants most likely show a phenotype comparable to a *wsc1* deletion strain because only a small fraction of the sensor is found at the plasma membrane while the majority accumulates in the vacuole (Figure 3.6). In cells with blocked endocytosis, on the other hand, no phenotype is observable even if Wsc1 does not form clusters. This could mean that clustering serves as a protection from endocytosis and is thus compensated when endocytosis is blocked by mutation. Wsc1 is presumably a sensor with a very rapid turnover and recycling which may explain its accumulation at sites of polarized growth (Piao *et al.*, 2007; Wilk *et al.*, 2010). The clustering could be a necessary sensor function to limit this rapid turnover for two reasons (Figure 4.1 middle and lower row): First, the clusters have been shown by atomic force microscopy to be limited to confined areas and their size even increases upon stress conditions (Heinisch *et al.*, 2010). They also do not seem to mix with markers for other plasma membrane domains making them a distinct microcompartment, the MCW (as discussed in chapter 4.3). This could limit the recruitment of proteins necessary for the formation of early endocytic sites like Ede1 or clathrin in this particular area of the compartment (Goode *et al.*, 2015). Furthermore, Sla1 is a protein that is involved in the formation of the endocytic coat in the late immobile phase of the endocytosis before the actin-myosin-driven ingression of the plasma membrane starts (Boettner *et al.*, 2011). Also, the physical interaction of Sla1 with the NPFDD endocytosis signal in the intracellular sensor domain is necessary for the internalization of the sensor (Piao *et al.*, 2007). As the endocytosis signal is located in the

middle of the intracellular domain in Wsc1 (see e.g. Figure 1.2) it may be inaccessible for Sla1 within a cluster to mediate the directed Wsc1 endocytosis. In contrast, the Rom2 interaction site is located at the very c-terminal end of the sensor and may be still accessible so that the sensor is still able to function in signaling (Vay *et al.*, 2004). It should be noted that this hypothesis is highly speculative as there are no studies on the folding of the intracellular domain of Wsc1. Alternatively, in the MCW, the tight arrangement of transmembrane domains may stiffen the membrane and prevent it from curvature that occurs during endocytic vesicle formation. Studies on membrane curvature revealed that some proteins show preferences for curved membranes and other proteins with many transmembrane domains seem to avoid curved membranes and influence the membrane stiffness (Aimon *et al.*, 2014).

Given this hypothesis, the membrane compartment occupied by Wsc1 (MCW) would be a cysteine-rich domain-dependent domain in the lateral plasma membrane to protect Wsc1 from endocytosis. This is a concept that has already been discussed for other plasma membrane domains as well. Although the first hypothesis for the membrane compartment occupied by Can1 or eisosomes stated, that they mark static sites of endocytosis in the plasma membrane (Walther *et al.*, 2006), it was later pointed out that internalization does not occur in this area and it rather forms a protective area for several plasma membrane proteins like Can1 or Tat2 to prevent their endocytosis (Grossmann *et al.*, 2008). Endocytosis of Can1 and Tat2 does still occur but it was later pointed out, that the proteins leave the protective area of the compartment to undergo endocytosis within the membrane compartment occupied by Pma1 (MCP, Brach *et al.*, 2011). In wild-type yeast cells, Wsc1 endocytosis does obviously also occur even though the cells are able to form clusters. The center of the clusters may be inaccessible for the endocytic machinery while endocytosis of Wsc1 may still occur at the edge of them, meaning the sensors are released from the cluster and the compartment to undergo endocytosis. A similar model has been proposed by Wilk *et al.*, 2010 for localization at sites of polarized growth where the sensor would be internalized by lateral diffusion away from the bud neck into an area competent for endocytosis. It should be noted here that there seems to be a high exocytosis/recycling rate for Wsc1 in these areas as well (Wilk *et al.*, 2010) and CRD-mutated sensors still accumulate in these areas (Figure

3.6). This might show that the amount of sensors needed in these areas for proper cell wall and septum formation is quite high and can only be maintained by a high recycling rate in addition to clustering.

Different results clearly show that the cysteine-rich domain and its conserved cysteine residues are needed for Wsc1 sensor clustering. But how the clustering is achieved on molecular level remains to be elucidated. Dupres *et al.*, 2011 showed by treatment of the cells with dithiothreitol (DTT) that disulfide bonds are required for clustering, but whether these are intra- or intermolecular remains unclear.

Edupaganti and Lipke (personal communication) identified a sequence motif within the cysteine-rich domain of Wsc1 that shows the potential to form amyloid-like protein aggregates (see Figure 1.4). These amyloids are insoluble protein aggregates that form *via* β -sheet interactions and are linked to various diseases like Alzheimer's but also have functional roles for example in microbial biofilm formation (Sawaya *et al.*, 2007; Garcia *et al.*, 2011; Alsteens *et al.*, 2012).

It was investigated here, whether the clustering of Wsc1 might be an amyloid-like protein aggregation by mutating the tyrosine residue at position 60 within the amyloid sequence to serine because TANGO analysis predicted a reduction in the aggregation potential from 41% to 2.63% for this amino acid exchange (Edupaganti and Lipke, personal communication). The life cell fluorescence microscopy and the integrative morphometrics analysis as already performed for the cysteine mutants revealed a reduction of clustering for this mutant which was about two-fold (Figure 3.9 C-D). In addition, preliminary results on the clustering of this mutant on single-molecule level using atomic force microscopy also show a strong decrease or complete loss of clustering (Alsteens and Dufrêne, personal communication), indicating an important role of the amyloid sequence for sensor clustering. Furthermore, the Y60S mutant showed a sensitivity to heat stress (37 °C) and Congo red and the phosphorylation of Slt2 was reduced to 70% of the wild type, also indicating a strong influence on sensor function. However, the reduction in clustering and the observed phenotype were less severe than in the C4,5A cysteine mutant or the *WSC1* deletion. The integrated morphometrics analysis suggests that the amount of sensor at the cell surface is strongly reduced (see Figure 3.9 E "average intensity") which is consistent with the atomic force microscopy data (Alsteens and

Dufrêne, personal communication). This could mean that the observed phenotype is most likely due to the reduced sensor amount at the surface and although the Y60S mutant still shows a signal in the plasma membrane and does not accumulate in the vacuole, the observations seem to be similar to mutants with mutated cysteine residues (Figure 3.6, Heinisch *et al.*, 2010; Wilk, 2010). The weaker effect in comparison to the cysteine-residue mutants may be explained by the fact that a single amino acid exchange in the amyloid motif may not completely abolish its β -aggregation potential, although the prediction by the TANGO algorithm has been shown to match the practical data almost completely (Fernandez-Escamilla *et al.*, 2004). While the Y60S mutation predicts a reduction in the aggregation potential from 41% to 2.63%, Y60R mutation would have reduced the potential to 0.19% and a Y64N mutation would also reduce the potential to 2.88% (Edupaganti and Lipke, personal communication), so that two amino acid exchanges may be more effective in this case. Therefore, a Y60R is currently investigated in our laboratory. In addition, two more motifs in the Wsc1 amino acid sequence show a potential to form amyloids. The first one is located in the serine/threonine-rich region at position 224-232 and shows an aggregation potential of 57% while another one is found in the intracellular part at position 368-372 showing an aggregation potential of 78,5%. Although these sequences have a higher predicted β -aggregation potential they were deemed less important in the light of the CRD mutants discussed above and were not further investigated due to time constraints in the preparation of this thesis. But an involvement of the other two motifs in clustering that may weaken the phenotype of the Y60S mutation cannot be excluded in this study.

As the Y60S mutation clearly does have an effect on sensor clustering and signaling it is highly possible that Wsc1 clusters are of amyloid nature. To match the definition of amyloid proteins several other criteria should apply to the Wsc1 clusters as well. Two of these criteria are that the aggregates should be stained by Congo red and Thioflavin S/T and that these dyes should inhibit the aggregation in higher concentrations (Garcia *et al.*, 2011). Attempts to demonstrate these features for Wsc1 clusters were not successful, so far. In future experiments, it would be interesting to see if it would also be possible to inhibit the clustering by treating the cells with short peptides containing the mutated amyloid motif or – *vice versa* – treatment of the mutant with short peptides containing the wild-type amyloid

sequence should restore the clustering capabilities as it was done in Garcia *et al.*, 2011. Also, if the Wsc1 amyloid sequence within the CRD would be exchanged with an already described amyloid motif for example from the human disease-associated A β protein (LVFFA), the Wsc1 clustering behavior shouldn't change as well (Rameau *et al.*, 2016).

If the Wsc1 clustering is achieved by amyloid-like protein aggregation dependent on the ASYFALY motif within the cysteine-rich domain, the function of the cysteine-residues needs to be elucidated. Intermolecular disulfide bonds may occur in cell wall proteins and even linkage to cell wall carbohydrates by cysteine residues may be possible (de Nobel *et al.*, 1990; Kollár *et al.*, 1997), so that the cysteines could therefore covalently link the sensor to the cell wall and other sensors. It is more likely that intramolecular disulfide bonds contribute to Wsc1 clustering and while Sawaya *et al.*, 2007 pointed out the importance of the steric zipper structure for β -amyloids, intramolecular disulfide bonds could stabilize the correct conformation within the CRD to govern the secondary structure of the amyloid β -sheets for correct protein aggregation or clustering (Figure 4.1 upper row). This is supported by the fact that the amyloid-forming sequence is located at a conserved position between the third and fourth cysteine-residue within the CRD of all three Wsc-type sensors (see Figure 1.4). Although the eight cysteine-residues are conserved in species like *Candida albicans*, *Ashbya gossypii*, *Aspergillus fumigatus*, *Schizosaccharomyces pombe* and *Kluyveromyces lactis*, similar amyloid sequences are only found in Wsc-type sensors in *K. lactis* (Heinisch *et al.*, 2010) and *C. albicans*, meaning that amyloid-like sensor clustering may be conserved in other fungi as well, but is hard to determine without further TANGO analysis.

If Wsc-type sensor clustering is achieved by amyloid protein aggregation, it may provide a new target for antifungal drugs. Components that abolish amyloid formation similar as shown for Congo red, Thioflavin or mutated amyloid peptides (Garcia *et al.*, 2011) could target all Wsc-type sensors simultaneously. Non-clustering Wsc1 mutants show phenotypes comparable to a deletion of the gene and cells lacking all three Wsc1 sensors show a significantly increased growth impairment in comparison to a single deletion (Verna *et al.*, 1997; Heinisch *et al.*, 2010). Paired with the decreased capability to form infectious biofilms in amyloid mutants as for example shown for Als5 in *Candida albicans* (Garcia *et al.*, 2011;

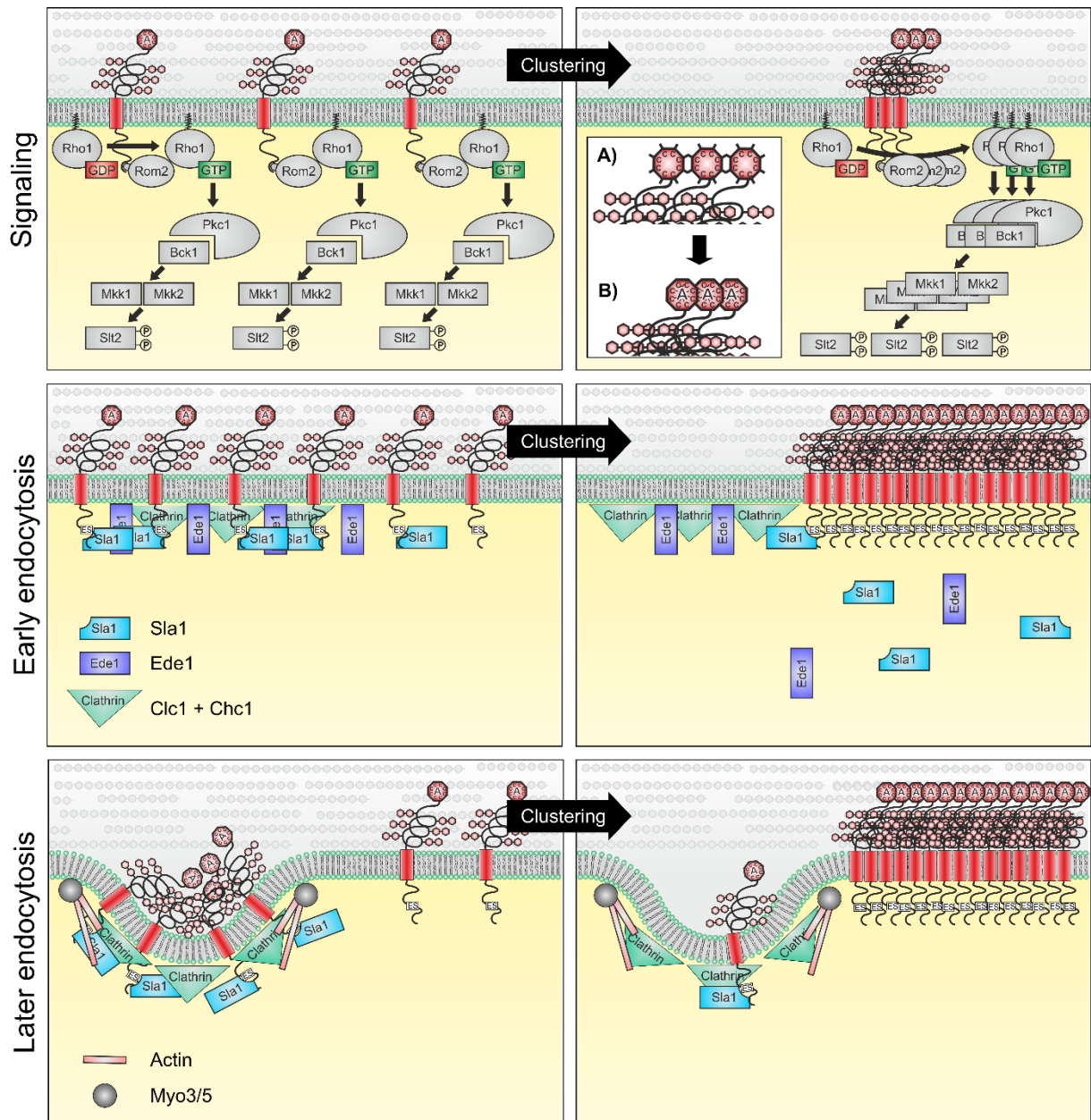


Figure 4.1: Model for Wsc1 clustering and its function for sensor signaling. The pathway activation and signaling capacity of Wsc1 is not determined by clustering of the sensor but by the amount of sensors at the cell surface (first row) while the clustering is achieved by interaction of the cysteine-rich domains of the sensors. The interaction is not mediated by intermolecular disulfide bridges (A) but by amyloid-like protein aggregation (B, see white box insert in the first row). The importance of clustering for sensor function could be to protect the sensors from endocytosis. During early endocytosis (second row), endocytic sites may not form within the cluster as early endocytic proteins like Clathrin and Ede1 may not attach at the plasma membrane. Furthermore, interaction of the Sla1 adaptor with the endocytosis signal of Wsc1 may not occur and prevent its endocytosis. As a second mechanism, the actin/myosin-driven membrane invagination that is necessary for endocytic vesicle formation may not occur within a Wsc1 cluster because the tight order of transmembrane domains could prevent membrane curvature (third row).

Alsteens *et al.*, 2012), these drugs could serve as a multi-target treatment in fighting diseases caused by fungal species. Furthermore, as many human diseases are linked to amyloid protein aggregations (Jahn *et al.*, 2010; Lipke *et al.*, 2012; Garcia-Sherman *et al.*, 2014), *Saccharomyces cerevisiae* and Wsc1 provide another an easy-to-handle model system to study amyloid protein biochemistry in addition to the well-studied prions (Bendheim *et al.*, 1985). Also, Wsc1 clusters may now be added to a diverse and continuously extending list of functional amyloids in organisms as for example described in microbial biofilms, mammals melanosoms or spider silk (Slotta *et al.*, 2007; Garcia *et al.*, 2011; Hu *et al.*, 2011; Rameau *et al.*, 2016).

4.7 Outlook

The quintuple deletion of all five CWI sensors genes provides a valuable tool to investigate the function of single sensors, even sensors like Wsc3 and partially also Wsc2 which lack strong phenotype in a single deletion mutant. Although the growth and transformation of the strain are difficult because of its strong growth defects, it should be possible to check fusion constructs or mutations within the sensors for its functionality – an important control for experiments which was not possible so far.

The new hypothesis on Wsc1 sensor clustering and its role for endocytosis protection is mostly based on fluorescent images and experiments on sensor functionality. To be sure that clustering influences the sensor amount in the plasma membrane a method is necessary which allows accurate quantification wild-type and cysteine-mutated sensors and their respective versions with blocked endocytosis at the cell surface as well. Single-molecule atomic force microscopy (AFM) is a promising method but the duration of a single surface scan does not allow quantifying dynamic processes like endocytosis yet. Furthermore, another method to investigate sensor functionality would be helpful as serial drop dilution assays and Slt2 phosphorylation quantification do not reliably allow to detect subtle changes in sensor functionality.

It was shown here that the sensors distribute in certain microdomains in the plasma membrane. The method applied here only provides static data for protein localization. Previous studies on plasma membrane microdomains found that most proteins show

dynamic movement in the membrane which leads to random overlap between domains. Modern microscopy methods like TIRF should provide better data on the dynamic domain localization of CWI sensors. TIRF microscopy combined with laser ablation technology could also help to gain insight on the spatio-temporal formation of sensors clusters.

This study provides evidence, that Wsc1 clustering is achieved by amyloid-like protein aggregation. TANGO analysis revealed that an Y60R mutation should show more severe phenotypes and therefore should be investigated as well. In addition, substances like Thioflavin T should influence the sensor clustering as well. Short peptides with either the Wsc1 wild-type amyloid amino acid sequence or the mutated peptide should be able to restore or disturb the sensor clustering as well and underline the amyloid-like protein aggregation hypothesis on Wsc1 clustering.

5. References

- Adler, J., and Parmryd, I. (2010) Quantifying colocalization by correlation: The pearson correlation coefficient is superior to the Mander's overlap coefficient. *Cytom Part A* **77**: 733–742.
- Aguilar, P.S., Fröhlich, F., Rehman, M., Shales, M., Ulitsky, I., Olivera-Couto, A., Braberg, H., Shamir, R., Walter, P., Mann, M., Eising, C.S., Krogan, N.J., and Walther, T.C. (2010) A plasma-membrane E-MAP reveals links of the eisosome with sphingolipid metabolism and endosomal trafficking. *Nat Struct Mol Biol* **17**: 901–908.
- Aimon, S., Callan-Jones, A., Berthaud, A., Pinot, M., Toombes, G.S., and Bassereau, P. (2014) Membrane Shape Modulates Transmembrane Protein Distribution. *Dev Cell* **28**: 212–218.
- Alberts, A.S., Bouquin, N., Johnston, L.H., and Treisman, R. (1998) Analysis of RhoA-binding proteins reveals an interaction domain conserved in heterotrimeric G protein beta subunits and the yeast response regulator protein Skn7. *J Biol Chem* **273**: 8616–22.
- Alsteens, D., Dupres, V., Yunus, S., Latgé, J.P., Heinisch, J.J., and Dufreîne, Y.F. (2012) High-resolution imaging of chemical and biological sites on living cells using peak force tapping atomic force microscopy. *Langmuir* **28**: 16738–16744.
- Alsteens, D., Ramsook, C.B., Lipke, P.N., and Dufreîne, Y.F. (2012) Unzipping a functional microbial amyloid. *ACS Nano* **6**: 7703–7711.
- Alvarez, F.J., Douglas, L.M., Rosebrock, A., and Konopka, J.B. (2008) The Sur7 protein regulates plasma membrane organization and prevents intracellular cell wall growth in *Candida albicans*. *Mol Biol Cell* **19**: 5214–25
- Ambesi, A., Miranda, M., Petrov, V. V., and Slayman, C.W. (2000) Biogenesis and function of the yeast plasma-membrane H(+)-ATPase. *J Exp Biol* **203**: 155–160.
- Amerik, A.Y., Nowak, J., Swaminathan, S., and Hochstrasser, M. (2000) The Doa4 deubiquitinating enzyme is functionally linked to the vacuolar protein-sorting and endocytic pathways. *Mol Biol Cell* **11**: 3365–80.
- Andrews, P.D., and Stark, M.J. (2000) Dynamic, Rho1p-dependent localization of Pkc1p to sites of polarized growth. *J Cell Sci* **113**: 2685–2693.
- Arlt, H., Auffarth, K., Kurre, R., Lisse, D., Piehler, J., and Ungermann, C. (2015) Spatiotemporal dynamics of membrane remodeling and fusion proteins during endocytic transport. *Mol Biol Cell* **26**: 1357–1370.

- Aronova, S., Wedaman, K., Anderson, S., Yates, J., and Powers, T. (2007) Probing the membrane environment of the TOR kinases reveals functional interactions between TORC1, actin, and membrane trafficking in *Saccharomyces cerevisiae*. *Mol Biol Cell* **18**: 2779–2794.
- Aronova, S., Wedaman, K., Aronov, P.A., Fontes, K., Ramos, K., Hammock, B.D., and Powers, T. (2008) Regulation of ceramide biosynthesis by TOR complex 2. *Cell Metab* **7**: 148–58.
- Arvanitidis, A., and Heinisch, J.J. (1994) Studies on the function of yeast phosphofructokinase subunits by in vitro mutagenesis. *J Biol Chem* **269**: 8911.
- Audhya, A., and Emr, S.D. (2002) Stt4 PI 4-kinase localizes to the plasma membrane and functions in the Pkc1-mediated MAP kinase cascade. *Dev Cell* **2**: 593–605.
- Backhaus, K., Rippert, D., Heilmann, C.J., Sorgo, A.G., de Koster, C.G., Klis, F.M., Rodicio, R., and Heinisch, J.J., (2013) Mutations in *SNF1* complex genes affect yeast cell wall strength. *Eur J Cell Biol* **92**: 383–395.
- Bagnat, M., Keränen, S., Shevchenko, A., and Simons, K. (2000) Lipid rafts function in biosynthetic delivery of proteins to the cell surface in yeast. *Proc Natl Acad Sci U S A* **97**: 3254–3259.
- Baird, G.S., Zacharias, D.A., and Tsien, R.Y. (2000) Biochemistry, mutagenesis, and oligomerization of DsRed, a red fluorescent protein from coral. *Proc Natl Acad Sci U S A* **97**: 11984–11989.
- Bastiani, M., and Parton, R.G. (2010) Caveolae at a glance. *J Cell Sci* **123**: 3831–3836.
- Baumgart, T., Hess, S.T., and Webb, W.W. (2003) Imaging coexisting fluid domains in biomembrane models coupling curvature and line tension. *Nature* **425**: 821–824.
- Bendheim, P.E., Bockman, J.M., McKinley, M.P., Kingsbury, D.T., and Prusiner, S.B. (1985) Scrapie and Creutzfeldt-Jakob disease prion proteins share physical properties and antigenic determinants. *Proc Natl Acad Sci U S A* **82**: 997–1001.
- Bénédicti, H., Raths, S., Crausaz, F., and Riezman, H. (1994) The *END3* gene encodes a protein that is required for the internalization step of endocytosis and for actin cytoskeleton organization in yeast. *Mol Biol Cell* **5**: 1023–37.
- Berchtold, D., and Walther, T.C. (2009) TORC2 plasma membrane localization is essential for cell viability and restricted to a distinct domain. *Mol Biol Cell* **20**: 1565–75.
- Bermejo, C., García, R., Straede, A., Rodríguez-Peña, J.M., Nombela, C., Heinisch, J.J., and Arroyo, J. (2010) Characterization of sensor-specific stress response by transcriptional profiling of *wsc1* and *mid2* deletion strains and chimeric sensors in *Saccharomyces cerevisiae*. *OMICS* **14**: 679–688.

- Boettner, D.R., Chi, R.J., and Lemmon, S.K. (2011) Lessons from yeast for clathrin-mediated endocytosis. *Nat Cell Biol* **14**: 2–10.
- Brach, T., Specht, T., and Kaksonen, M. (2011) Reassessment of the role of plasma membrane domains in the regulation of vesicular traffic in yeast. *J Cell Sci* **124**: 328–337.
- Breeden, L.L. (1997) Alpha-factor synchronization of budding yeast. *Methods Enzymol* **283**: 332–341.
- Breeden, L.L. (2003) Periodic transcription: A cycle within a cycle. *Curr Biol* **13**: 31–38.
- Capra, E.J., and Laub, M.T. (2012) Evolution of two-component signal transduction systems. *Annu Rev Microbiol* **66**: 325–47.
- Chen, R.E., and Thorner, J. (2007) Function and Regulation in MAPK Signaling Pathways. *Biochim Biophys Acta* **1773**: 1311–1340.
- Compagno, C., Ranzi, B.M., and Martegani, E. (1989) Yeast 2 micron vectors replicate and undergo recombination in *Torulospira delbrueckii*. *Mol Microbiol* **3**: 1003–1010.
- Córcoles-Sáez, I., Ballester-Tomas, L., de la Torre-Ruiz, M.A., Prieto, J.A., and Randez-Gil, F. (2012) Low temperature highlights the functional role of the cell wall integrity pathway in the regulation of growth in *Saccharomyces cerevisiae*. *Biochem J* **446**: 477–88.
- de Bony, J., Lopez, A., Gilleron, M., Welby, M., Lanéelle, G., Rousseau, B., Beaucourt, J.P., and Tocanne, J.F. (1989) Transverse and lateral distribution of phospholipids and glycolipids in the membrane of the bacterium *Micrococcus luteus*. *Biochemistry* **28**: 3728–37.
- de Hart, A.K.A., Schnell, J.D., Allen, D.A., and Hicke, L. (2002) The conserved Pkh-Ypk kinase cascade is required for endocytosis in yeast. *J Cell Biol* **156**: 241–248.
- Dhillon, A.S., Hagan, S., Rath, O., and Kolch, W. (2007) MAP kinase signalling pathways in cancer. *Oncogene* **26**: 3279–3290.
- Dodou, E., and Treisman, R. (1997) The *Saccharomyces cerevisiae* MADS-box transcription factor Rlm1 is a target for the Mpk1 mitogen-activated protein kinase pathway. *Mol Cell Biol* **17**: 1848–1859.
- Douglas, L.M., and Konopka, J.B. (2014) Fungal Membrane Organization: The Eisosome Concept. *Annu Rev Microbiol* **68**: 377–393.
- Douglas, L.M., Wang, H.X., and Keppler-Ross, S. (2012) Sur7 promotes plasma membrane organization and is needed for resistance to stressful conditions and to the invasive growth and virulence of *Candida albicans*. *MBio* **3**: 1–12.

- van Drogen, F., and Peter, M. (2002) Spa2p functions as a scaffold-like protein to recruit the Mpk1p MAP kinase module to sites of polarized growth. *Curr Biol* **12**: 1698–1703.
- Dupres, V., Alsteens, D., Wilk, S., Hansen, B., Heinisch, J.J., and Dufrêne, Y.F. (2009) The yeast Wsc1 cell surface sensor behaves like a nanospring in vivo. *Nat Chem Biol* **5**: 857–862.
- Dupres, V., Dufrêne, Y.F., and Heinisch, J.J. (2010) Measuring cell wall thickness in living yeast cells using single molecular rulers. *ACS Nano* **4**: 5498–5504.
- Dupres, V., Heinisch, J.J., and Dufrêne, Y.F. (2011) Atomic force microscopy demonstrates that disulfide bridges are required for clustering of the yeast cell wall integrity sensor Wsc1. *Langmuir* **27**: 15129–15134.
- Eggeling, C., Ringemann, C., Medda, R., Schwarzmann, G., Sandhoff, K., Polyakova, S., Belov, V.N., Hein, B., von Middendorff, C., Schönle, A., and Hell, S.W. (2009) Direct observation of the nanoscale dynamics of membrane lipids in a living cell. *Nature* **457**: 1159–62.
- Elorza, M. V., Rico, H., and Sentandreu, R. (1983) Calcofluor white alters the assembly of chitin fibrils in *Saccharomyces cerevisiae* and *Candida albicans* cells. *J Gen Microbiol* **129**: 1577–1582.
- Ernsting, B.R., and Dixon, J.E. (1997) The PPS1 gene of *Saccharomyces cerevisiae* codes for a dual specificity protein phosphatase with a role in the DNA synthesis phase of the cell cycle. *J Biol Chem* **272**: 9332–9343.
- Fernandez-Escamilla, A.-M., Rousseau, F., Schymkowitz, J.W.H., and Serrano, L. (2004) Prediction of sequence-dependent and mutational effects on the aggregation of peptides and proteins. *Nat Biotechnol* **22**: 1302–1306.
- Fishov, I., and Woldringh, C.L. (1999) Visualization of membrane domains in *Escherichia coli*. *Mol Microbiol* **32**: 1166–72.
- Frohlich, F., Moreira, K., Aguilar, P.S., Hubner, N.C., Mann, M., Walter, P., and Walther, T.C. (2009) A genome-wide screen for genes affecting eisosomes reveals Nce102 function in sphingolipid signaling. *J Cell Biol* **185**: 1227–1242.
- Garcia, M.C., Lee, J.T., Ramsook, C.B., Alsteens, D., Dufrêne, Y.F., and Lipke, P.N. (2011) A Role for Amyloid in Cell Aggregation and Biofilm Formation. *PLoS One* **6**: e17632.
- Garcia-Garcia, E., Grayfer, L., Stafford, J.L., and Belosevic, M. (2012) Evidence for the presence of functional lipid rafts in immune cells of ectothermic organisms. *Dev Comp Immunol* **37**: 257–269.

- Garcia-Sherman, M.C., Lysak, N., Filonenko, A., Richards, H., Sobonya, R.E., Klotz, S.A., and Lipke, P.N. (2014) Peptide Detection of Fungal Functional Amyloids in Infected Tissue. *PLoS One* **9**: e86067.
- Gietz, R., St. Jean, A., Woods, R.A., and Schiestl, R.H. (1992) Improved method for high efficiency transformation of intact yeast cells. *Nucl Acid Res* **20**: 1425.
- Gietz, R.D., and Akio, S. (1988) New yeast-*Escherichia coli* shuttle vectors constructed with in vitro mutagenized yeast genes lacking six-base pair restriction sites. *Gene* **74**: 527–534.
- Goode, B.L., Eskin, J.A., and Wendland, B. (2015) Actin and Endocytosis in Budding Yeast. *Genetics* **199**: 315–358.
- Grossmann, G., Malinsky, J., Stahlschmidt, W., Loibl, M., Weig-Meckl, I., Frommer, W.B., Opekarová, M., and Tanner, W. (2008) Plasma membrane microdomains regulate turnover of transport proteins in yeast. *J Cell Biol* **183**: 1075–1088.
- Grossmann, G., Opekarová, M., Malinsky, J., Weig-Meckl, I., and Tanner, W. (2007) Membrane potential governs lateral segregation of plasma membrane proteins and lipids in yeast. *EMBO J* **26**: 1–8.
- Guo, W., Tamanoi, F., and Novick, P. (2001) Spatial regulation of the exocyst complex by Rho1 GTPase. *Nat Cell Biol* **3**: 353–360.
- Hanahan, D. (1985) Techniques for transformation of *E. coli*. In: Glover D. M., editor. *DNA cloning: a practical approach. Vol. 1. Oxford, United Kingdom: IRL Press.* pp. 109–135.
- Hartwell, L.H., Culotti, J., and Reid, B. (1970) Genetic control of the cell-division cycle in yeast. I. Detection of mutants. *Proc Natl Acad Sci U S A* **66**: 352–359.
- Heinisch, J.J. (1993) PFK2, ISP42, ERG2 and RAD14 are located on the right arm of chromosome XIII. *Yeast* **9**: 1103–1105.
- Heinisch, J.J., Dupres, V., Alsteens, D., and Dufrêne, Y.F. (2010) Measurement of the mechanical behavior of yeast membrane sensors using single-molecule atomic force microscopy. *Nat Protoc* **5**: 670–677.
- Heinisch, J.J., Dupres, V., Wilk, S., Jendretzki, A., and Dufrêne, Y.F. (2010) Single-Molecule Atomic Force Microscopy Reveals Clustering of the Yeast Plasma-Membrane Sensor Wsc1. *PLoS One* **5**: e111104.
- Heinisch, J.J., Lorberg, A., Schmitz, H.P., and Jacoby, J.J. (1999) The protein kinase C-mediated MAP kinase pathway involved in the maintenance of cellular integrity in *Saccharomyces cerevisiae*. *Mol Microbiol* **32**: 671–80.

- Hill, J.E., Myers, A.M., Koerner, T.J., and Tzagoloff, A. (1986) Yeast/*E. coli* shuttle vectors with multiple unique restriction sites. *Yeast* **2**: 163–167.
- Hu, C.D., Chinenov, Y., and Kerppola, T.K. (2002) Visualization of interactions among bZIP and Rel family proteins in living cells using bimolecular fluorescence complementation. *Mol Cell* **9**: 789–798.
- Hu, K.N., McGlinchey, R.P., Wickner, R.B., and Tycko, R. (2011) Segmental polymorphism in a functional amyloid. *Biophys J* **101**: 2242–2250.
- Hutzler, F., Gerstl, R., Lommel, M., and Strahl, S. (2008) Protein N-glycosylation determines functionality of the *Saccharomyces cerevisiae* cell wall integrity sensor Mid2p. *Mol Microbiol* **68**: 1438–1449.
- Inagaki, M., Schmelzle, T., Yamaguchi, K., Irie, K., Hall, M.N., and Matsumoto, K. (1999) PDK1 homologs activate the Pkc1-mitogen-activated protein kinase pathway in yeast. *Mol Cell Biol* **19**: 8344–8352.
- Irie, K., Takase, M., Lee, K.S., Levin, D.E., Araki, H., Matsumoto, K., and Oshima, Y. (1993) *MKK1* and *MKK2*, which encode *Saccharomyces cerevisiae* mitogen-activated protein kinase-kinase homologs, function in the pathway mediated by protein kinase C. *Mol Cell Biol* **13**: 3076–3083.
- Iwabuchi, K., Nakayama, H., Masuda, H., Kina, K., Ogawa, H., and Takamori, K. (2012) Membrane microdomains in immunity: glycosphingolipid-enriched domain-mediated innate immune responses. *Biofactors* **38**: 275–283.
- Jacoby, J.J., Nilius, S.M., and Heinisch, J.J. (1998) A screen for upstream components of the yeast protein kinase C signal transduction pathway identifies the product of the *SLG1* gene. *Mol Gen Genet* **258**: 148–55.
- Jahn, T.R., Makin, O.S., Morris, K.L., Marshall, K.E., Tian, P., Sikorski, P., and Serpell, L.C. (2010) The Common Architecture of Cross- β Amyloid. *J Mol Biol* **395**: 717–727.
- Jin, C., Parshin, A. V, Daly, I., Strich, R., and Cooper, K.F. (2013) The cell wall sensors Mtl1, Wsc1, and Mid2 are required for stress-induced nuclear to cytoplasmic translocation of cyclin C and programmed cell death in yeast. *Oxid Med Cell Longev* **2013**: 320823.
- Jung, U.S., and Levin, D.E. (1999) Genome-wide analysis of gene expression regulated by the yeast cell wall integrity signalling pathway. *Mol Microbiol* **34**: 1049–1057.
- Kabeche, R., Baldissard, S., Hammond, J., Howard, L., and Moseley, J.B. (2011) The filament-forming protein Pil1 assembles linear eisosomes in fission yeast. *Mol Biol Cell* **22**: 4059–4067.

- Kabeche, R., Howard, L., and Moseley, J.B. (2015) Eisosomes provide membrane reservoirs for rapid expansion of the yeast plasma membrane. *J Cell Sci* **128**: 4057-4062.
- Kaksonen, M. (2008) Taking apart the endocytic machinery. *J Cell Biol* **180**: 1059–1060.
- Kamada, Y., Jung, U.S., Piotrowski, J., and Levin, D.E. (1995) The protein kinase C-activated MAP kinase pathway of *Saccharomyces cerevisiae* mediates a novel aspect of the heat shock response. *Genes Dev* **9**: 1559–1571.
- Kamble, C., Jain, S., Murphy, E., and Kim, K. (2011) Requirements of Slm proteins for proper eisosome organization, endocytic trafficking and recycling in the yeast *Saccharomyces cerevisiae*. *J Biosci* **36**: 79–96.
- Kapteyn, J.C., van den Ende, H., and Klis, F.M. (1999) The contribution of cell wall proteins to the organization of the yeast cell wall. *Biochim Biophys Acta* **1426**: 373–383.
- Karotki, L., Huiskonen, J.T., Stefan, C.J., Ziolkowska, N.E., Roth, R., Surma, M.A., Krogan, N.J., Emr, S.D., Heuser, J., Grünwald, K., and Walther, T.C. (2011) Eisosome proteins assemble into a membrane scaffold. *J Cell Biol* **195**: 889–902.
- Kaufmann, A. (2009) A plasmid collection for PCR-based gene targeting in the filamentous ascomycete *Ashbya gossypii*. *Fungal Genet Biol* **46**: 595–603.
- Ketela, T., Green, R., and Bussey, H. (1999) *Saccharomyces cerevisiae* Mid2p is a potential cell wall stress sensor and upstream activator of the PKC1-MPK1 cell integrity pathway. *J Bacteriol* **181**: 3330–3340.
- Kim, E.K., and Choi, E.-J. (2010) Pathological roles of MAPK signaling pathways in human diseases. *Biochim Biophys Acta - Mol Basis Dis* **1802**: 396–405.
- Kim, K.-Y., Truman, A.W., and Levin, D.E. (2008) Yeast Mpk1 mitogen-activated protein kinase activates transcription through Swi4/Swi6 by a noncatalytic mechanism that requires upstream signal. *Mol Cell Biol* **28**: 2579–89.
- Kirchrath, L., Lorberg, A., Schmitz, H.P., Gengenbacher, U., and Heinisch, J.J. (2000) Comparative genetic and physiological studies of the MAP kinase Mpk1p from *Kluyveromyces lactis* and *Saccharomyces cerevisiae*. *J Mol Biol* **300**: 743–758.
- Klebe, R.J., Harriss, J.V., Sharp, Z.D., and Douglas, M.G. (1983) A general method for polyethylene-glycol-induced genetic transformation of bacteria and yeast. *Gene* **25**: 333–341.
- Klis, F. (2002) Dynamics of cell wall structure in *Saccharomyces cerevisiae*. *FEMS Microbiol Rev* **26**: 239–256.

- Kock, C., Dufrêne, Y.F., and Heinisch, J.J. (2015) Up against the Wall: Is Yeast Cell Wall Integrity Ensured by Mechanosensing in Plasma Membrane Microdomains? *Appl Environ Microbiol* **81**: 806–811.
- Kock, C., Arlt, H., Ungermann, C., and Heinisch, J.J. (2016) Yeast cell wall integrity sensors form specific plasma membrane microdomains important for signaling. *Cell Microbiol*, revision submitted, publication presumably in september 2016.
- Kollár, R., Reinhold, B.B., Petráková, E., Yeh, H.J., Ashwell, G., Drgonová, J., Kapteyn, J.C., Klis, F.M., and Cabib, E. (1997) Architecture of the yeast cell wall. Beta(1,6)-glucan interconnects mannoprotein, beta(1,3)-glucan, and chitin. *J Biol Chem* **272**: 17762–75.
- Kono, K., Nogami, S., Abe, M., Nishizawa, M., Morishita, S., Pellman, D., and Ohya, Y. (2008) G1/S cyclin-dependent kinase regulates small GTPase Rho1p through phosphorylation of RhoGEF Tus1p in *Saccharomyces cerevisiae*. *Mol Biol Cell* **19**: 1763–71.
- Kusumi, A., Nakada, C., Ritchie, K., Murase, K., Suzuki, K., Murakoshi, H., Kasai, R.S., Kondo, J., and Fujiwara, T. (2005) Paradigm Shift of the Plasma Membrane Concept from the Two-Dimensional Continuum Fluid to the Partitioned Fluid: High-Speed Single-Molecule Tracking of Membrane Molecules. *Annu Rev Biophys Biomol Struct* **34**: 351–378.
- Lee, K.S., and Levin, D.E. (1992) Dominant mutations in a gene encoding a putative protein kinase (*BCK1*) bypass the requirement for a *Saccharomyces cerevisiae* protein kinase C homolog. *Mol Cell Biol* **12**: 172–182.
- Levin, D.E. (2005) Cell Wall Integrity Signaling in *Saccharomyces cerevisiae*. *Microbiol Mol Biol Rev* **69**: 262–291.
- Levin, D.E. (2011) Regulation of Cell Wall Biogenesis in *Saccharomyces cerevisiae*: The Cell Wall Integrity Signaling Pathway. *Genetics* **189**: 1145–1175.
- Levin-Salomon, V., Maayan, I., Avrahami-Moyal, L., Marbach, I., Livnah, O., and Engelberg, D. (2009) When expressed in yeast, mammalian mitogen-activated protein kinases lose proper regulation and become spontaneously phosphorylated. *Biochem J* **417**: 331–342.
- Lipke, P.N., Garcia, M.C., Alsteens, D., Ramsook, C.B., Klotz, S. a, and Dufrêne, Y.F. (2012) Strengthening relationships: amyloids create adhesion nanodomains in yeasts. *Trends Microbiol* **20**: 59–65.
- Lodder, A.L., Lee, T.K., and Ballester, R. (1999) Characterization of the Wsc1 protein, a putative receptor in the stress response of *Saccharomyces cerevisiae*. *Genetics* **152**: 1487–1499.

- Lommel, M., Bagnat, M., and Strahl, S. (2004) Aberrant processing of the WSC family and Mid2p cell surface sensors results in cell death of *Saccharomyces cerevisiae* O-mannosylation mutants. *Mol Cell Biol* **24**: 46–57.
- Longtine, M.S., McKenzie, A., Demarini, D.J., Shah, N.G., Wach, A., Brachat, A., Philippsen, P., and Pringle, J.R. (1998) Additional modules for versatile and economical PCR-based gene deletion and modification in *Saccharomyces cerevisiae*. *Yeast* **14**: 953–61.
- Lorberg, A., Schmitz, H.P., Jacoby, J.J., and Heinisch, J.J. (2001) Lrg1p functions as a putative GTPase-activating protein in the Pkc1p-mediated cell integrity pathway in *Saccharomyces cerevisiae*. *Mol Genet Genomics* **266**: 514–26. Accessed April 24, 2016.
- Luo, G., Gruhler, A., Liu, Y., Jensen, O.N., and Dickson, R.C. (2008) The Sphingolipid Long-chain Base-Pkh1/2-Ypk1/2 Signaling Pathway Regulates Eisosome Assembly and Turnover. *J Biol Chem* **283**: 10433–10444.
- Malinska, K., Malinsky, J., Opekarova, M., and Tanner, W. (2004) Distribution of Can1p into stable domains reflects lateral protein segregation within the plasma membrane of living *S. cerevisiae* cells. *J Cell Sci* **117**: 6031–6041.
- Malínská, K., Malínský, J., Opekarová, M., and Tanner, W. (2003) Visualization of protein compartmentation within the plasma membrane of living yeast cells. *Mol Biol Cell* **14**: 4427–36.
- Mao, K., Wang, K., Zhao, M., Xu, T., and Klionsky, D.J. (2011) Two MAPK-signaling pathways are required for mitophagy in *Saccharomyces cerevisiae*. *J Cell Biol* **193**: 755–767.
- Martín, H., Flández, M., Nombela, C., and Molina, M. (2005) Protein phosphatases in MAPK signalling: we keep learning from yeast. *Mol Microbiol* **58**: 6–16.
- Mascaraque, V., Hernández, M.L., Jiménez-Sánchez, M., Hansen, R., Gil, C., Martín, H., Cid, V.J., and Molina, M. (2013) Phosphoproteomic analysis of protein kinase C signaling in *Saccharomyces cerevisiae* reveals Slt2 mitogen-activated protein kinase (MAPK)-dependent phosphorylation of eisosome core components. *Mol Cell Proteomics* **12**: 557–74.
- Merzendorfer, H., and Heinisch, J.J. (2013) Microcompartments within the yeast plasma membrane. *Biol Chem* **394**: 189–202.
- Mo, C., Valachovic, M., and Bard, M. (2004) The ERG28-encoded protein, Erg28p, interacts with both the sterol C-4 demethylation enzyme complex as well as the late biosynthetic protein, the C-24 sterol methyltransferase (Erg6p). *Biochim Biophys Acta - Mol Cell Biol Lipids* **1686**: 30–36.
- Molano, J., Bowers, B., and Cabib, E. (1980) Distribution of chitin in the yeast cell wall. An ultrastructural and chemical study. *J Cell Biol* **85**: 199–212.

- Moreira, K.E., Schuck, S., Schrul, B., Frohlich, F., Moseley, J.B., Walther, T.C., and Walter, P. (2012) Seg1 controls eisosome assembly and shape. *J Cell Biol* **198**: 405–420.
- Nishida, N., Jing, D., Kuroda, K., and Ueda, M. (2014) Activation of signaling pathways related to cell wall integrity and multidrug resistance by organic solvent in *Saccharomyces cerevisiae*. *Curr Genet* **60**: 149–162.
- de Nobel, H., Ruiz, C., Martin, H., Morris, W., Brul, S., Molina, M., and Klis, F.M. (2000) Cell wall perturbation in yeast results in dual phosphorylation of the Slt2/Mpk1 MAP kinase and in an Slt2-mediated increase in FKS2-lacZ expression, glucanase resistance and thermotolerance. *Microbiology* **146**: 2121–32.
- de Nobel, J.G., Klis, F.M., Priem, J., Munnik, T., and van den Ende, H. (1990) The glucanase-soluble mannoproteins limit cell wall porosity in *Saccharomyces cerevisiae*. *Yeast* **6**: 491–499.
- Olivera-Couto, A., and Aguilar, P.S. (2012) Eisosomes and plasma membrane organization. *Mol Genet Genomics* **287**: 607–620.
- Olivera-Couto, A., Grana, M., Harispe, L., and Aguilar, P.S. (2011) The eisosome core is composed of BAR domain proteins. *Mol Biol Cell* **22**: 2360–2372.
- Olson, D.K., Fröhlich, F., Christiano, R., Hannibal-Bach, H.K., Ejsing, C.S., and Walther, T.C. (2015) Rom2-dependent phosphorylation of Elo2 controls the abundance of very long-chain fatty acids. *J Biol Chem* **290**: 4238–4247.
- Onishi, M., Nolan, K., Nishihama, R., and Pringle, J.R. (2013) Distinct roles of Rho1, Cdc42, and Cyk3 in septum formation and abscission during yeast cytokinesis. *J Cell Biol* **202**: 311–329.
- Ono, T., Suzuki, T., Anraku, Y., and Iida, H. (1994) The MID2 gene encodes a putative integral membrane protein with a Ca(2+)-binding domain and shows mating pheromone-stimulated expression in *Saccharomyces cerevisiae*. *Gene* **151**: 203–208.
- Orlean, P. (2012) Architecture and Biosynthesis of the *Saccharomyces cerevisiae* Cell Wall. *Genetics* **192**: 775–818.
- Otoo, H.N., Lee, K.G., Qiu, W., and Lipke, P.N. (2008) *Candida albicans* Als Adhesins Have Conserved Amyloid-Forming Sequences. *Eukaryot Cell* **7**: 776–782.
- Ozaki, K., Tanaka, K., Imamura, H., Hihara, T., Kameyama, T., Nonaka, H., *et al.* (1996) Rom1p and Rom2p are GDP/GTP exchange proteins (GEPs) for the Rho1p small GTP binding protein in *Saccharomyces cerevisiae*. *EMBO J* **15**: 2196–207.

- Petkova, M.I., Pujol-Carrion, N., Arroyo, J., Garcia-Cantalejo, J., and de la Torre-Ruiz, M, A. (2010) Mtl1 Is Required to Activate General Stress Response through Tor1 and Ras2 Inhibition under Conditions of Glucose Starvation and Oxidative Stress. *J Biol Chem* **285**: 19521–19531.
- Petkova, M.I., Pujol-Carrion, N., and de la Torre-Ruiz, M.A. (2012) Mtl1 O-mannosylation mediated by both Pmt1 and Pmt2 is important for cell survival under oxidative conditions and TOR blockade. *Fungal Genet Biol* **49**: 903–914.
- Philip, B., and Levin, D.E. (2001) Wsc1 and Mid2 Are Cell Surface Sensors for Cell Wall Integrity Signaling That Act through Rom2 , a Guanine Nucleotide Exchange Factor for Rho1. *Mol Cell Biol* **21**: 271–280.
- Piao, H.L., Machado, I.M.P., and Payne, G.S. (2007) NPFxD-mediated endocytosis is required for polarity and function of a yeast cell wall stress sensor. *Mol Biol Cell* **18**: 57–65.
- Proszynski, T.J., Klemm, R.W., Gravert, M., Hsu, P.P., Gloor, Y., Wagner, J., Kozak, K., Grabner, H., Walzer, K., Bagnat, M., Simons, K., and Walch-Solimena, C. (2005) A genome-wide visual screen reveals a role for sphingolipids and ergosterol in cell surface delivery in yeast. *Proc Natl Acad Sci U S A* **102**: 17981–17986.
- Proszynski, T.J., Simons, K., and Bagnat, M. (2004) O-glycosylation as a sorting determinant for cell surface delivery in yeast. *Mol Biol Cell* **15**: 1533–1543.
- Pujol-Carrion, N., Petkova, M.I., Serrano, L., and de la Torre-Ruiz, M.A. (2013) The MAP Kinase Slt2 Is Involved in Vacuolar Function and Actin Remodeling in *Saccharomyces cerevisiae* Mutants Affected by Endogenous Oxidative Stress. *Appl Environ Microbiol* **79**: 6459–6471.
- Qadota, H., Python, C.P., Inoue, S.B., Arisawa, M., Anraku, Y., Zheng, Y., Watanabe, T., Levin, D.E., and Ohya, Y. (1996) Identification of yeast Rho1p GTPase as a regulatory subunit of 1,3-beta-glucan synthase. *Science* **272**: 279–81.
- Qi, M., and Elion, E.A. (2005) MAP kinase pathways. *J Cell Sci* **118**: 3569–3572.
- Rajavel, M., Philip, B., Buehrer, B.M., Errede, B., and Levin, D.E. (1999) Mid2 is a putative sensor for cell integrity signaling in *Saccharomyces cerevisiae*. *Mol Cell Biol* **19**: 3969–3976.
- Rameau, R.D., Jackson, D.N., Beaussart, A., Dufrêne, Y.F., and Lipke, N. (2016) The Human Disease-Associated A β Amyloid Core Sequence Forms Functional Amyloids in a Fungal Adhesin. **7**: 1–9.
- Reggiori, F., Tucker, K.A., Stromhaug, P.E., and Klionsky, D.J. (2004) The Atg1-Atg13 complex regulates Atg9 and Atg23 retrieval transport from the pre-autophagosomal structure. *Dev Cell* **6**: 79–90.

- Reinoso-Martín, C., Schüller, C., Schuetzer-Muehlbauer, M., and Kuchler, K. (2003) The Yeast Protein Kinase C Cell Integrity Pathway Mediates Tolerance to the Antifungal Drug Caspofungin through Activation of Slt2p Mitogen-Activated Protein Kinase Signaling. *Eukaryot Cell* **2**: 1200–1210.
- Roberts, B.T., Farr, K. a, and Hoyt, M. a (1994) The *Saccharomyces cerevisiae* checkpoint gene BUB1 encodes a novel protein kinase. *Mol Cell Biol* **14**: 8282–8291.
- Rodicio, R., and Heinisch, J.J. (2010) Together we are strong—cell wall integrity sensors in yeasts. *Yeast* **27**: 531–540.
- Rodriguez-Pena, J.M., Garcia, R., Nombela, C., and Arroyo, J. (2010) The high-osmolarity glycerol (HOG) and cell wall integrity (CWI) signalling pathways interplay: A yeast dialogue between MAPK routes. *Yeast* **27**: 495–502.
- Roncero, C. (2002) The genetic complexity of chitin synthesis in fungi. *Curr Genet* **41**: 367–378.
- Roncero, C., and Duran, A. (1985) Effect of Calcofluor White and Congo Red on Fungal Cell Wall Morphogenesis : In Vivo Activation of Chitin Polymerization. *J Bacteriol* **163**: 1180–1185.
- Roux, K.J., Kim, D.I., Raida, M., and Burke, B. (2012) A promiscuous biotin ligase fusion protein identifies proximal and interacting proteins in mammalian cells. *J Cell Biol* **196**: 801–810.
- Sagot, I., Klee, S.K., and Pellman, D. (2002) Yeast formins regulate cell polarity by controlling the assembly of actin cables. *Nat Cell Biol* **4**: 42–50.
- Sawaya, M.R., Sambashivan, S., Nelson, R., Ivanova, M.I., Sievers, S.A., Apostol, M.I., Thompson, M.J., Balbirnie, M., Wiltzius, J.J., McFarlane, H.T., Madsen, A.Ø., Riek, C., and Eisenberg, D. (2007) Atomic structures of amyloid cross- β spines reveal varied steric zippers. *Nature* **447**: 453–457.
- Schmidt, A., Bickle, M., Beck, T., and Hall, M.N. (1997) The yeast phosphatidylinositol kinase homolog *TOR2* activates *RHO1* and *RHO2* via the exchange factor *ROM2*. *Cell* **88**: 531–542.
- Schmitz, H.-P., and Heinisch, J.J. (2003) Evolution, biochemistry and genetics of protein kinase C in fungi. *Curr Genet* **43**: 245–254.
- Schmitz, H.-P., Jendretzki, A., Wittland, J., Wiechert, J., and Heinisch, J.J. (2015) Identification of Dck1 and Lmo1 as upstream regulators of the small GTPase Rho5 in *Saccharomyces cerevisiae*. *Mol Microbiol* **96**: 306–324.

- Schmitz, H.-P., Lorberg, A., and Heinisch, J.J. (2002) Regulation of yeast protein kinase C activity by interaction with the small GTPase Rho1p through its amino-terminal HR1 domain. *Mol Microbiol* **44**: 829–840.
- Sclafani, R.A., and Jackson, A.L. (1994) Cdc7 protein kinase for DNA metabolism comes of age. *Mol Microbiol* **11**: 805–810.
- Seger, S., Rischatsch, R., and Philippsen, P. (2011) Formation and stability of eisosomes in the filamentous fungus *Ashbya gossypii*. *J Cell Sci* **124**: 1629–1634.
- Sheff, M.A., and Thorn, K.S. (2004) Optimized cassettes for fluorescent protein tagging in *Saccharomyces cerevisiae*. *Yeast* **21**: 661–670.
- Shibata, Y., Hu, J., Kozlov, M.M., and Rapoport, T. a. (2009) Mechanisms Shaping the Membranes of Cellular Organelles. *Annu Rev Cell Dev Biol* **25**: 329–354.
- Sia, R.A., Herald, H.A., and Lew, D.J. (1996) Cdc28 tyrosine phosphorylation and the morphogenesis checkpoint in budding yeast. *Mol Biol Cell* **7**: 1657–66.
- Simons, K., and Sampaio, J.L. (2011) Membrane organization and lipid rafts. *Cold Spring Harb Perspect Biol* **3**: a004697.
- Singer, S.J., and Nicolson, G.L. (1972) The fluid mosaic model of the structure of cell membranes. *Science* **175**: 720–731.
- Slotta, U., Hess, S., Spieß, K., Stromer, T., Serpell, L., and Scheibel, T. (2007) Spider Silk and Amyloid Fibrils: A Structural Comparison. *Macromol Biosci* **7**: 183–188.
- Sonnino, S., and Prinetti, a (2013) Membrane domains and the “lipid raft” concept. *Curr Med Chem* **20**: 4–21.
- Sowa, G. (2012) Caveolae, caveolins, cavins, and endothelial cell function: new insights. *Front Physiol* **2**: 1–13.
- Spira, F., Mueller, N.S., Beck, G., Olshausen, P. von, Beig, J., and Wedlich-Söldner, R. (2012) Patchwork organization of the yeast plasma membrane into numerous coexisting domains. *Nat Cell Biol* **14**: 640–648.
- Stradalova, V., Stahlschmidt, W., Grossmann, G., Blazikova, M., Rachel, R., Tanner, W., and Malinsky, J. (2009) Furrow-like invaginations of the yeast plasma membrane correspond to membrane compartment of Can1. *J Cell Sci* **122**: 2887–2894.
- Straede, A., Corran, A., Bundy, J., and Heinisch, J.J. (2007) The effect of tea tree oil and antifungal agents on a reporter for yeast cell integrity signalling. *Yeast* **24**: 321–34.

Straede, A., and Heinisch, J.J. (2007) Functional analyses of the extra- and intracellular domains of the yeast cell wall integrity sensors Mid2 and Wsc1. *FEBS Lett* **581**: 4495–4500.

Tang, H.Y., Munn, A., and Cai, M. (1997) EH domain proteins Pan1p and End3p are components of a complex that plays a dual role in organization of the cortical actin cytoskeleton and endocytosis in *Saccharomyces cerevisiae*. *Mol Cell Biol* **17**: 4294–4304.

Terskikh, A. V., Fradkov, A.F., Zraisky, A.G., Kajava, A. V., and Angres, B. (2002) Analysis of DsRed Mutants: SPACE AROUND THE FLUOROPHORE ACCELERATES FLUORESCENCE DEVELOPMENT. *J Biol Chem* **277**: 7633–7636.

Torres, L., Martín, H., García-Saez, M.I., Arroyo, J., Molina, M., Sánchez, M., and Nombela, C. (1991) A protein kinase gene complements the lytic phenotype of *Saccharomyces cerevisiae* *lyt2* mutants. *Mol Microbiol* **5**: 2845–54.

Tu, Y. (2013) Quantitative modeling of bacterial chemotaxis: signal amplification and accurate adaptation. *Annu Rev Biophys* **42**: 337–59.

Valdivia, R.H., and Schekman, R. (2003) The yeasts Rho1p and Pkc1p regulate the transport of chitin synthase III (Chs3p) from internal stores to the plasma membrane. *Proc Natl Acad Sci U S A* **100**: 10287–92.

Vangelatos, I., Roumelioti, K., Gournas, C., Suarez, T., Scazzocchio, C., and Sophianopoulou, V. (2010) Eisosome organization in the filamentous ascomycete *Aspergillus nidulans*. *Eukaryot Cell* **9**: 1441–54.

Vartak, R., Porras, C.A.M., and Bai, Y. (2013) Respiratory supercomplexes: Structure, function and assembly. *Protein Cell* **4**: 582–590.

Vay, H.A., Philip, B. and Levin, D.E. (2004) Mutational analysis of the cytoplasmic domain of the Wsc1 cell wall stress sensor. *Microbiology* **150**: 3281–3288.

Verna, J., Lodder, A., Lee, K., Vagts, A., and Ballester, R. (1997) A family of genes required for maintenance of cell wall integrity and for the stress response in *Saccharomyces cerevisiae*. *Proc Natl Acad Sci U S A* **94**: 13804–13809.

Vieira, J., and Messing, J. (1991) New pUC-derived cloning vectors with different selectable markers and DNA replication origins. *Gene* **100**: 189–94.

Vilella, F., Herrero, E., Torres, J., and de la Torre-Ruiz, M.A. (2005) Pkc1 and the upstream elements of the cell integrity pathway in *Saccharomyces cerevisiae*, Rom2 and Mtl1, are required for cellular responses to oxidative stress. *J Biol Chem* **280**: 9149–59.

Walther, T.C., Aguilar, P.S., Fröhlich, F., Chu, F., Moreira, K., Burlingame, A.L., and Walter, P. (2007) Pkh-kinases control eisosome assembly and organization. *EMBO J* **26**: 4946–4955.

- Walther, T.C., Brickner, J.H., Aguilar, P.S., Bernales, S., Pantoja, C., and Walter, P. (2006) Eisosomes mark static sites of endocytosis. *Nature* **439**: 998–1003.
- Watanabe, D., Abe, M., and Ohya, Y. (2001) Yeast Lrg1p acts as a specialized RhoGAP regulating 1,3-beta-glucan synthesis. *Yeast* **18**: 943–51. Accessed April 24, 2016.
- Watanabe, Y., Takaesu, G., Hagiwara, M., Irie, K., and Matsumoto, K. (1997) Characterization of a serum response factor-like protein in *Saccharomyces cerevisiae*, Rlm1, which has transcriptional activity regulated by the Mpk1 (Slr2) mitogen-activated protein kinase pathway. *Mol Cell Biol* **17**: 2615–23.
- Weinberg, J., and Drubin, D.G. (2012) Clathrin-mediated endocytosis in budding yeast. *Trends Cell Biol* **22**: 1–13.
- Westermarck, P., Benson, M.D., Buxbaum, J.N., Cohen, A.S., Frangione, B., Ikeda, S.-I., Master, C.L., Merlini, G., Saraiva, M.J., Sipe, and J.D. (2005) Amyloid: toward terminology clarification. Report from the Nomenclature Committee of the International Society of Amyloidosis. *Amyloid* **12**: 1–4.
- Wilk, S. (2010) Charakterisierung der Sensoren des Zellintegritätswegs der Hefe *Saccharomyces cerevisiae*. Osnabrück, Univ., Diss.
- Wilk, S., Wittland, J., Thywissen, A., Schmitz, H.-P., and Heinisch, J.J. (2010) A block of endocytosis of the yeast cell wall integrity sensors Wsc1 and Wsc2 results in reduced fitness in vivo. *Mol Genet Genomics* **284**: 217–229.
- Wilson, K.L., and Dawson, S.C. (2011) Evolution: Functional evolution of nuclear structure. *J Cell Biol* **195**: 171–181.
- Wittland, J. (2012) Charakterisierung der physiologischen Bedeutung und der Wechselwirkungen der Sensoren des Zellintegritätswegs der Hefe *Saccharomyces cerevisiae*. Osnabrück, Univ., Diss..
- Wong, J., Nakajima, Y., Westermann, S., Shang, C., Kang, J.-S., Goodner, C., Houshmand, P., Fields, S., Chan, C.S.M., Drubin, D., Barnes, G., and Hazbun, T. (2007) A protein interaction map of the mitotic spindle. *Mol Biol Cell* **18**: 3800–3809.
- Young, M.E., Karpova, T.S., Brügger, B., Moschenross, D.M., Wang, G.K., Schneiter, R., Wieland, F.T., and Cooper, J.A. (2002) The Sur7p family defines novel cortical domains in *Saccharomyces cerevisiae*, affects sphingolipid metabolism, and is involved in sporulation. *Mol Cell Biol* **22**: 927–934.
- Ziółkowska, N.E., Christiano, R., and Walther, T.C. (2012) Organized living: formation mechanisms and functions of plasma membrane domains in yeast. *Trends Cell Biol* **22**: 151–158.

6. Supplementary

6.1 Plasma membrane domain colocalization controls

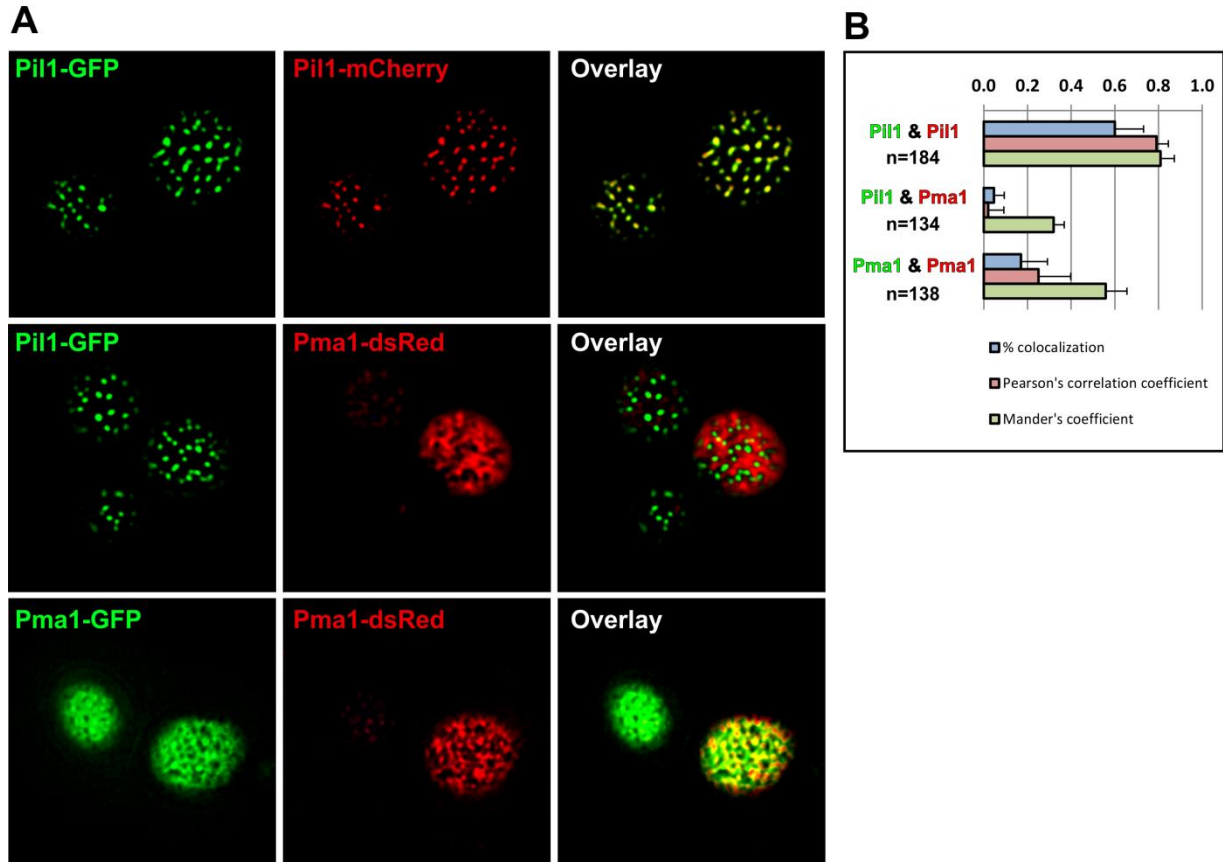


Figure 6.1: Colocalization analysis control experiments. The strains HCK18-3C/pOCK002 (*MATalpha PIL1-GFP-SpHIS5 ura3::PIL1-mCherry*), HCK37-5C (*MATalpha PIL1-GFP SpHIS5 PMA1-dsRed-kanMX*) and DCK40-2 (*PMA1-GFP-kanMX/PMA1-dsRed-kanMX*) were investigated by life cell epifluorescence microscopy with a DeltaVision Elite microscope and overlays of top-sections were created (**A**). The median of the percentage of colocalized spots (% colocalization, PCOL) was then determined by a “count & colocalize” software plugin together with the “Pearson’s correlation coefficient” (PCC) and the “Mander’s overlap coefficient” (MOC) to quantify the colocalization. Pil1 & Pil1: PCOL = 60 ± 13 %, PCC = 0.79 ± 0.05 and MOC = 0.81 ± 0.06 (n=184), Pil1 & Pma1: PCOL = 4.7 ± 4.7, PCC = 0.02 ± 0.07 and MOC = 0.32 ± 0.05 (n=134), Pma1 & Pma1: PCOL = 17 ± 12 %, PCC = 0.25 ± 0.15 and MOC = 0.56 ± 0.1 (n=138).

6.2 List of potential Wsc1 interaction partners identified by BioID

Gene	Name	Function	score	Analysis	Category
<i>ATG2</i>	AuTophagy related	Peripheral membrane protein required for autophagic vesicle formation; also required for vesicle formation during pexophagy and the cytoplasm-to-vacuole targeting (Cvt) pathway; involved in Atg9p cycling between the phagophore assembly site and mitochondria; essential for cell cycle progression from G2/M to G1 under nitrogen starvation; forms cytoplasmic foci upon DNA replication stress	score 26, 16 peptides	2	cell cycle / signaling
<i>ATG9</i>	AuTophagy related	Transmembrane protein involved in forming Cvt and autophagic vesicles; cycles between the phagophore assembly site (PAS) and other cytosolic punctate structures, not found in autophagosomes; may be involved in membrane delivery to the PAS	score 21, 13 peptides	2	cell cycle / signaling
<i>BUB1</i>	Budding Uninhibited by Benzimidazole	Protein kinase involved in the cell cycle checkpoint into anaphase; forms complex with Mad1p and Bub3p crucial to preventing cell cycle progression into anaphase in presence of spindle damage; CDC28-mediated phosphorylation at Bub1p-T566 is important for degradation in anaphase and adaptation of checkpoint to prolonged mitotic arrest; associates with centromere DNA via Skp1p; BUB1 has a paralog, MAD3, that arose from the whole genome duplication	score 18, 2 peptides	1	cell cycle / signaling
<i>CDC7</i>	Cell Division Cycle	DDK (Dbf4-dependent kinase) catalytic subunit; required for origin firing and replication fork progression in mitotic S phase through phosphorylation of Mcm2-7p complexes and Cdc45p; kinase activity correlates with cyclical DBF4 expression; required for pre-meiotic DNA replication, meiotic DSB formation, recruitment of the monopolin complex to kinetochores during meiosis I and as a gene-specific regulator of the meiosis-specific transcription factor Ndt80p	score 34, 6 peptides	2	cell cycle / signaling
<i>IRA1</i>	Inhibitory Regulator of the RAS-cAMP pathway	GTPase-activating protein; negatively regulates RAS by converting it from the GTP- to the GDP-bound inactive form, required for reducing cAMP levels under nutrient limiting conditions, mediates membrane association of adenylate cyclase; IRA1 has a paralog, IRA2, that arose from the whole genome duplication	score 29, 14 peptides	2	cell cycle / signaling

Gene	Name	Function	score	Analysis	Category
<i>IST2</i>	Increased Sodium Tolerance	Cortical ER protein involved in ER-plasma membrane tethering; one of 6 proteins (Ist2p, Scs2p, Scs22p, Tcb1p, Tcb3p) that connect ER to the plasma membrane (PM) and regulate PM phosphatidylinositol-4-phosphate (PI4P) levels by controlling access of Sac1p phosphatase to its substrate PI4P in the PM; localizes to the mother cell in small-budded cells and to the bud in medium- and large-budded cells; mRNA is transported to the bud tip by an actomyosin-driven process	score 58, 9 peptides	2	cell cycle / signaling
<i>MIH1</i>	Mitotic Inducer Homolog	Protein tyrosine phosphatase involved in cell cycle control; regulates the phosphorylation state of Cdc28p; homolog of <i>S. pombe</i> cdc25	score 17, 6 peptides	1	cell cycle / signaling
<i>MPT5</i>	Multicopy suppressor of Pop Two	mRNA-binding protein of the PUF family; binds to the 3' UTR of specific mRNAs, including those involved in mating type switching, cell wall integrity, chronological lifespan, chromatin modification, and spindle pole body architecture; recruits the CCR4-NOT deadenylase complex to mRNAs along with Dhh1p and Dcp1p to promote deadenylation, decapping, and decay; also interacts with the Caf20p translational initiation repressor, affecting its mRNA target specificity	score 28, 6 peptides	2	cell cycle / signaling
<i>NIP100</i>	Nuclear Import	Large subunit of the dynactin complex; dynactin is involved in partitioning the mitotic spindle between mother and daughter cells; putative ortholog of mammalian p150(glued)	score 25, 10 peptides	1	cell cycle / signaling
<i>OLA1</i>	Obg-Like ATPase	P-loop ATPase with similarity to human OLA1 and bacterial YchF; identified as specifically interacting with the proteasome; protein abundance increases in response to hydrogen peroxide and to DNA replication stress	score 24, 5 peptides	1	cell cycle / signaling
<i>PMR1</i>	Plasma Membrane ATPase Related	High affinity Ca ²⁺ /Mn ²⁺ P-type ATPase; required for Ca ²⁺ and Mn ²⁺ transport into Golgi; involved in Ca ²⁺ dependent protein sorting and processing; mutations in human homolog ATP2C1 cause acantholytic skin condition Hailey-Hailey disease	score 34, 7 peptides	2	cell cycle / signaling

Gene	Name	Function	score	Analysis	Category
<i>PPS1</i>	Protein Phosphatase S phase	Protein phosphatase; has specificity for serine, threonine, and tyrosine residues; has a role in the DNA synthesis phase of the cell cycle	score 13, 3 peptides	1	cell cycle / signaling
<i>PRM10</i>	Pheromone-Regulated Membrane protein	Pheromone-regulated protein; proposed to be involved in mating; predicted to have 5 transmembrane segments; induced by treatment with 8-methoxyorsoralen and UVA irradiation	score 15, 6 peptides	1	cell cycle / signaling
<i>RHO1</i>	Ras HOMolog	GTP-binding protein of the rho subfamily of Ras-like proteins; involved in establishment of cell polarity; regulates protein kinase C (Pkc1p) and the cell wall synthesizing enzyme 1,3-beta-glucan synthase (Fks1p and Gsc2p)	score 62, 1 peptide	2	cell cycle / signaling
<i>ROM2</i>	RHO1 Multicopy suppressor	GDP/GTP exchange factor (GEF) for Rho1p and Rho2p; mutations are synthetically lethal with mutations in rom1, which also encodes a GEF; Rom2p localization to the bud surface is dependent on Ack1p; ROM2 has a paralog, ROM1, that arose from the whole genome duplication	score 19, 14 peptides	1	cell cycle / signaling
<i>SCS2</i>	Suppressor of Choline Sensitivity	Integral ER membrane protein, regulates phospholipid metabolism; one of 6 proteins (1st2p, Scs2p, Scs22p, Tcb1p, Tcb2p, Tcb3p) that connect ER to the plasma membrane (PM) and regulate PI4P levels by controlling access of Sac1p phosphatase to its substrate PI4P in the PM; interacts with FFAT motif of Opi1p; involved in telomeric silencing; null shows inositol auxotrophy above 34 deg C; VAP homolog; SCS2 has a paralog, SCS22, that arose from the whole genome duplication	score 36, 9 peptides	2	cell cycle / signaling
<i>UGA1</i>	Utilization of GABA	Gamma-aminobutyrate (GABA) transaminase; also known as 4-aminobutyrate aminotransferase; involved in the 4-aminobutyrate and glutamate degradation pathways; required for normal oxidative stress tolerance and nitrogen utilization; protein abundance increases in response to DNA replication stress	score 26, 7 peptides	2	cell cycle / signaling

Gene	Name	Function	score	Analysis	Category
<i>YHB1</i>	Yeast HemogloBin-like protein	Nitric oxide oxidoreductase; flavohemoglobin involved in nitric oxide detoxification; plays a role in the oxidative and nitrosative stress responses; protein increases in abundance and relocalizes from nucleus to cytoplasmic foci upon DNA replication stress	score 124, 10 peptides	2	cell cycle / signaling
<i>ZRC1</i>	Zinc Resistance Conferring	Vacuolar membrane zinc transporter; transports zinc from cytosol to vacuole for storage; also has role in resistance to zinc shock resulting from sudden influx of zinc into cytoplasm; human ortholog SLC30A10 functions as a Mn transporter and mutations in SLC30A10 cause neurotoxic accumulation of Mn in liver and brain; ZRC1 has a paralog, COT1, that arose from the whole genome duplication	score 32, 4 peptides	2	cell cycle / signaling
<i>FKS1</i>	FK506 Sensitivity	Catalytic subunit of 1,3-beta-D-glucan synthase; functionally redundant with alternate catalytic subunit Gsc2p; binds to regulatory subunit Rho1p; involved in cell wall synthesis and maintenance; localizes to sites of cell wall remodeling; FKS1 has a paralog, GSC2, that arose from the whole genome duplication	score 39, 9 peptides	2	cell wall / plasma membrane
<i>HXT3</i>	Hexose Transporter	Low affinity glucose transporter of the major facilitator superfamily; expression is induced in low or high glucose conditions; HXT3 has a paralog, HXT5, that arose from the whole genome duplication	score 42, 9 peptides	2	cell wall / plasma membrane
<i>KNH1</i>	Kre9(Nine) Homolog	Protein with similarity to Kre9p; Kre9p is involved in cell wall beta 1,6-glucan synthesis; overproduction suppresses growth defects of a kre9 null mutant; required for propionic acid resistance	score 22, 1 Peptid	1	cell wall / plasma membrane
<i>KRE6</i>	Killer toxin RESistant	Type II integral membrane protein; required for beta-1,6 glucan biosynthesis; putative beta-glucan synthase; localizes to ER, plasma membrane, sites of polarized growth and secretory vesicles; functionally redundant with Skn1p; KRE6 has a paralog, SKN1, that arose from the whole genome duplication	score 23, 4 peptides	1	cell wall / plasma membrane
<i>MRH1</i>	Membrane protein Related to Hsp30p	Protein that localizes primarily to the plasma membrane; also found at the nuclear envelope; the authentic, non-tagged protein is detected in mitochondria in a phosphorylated state; MRH1 has a paralog, YRO2, that arose from the whole genome duplication	score 21, 1 Peptid	1	cell wall / plasma membrane

Gene	Name	Function	score	Analysis	Category
<i>PMA1</i>	Plasma Membrane ATPase	Plasma membrane P2-type H ⁺ -ATPase; pumps protons out of cell; major regulator of cytoplasmic pH and plasma membrane potential; long-lived protein asymmetrically distributed at plasma membrane between mother cells and buds; accumulates at high levels in mother cells during aging, buds emerge with very low levels of Pma1p, newborn cells have low levels of Pma1p; Hsp30p plays a role in Pma1p regulation; interactions with Std1p appear to propagate [GAR+]	score 433, 24 peptides	2	cell wall / plasma membrane
<i>PSA1</i>		GDP-mannose pyrophosphorylase (mannose-1-phosphate guanyltransferase); synthesizes GDP-mannose from GTP and mannose-1-phosphate in cell wall biosynthesis; required for normal cell wall structure	score 38, 10 peptides	2	cell wall / plasma membrane
<i>CRN1</i>	CoRoNin	Coronin; cortical actin cytoskeletal component that associates with the Arp2p/Arp3p complex to regulate its activity; plays a role in regulation of actin patch assembly	score 21, 7 peptides	2	cytoskeleton
<i>MHP1</i>	MAP-Homologous Protein	Microtubule-associated protein involved in microtubule organization; involved in assembly and stabilization of microtubules; overproduction results in cell cycle arrest at G2 phase; similar to Drosophila protein MAP and to mammalian MAP4 proteins	score 22, 16 peptides	2	cytoskeleton
<i>MYO5</i>	MYOsin	One of two type I myosins; contains proline-rich tail homology 2 (TH2) and SH3 domains; MYO5 deletion has little effect on growth, but myo3 myo5 double deletion causes severe defects in growth and actin cytoskeleton organization; MYO5 has a paralog, MYO3, that arose from the whole genome duplication	score 14, 12 peptides	2	cytoskeleton
<i>TUB1</i>	TUBulin	Alpha-tubulin; associates with beta-tubulin (Tub2p) to form tubulin dimer, which polymerizes to form microtubules; relative distribution to nuclear foci increases upon DNA replication stress; TUB1 has a paralog, TUB3, that arose from the whole genome duplication	score 37, 3 peptides	2	cytoskeleton

Gene	Name	Function	score	Analysis	Category
<i>AYR1</i>	1-Acyldihydroxyacetone-phosphate Reductase	NADPH-dependent 1-acyl dihydroxyacetone phosphate reductase found in lipid particles, ER, and mitochondrial outer membrane; involved in phosphatidic acid biosynthesis; required for spore germination; capable of metabolizing steroid hormones	score 16, 6 peptides	1	lipid metabolism
<i>CHO2</i>	CHoline requiring	Phosphatidylethanolamine methyltransferase (PEMT); catalyzes the first step in the conversion of phosphatidylethanolamine to phosphatidylcholine during the methylation pathway of phosphatidylcholine biosynthesis	score 34, 9 peptides	2	lipid metabolism
<i>ERG1</i>	ERGosterol biosynthesis	Squalene epoxidase; catalyzes the epoxidation of squalene to 2,3-oxidosqualene; plays an essential role in the ergosterol-biosynthesis pathway and is the specific target of the antifungal drug terbinafine	score 28, 6 peptides	2	lipid metabolism
<i>ERG11</i>	ERGosterol biosynthesis	Lanosterol 14-alpha-demethylase; catalyzes the C-14 demethylation of lanosterol to form 4,4"-dimethyl cholesta-8,14,24-triene-3-beta-ol in the ergosterol biosynthesis pathway; member of the cytochrome P450 family; associated and coordinately regulated with the P450 reductase Ncp1p	score 72, 11 peptides	2	lipid metabolism
<i>ERG28</i>	ERGosterol biosynthesis	Endoplasmic reticulum membrane protein; may facilitate protein-protein interactions between the Erg26p dehydrogenase and the Erg27p 3-ketoreductase and/or tether these enzymes to the ER, also interacts with Erg6p	score 45, 2 peptides	2	lipid metabolism
<i>ERG3</i>	ERGosterol biosynthesis	C-5 sterol desaturase; glycoprotein that catalyzes the introduction of a C-5(6) double bond into episterol, a precursor in ergosterol biosynthesis; mutants are viable, but cannot grow on non-fermentable carbon sources; substrate of the HRD ubiquitin ligase	score 15, 1 peptides	2	lipid metabolism
<i>ERG5</i>	ERGosterol biosynthesis	C-22 sterol desaturase; a cytochrome P450 enzyme that catalyzes the formation of the C-22(23) double bond in the sterol side chain in ergosterol biosynthesis; may be a target of azole antifungal drugs	score 34, 6 peptides	2	lipid metabolism

Gene	Name	Function	score	Analysis	Category
<i>FAA2</i>	Fatty Acid Activation	Medium chain fatty acyl-CoA synthetase; activates imported fatty acids; accepts a wide range of fatty acid chain lengths with a preference for medium chains, C9:0-C13:0; localized to the peroxisome	score 18, 9 peptides	2	lipid metabolism
<i>FMP30</i>	Found in Mitochondrial Proteome	Mitochondrial inner membrane protein with a role in maintaining mitochondrial morphology and normal cardiolipin levels; proposed to be involved in N-acyl ethanolamine metabolism; related to mammalian N-acylPE-specific phospholipase D	score 22, 4 peptides	1	lipid metabolism
<i>LCB1</i>	Long-Chain Base	Component of serine palmitoyltransferase; responsible along with Lcb2p for the first committed step in sphingolipid synthesis, which is the condensation of serine with palmitoyl-CoA to form 3-ketosphinganine	score 27, 5 peptides	2	lipid metabolism
<i>SLC1</i>	SphingoLipid Compensation	1-acyl-sn-glycerol-3-phosphate acyltransferase; catalyzes the acylation of lysophosphatidic acid to form phosphatidic acid, a key intermediate in lipid metabolism; enzymatic activity detected in lipid particles and microsomes	score 20, 3 peptides	1	lipid metabolism
<i>SRF1</i>	Spo14 Regulatory Factor	Regulator of phospholipase D (Spo14p); interacts with Spo14p and regulates its catalytic activity; capable of buffering the toxicity of C16:0 platelet activating factor, a lipid that accumulates intraneuronally in Alzheimer's patients	score 13, 3 peptides	1	lipid metabolism
<i>HVG1</i>	Homologous to VRG4	Protein of unknown function; HVG1 has a paralog, VRG4 (Golgi GDP-mannose transporter; regulates Golgi function and glycosylation in Golgi; VRG4 has a paralog, HVG1, that arose from the whole genome duplication), that arose from the whole genome duplication	score 13, 3 peptides	1	posttranslational modification
<i>KTR5</i>	Kre Two Related	Putative mannosyltransferase involved in protein glycosylation; member of the KRE2/MNT1 mannosyltransferase family; KTR5 has a paralog, KTR7, that arose from the whole genome duplication	score 19, 5 peptides	1	posttranslational modification

Gene	Name	Function	score	Analysis	Category
<i>MNN10</i>	MaNnosyltransferase	Subunit of a Golgi mannosyltransferase complex; complex mediates elongation of the polysaccharide mannan backbone; membrane protein of the mannosyltransferase family; other members of the complex are Anp1p, Mnn9p, Mnn11p, and Hoc1p	score 30, 6 peptides	2	posttranslational modification
<i>PMT2</i>	Protein O-MannosylTransferase	Protein O-mannosyltransferase of the ER membrane; transfers mannose residues from dolichyl phosphate-D-mannose to protein serine/threonine residues; involved in ER quality control; acts in a complex with Pmt1p, can instead interact with Pmt5p; antifungal drug target; PMT2 has a paralog, PMT3, that arose from the whole genome duplication	score 27, 12 peptides	1	posttranslational modification
<i>PMT4</i>	Protein O-MannosylTransferase	Protein O-mannosyltransferase; transfers mannose residues from dolichyl phosphate-D-mannose to protein serine/threonine residues; appears to form homodimers in vivo and does not complex with other Pmt proteins; target for new antifungals	score 50, 14 peptides	2	posttranslational modification
<i>APM1</i>	clathrin Adaptor Protein complex Medium chain	Mu1-like medium subunit of the clathrin-associated protein complex (AP-1); binds clathrin; involved in clathrin-dependent Golgi protein sorting	score 29, 4 peptides score 34, 6 peptides	1, 2	secretion / endocytosis
<i>BRO1</i>	BCK1-like Resistance to Osmotic shock	Cytoplasmic class E vacuolar protein sorting (VPS) factor; coordinates deubiquitination in the multivesicular body (MVB) pathway by recruiting Doa4p to endosomes	score 31, 11 peptides	2	secretion / endocytosis
<i>CLC1</i>	Clathrin Light Chain	Clathrin light chain; subunit of the major coat protein involved in intracellular protein transport and endocytosis; thought to regulate clathrin function; the clathrin triskelion is a trimeric molecule composed of three heavy chains that radiate from a vertex and three light chains which bind noncovalently near the vertex of the triskelion	score 35, 5 peptides	2	secretion / endocytosis
<i>CPS1</i>	CarboxyPeptidase yscS	Vacuolar carboxypeptidase S; expression is induced under low-nitrogen conditions	score 126, 9 peptides	2	secretion / endocytosis

Gene	Name	Function	score	Analysis	Category
<i>EDE1</i>	EH Domains and Endocytosis	Scaffold protein involved in the formation of early endocytic sites; putative regulator of cytokinesis; homo-oligomerization is required for localization to and organization of endocytic sites; has a network of interactions with other endocytic proteins; binds membranes in a ubiquitin-dependent manner; may also bind ubiquitinated membrane-associated proteins; interacts with Cmk2 and functions upstream of CMK2 in regulating non-apoptotic cell death; homolog of mammalian Eps15	score 21, 21 peptides	2	secretion / endocytosis
<i>SAR1</i>	Secretion-Associated, Ras-related	GTPase, GTP-binding protein of the ARF family; component of COPII coat of vesicles; required for transport vesicle formation during ER to Golgi protein transport; lowers membrane rigidity helping in vesicle formation	score 17, 5 peptides score 59, 5 peptides	1,2	secretion / endocytosis
<i>SBH2</i>	Sec61 beta homolog 2	Ssh1p-Sss1p-Sbh2p complex component; involved in protein translocation into the endoplasmic reticulum; SBH2 has a paralog, SBH1, that arose from the whole genome duplication	score 26, 2 peptides	1	secretion / endocytosis
<i>SEC31</i>	SECRETORY	Component of the Sec13p-Sec31p complex of the COPII vesicle coat; COPII coat is required for vesicle formation in ER to Golgi transport; mutant has increased aneuploidy tolerance	score 14, 10 peptides	1	secretion / endocytosis
<i>SEC61</i>	SECRETORY	Conserved ER protein translocation channel; essential subunit of Sec61 complex (Sec61p, Sbh1p, and Sss1p); forms a channel for SRP-dependent protein import and may be responsible for retrograde transport of misfolded proteins out of the ER; with Sec63 complex allows SRP-independent protein import into ER	score 31, 6 peptides	2	secretion / endocytosis
<i>SEC8</i>	SECRETORY	Essential 121 kDa subunit of the exocyst complex; the exocyst mediates polarized targeting and tethering of post-Golgi secretory vesicles to active sites of exocytosis at the plasma membrane prior to SNARE-mediated fusion; involved in ER and Golgi inheritance in small buds; relocalizes away from bud neck upon DNA replication stress	score 17, 6 peptides	1	secretion / endocytosis

Gene	Name	Function	score	Analysis	Category
ARN2	AFT1 ReguloN	Transporter; member of the ARN family of transporters that specifically recognize siderophore-iron chelates; responsible for uptake of iron bound to the siderophore triacetylfusarinine C	score 22, 8 peptides	1	no group
DUF1	DUB-associated Factor	Ubiquitin-binding protein of unknown function; contains one WD40 repeat in a beta-propeller fold; green fluorescent protein (GFP)-fusion protein localizes to the cytoplasm; homolog of human WDR48/UAF1, which is involved in regulating the Fanconi anemia pathway; deletion mutant is sensitive to various chemicals including phenanthroline, sanguinarine, and nordihydroguaiaretic acid	score 18, 9 peptides	2	no group
YLR456W		Putative pyridoxal 5'-phosphate synthase; null mutant displays increased resistance to antifungal agents gliotoxin, cycloheximide and H2O2; YLR456W has a paralog, YPR172W, that arose from the whole genome duplication	score 18, 5 peptides	1	no group

6.3 List of abbreviations

6.3.1 Gene abbreviations

<i>BCK1</i>	b <u>ypass</u> of <u>C</u> <u>kinase</u>
<i>BEM2</i>	b <u>ud</u> e <u>mergence</u>
<i>BIT61</i>	b <u>inding</u> partner of <u>T</u> or2p
<i>CAN1</i>	c <u>anavanine</u> resistance
<i>DOA4</i>	d <u>egradation</u> of <u>a</u> lpha
<i>END3</i>	e <u>ndocytosis</u> defective
<i>LRG1</i>	<u>L</u> im- <u>R</u> ho <u>G</u> ap homolog
<i>LSP1</i>	l <u>ong</u> chain bases s <u>t</u> imulate p <u>hosphorylation</u>
<i>MID2</i>	m <u>ating</u> pheromone- <u>I</u> nduced <u>D</u> eath
<i>MLP1</i>	<u>M</u> pk1-like p <u>rotein</u>
<i>MTL1</i>	<u>M</u> id <u>T</u> wo-like
<i>NCE102</i>	n <u>on</u> -c <u>lassical</u> e <u>xport</u>
<i>PIL1</i>	p <u>hosphorylation</u> <u>I</u> nhibited by <u>L</u> ong chain bases
<i>PKC1</i>	p <u>rotein</u> <u>k</u> inase <u>C</u>
<i>PKH1/2</i>	P <u>kb</u> -activating <u>k</u> inase <u>h</u> omolog
<i>PMA1</i>	p <u>lasma</u> m <u>embrane</u> <u>A</u> TPase
<i>SLM1/2</i>	s <u>ynthetic</u> l <u>ethal</u> with <u>M</u> ss4
<i>SLT2</i>	s <u>uppressor</u> of the l <u>ytic</u> phenotype
<i>SUR7</i>	s <u>uppressor</u> of <u>R</u> vs167 mutation
<i>WSC1-3</i>	cell <u>w</u> all integrity s <u>t</u> ress response <u>c</u> omponent
<i>RHO1</i>	<u>R</u> as <u>h</u> omolog
<i>RLM1</i>	r <u>esistance</u> to l <u>ethality</u> of <u>M</u> KK1 ^{P386} overexpression
<i>ROM2</i>	<u>R</u> h <u>o</u> 1 m <u>ulticopy</u> suppressor
<i>SAC7</i>	s <u>uppressor</u> of <u>a</u> ctin
<i>SBF</i>	<u>S</u> CB b <u>inding</u> f <u>actor</u>
<i>SWI4/6</i>	s <u>witching</u> deficient

6.3.2 Cell wall integrity pathway-related abbreviations

CRD	c <u>ysteine</u> -r <u>ich</u> <u>d</u> omain
CT	c <u>ytoplasmic</u> t <u>ail</u>
CWI	cell <u>w</u> all <u>i</u> ntegrity
STR	s <u>erine</u> / <u>t</u> hreonine-r <u>ich</u> region
TMD	t <u>rans</u> m <u>embrane</u> <u>d</u> omain

6.3.3 General abbreviations

APS	a <u>mmonium</u> p <u>ersulfate</u>
BiFC	b <u>imolecular</u> f <u>luorescence</u> <u>c</u> omplementation
BioID	proximity-dependent b <u>iotin</u> <u>i</u> dentification
DIC	d <u>ifferential</u> <u>i</u> nterference <u>c</u> ontrast
DMSO	d <u>imethyl</u> s <u>ulfoxide</u>

DNA	<u>d</u> eoxyribo <u>n</u> ucleic <u>a</u> cid
dNTP	<u>d</u> eoxy <u>n</u> ucleoside <u>t</u> riphosphate
DTT	<u>d</u> ithio <u>t</u> hreit <u>o</u> l
EDTA	<u>e</u> thylene <u>d</u> iamine <u>t</u> etra <u>a</u> ctic acid
ER	<u>e</u> ndoplasmic <u>r</u> eticulum
GAP	<u>G</u> TPase-activating <u>p</u> rotein
GEF	<u>G</u> uanine nucleotide <u>e</u> xchange <u>f</u> actor
GFP	<u>g</u> reen <u>f</u> luorescent <u>p</u> rotein
IgG	<u>i</u> mmunoglobulin <u>G</u>
LB	<u>l</u> ysogeny <u>b</u> roth medium
MCC	<u>m</u> embrane <u>c</u> ompartment occupied by <u>C</u> an1
MCP	<u>m</u> embrane <u>c</u> ompartment occupied by <u>P</u> ma1
MCT	<u>m</u> embrane <u>c</u> ompartment containing <u>T</u> ORC2
MOC	<u>M</u> ander's <u>o</u> verlap <u>c</u> oefficient
OD	<u>o</u> ptical <u>d</u> ensity
PBST	<u>p</u> hosphate <u>b</u> uffered <u>s</u> aline with <u>T</u> ween-20
PCC	<u>P</u> earson's <u>c</u> orrelation <u>c</u> oefficient
PCOL	<u>P</u> ercentage of <u>c</u> olocalization
PCR	<u>p</u> olymerase <u>c</u> hain <u>r</u> eaction
PEG	<u>p</u> oly <u>e</u> thylene <u>g</u> lycol
POL	<u>p</u> olarized <u>l</u> ight
SCD	<u>s</u> ynthetic <u>c</u> omplete <u>d</u> extrose medium
SCGal	<u>s</u> ynthetic <u>c</u> omplete <u>g</u> alactose medium
sCMOS	<u>s</u> cientific <u>c</u> omplementary <u>m</u> etal- <u>o</u> xide- <u>s</u> emiconductor
SDS	<u>s</u> odium <u>d</u> odecyl <u>s</u> ulfate
SDS-PAGE	<u>s</u> odium <u>d</u> odecyl <u>s</u> ulfate <u>p</u> oly <u>a</u> crylamide gel <u>e</u> lectrophoresis
SMD	<u>s</u> ynthetic <u>m</u> inimal <u>d</u> extrose medium
TAE	<u>t</u> ris/ <u>a</u> cetate/ <u>E</u> DTA buffer
TBST	<u>t</u> ris <u>b</u> uffered <u>s</u> aline with <u>T</u> ween-20
TEMED	<u>t</u> etra <u>m</u> e <u>t</u> hyle <u>t</u> hylene <u>d</u> iamine
UV	<u>u</u> ltra- <u>v</u> iolette
YEPD	<u>y</u> east <u>e</u> xtract <u>p</u> eptone <u>d</u> extrose medium
YEPGal	<u>y</u> east <u>e</u> xtract <u>p</u> eptone <u>g</u> alactose medium
YFP	<u>y</u> ellow <u>f</u> luorescent <u>p</u> rotein
YNB	<u>y</u> east <u>n</u> itrogen <u>b</u> ase

7. Acknowledgements / Danksagung

First of all, I want to thank Professor Dr. Jürgen J. Heinisch for giving me the opportunity to work on my PhD thesis in his lab, for supervising my thesis and for being a nice boss.

Second, I want to thank Professor Dr. Achim Paululat for supervising me in all my academic degrees so far (this is indeed true!) and especially this work.

I also want to thank PD Dr. Hans-Peter Schmitz for technical and scientific support over the last years and as a consequence I also want to thank him for taking a part in my dissertation committee.

I want to thank Dr. Heiko Harten for joining my dissertation committee.

I'd like to thank Dr. Henning Arlt and Professor Dr. Christian Ungermann for support in the colocalization analysis and letting me use the Deltavision microscope which was a cornerstone in the progress of my thesis.

I'd like to thank Bernadette Sander-Turgut for great help with my Western Blot experiments, for the numerous hours of work, the patience and also advice.

In addition, I want to thank the whole genetics department for creating a nice environment for work. Janina, Arne and Nele for all the help at the beginning of my thesis, Severin and Caro for years of continuing the "Nerd-lab" tradition and Anne, Dorte and Doris, but also Sascha and Katja for being good colleagues.

I thank all my students for making the "teaching duties" to one of my favorite part of the work and for putting so much effort into their theses.

To all my friends who supported me over all these years, to new friends, to people who stayed friends: Thank you for being the great persons you are and for not giving up on me!

Zu guter Letzt und auf Deutsch möchte ich mich herzlichst bei meiner Familie bedanken. Speziell ohne die fortwährende Unterstützung und Geduld meiner Eltern auf meinem langen Ausbildungsweg wäre all dies sowieso niemals möglich gewesen. Vielen Dank für alles!

8. Statutory declaration

Erklärung über die Eigenständigkeit der erbrachten wissenschaftlichen Leistung

Ich erkläre hiermit, dass ich die vorliegende Arbeit ohne unzulässige Hilfe Dritter und ohne Benutzung anderer als der angegebenen Hilfsmittel angefertigt habe. Die aus anderen Quellen direkt oder indirekt übernommenen Daten und Konzepte sind unter Angabe der Quelle gekennzeichnet.

Bei der Auswahl und Auswertung folgenden Materials haben mir die nachstehend aufgeführten Personen in der jeweils beschriebenen Weise unentgeltlich geholfen.

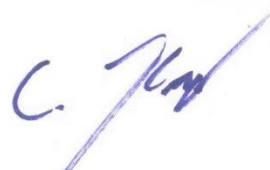
1. Die Slt2 Phosphorylierungs-Western Blot Analysen in Kapitel 3.3 (Figures 3.7 B, 3.8 B und 3.9 B) wurden in Zusammenarbeit mit der technischen Assistentin Bernadette Sander-Turgut durchgeführt
2. Die Massenspektrometrie – Analyse und MASCOT Datenbanksuche zur Identifikation von Wsc1-Interaktionspartnern (Kapitel 3.4) wurde in Zusammenarbeit mit Dr. rer. nat. Stefan Walter (Universität Osnabrück) durchgeführt
3. Die TANGO Analysen als Grundlage des Wsc1 Amyloid-Mutanten (Kapitel 1.3, 3.3.4, 4.4 und 4.7) stammen von Peter Lipke (Brooklyn College, New York) nach persönlicher Mitteilung und sind zum Zeitpunkt der Veröffentlichung dieser Arbeit unpubliziert.

Weitere Personen waren an der inhaltlichen materiellen Erstellung der vorliegenden Arbeit nicht beteiligt. Insbesondere habe ich hierfür nicht die entgeltliche Hilfe von Vermittlungs- bzw. Beratungsdiensten (Promotionsberater oder andere Personen) in Anspruch genommen. Niemand hat von mir unmittelbar oder mittelbar geldwerte Leistungen für Arbeiten erhalten, die im Zusammenhang mit dem Inhalt der vorgelegten Dissertation stehen.

Die Arbeit wurde bisher weder im In- noch im Ausland in gleicher oder ähnlicher Form einer anderen Prüfungsbehörde vorgelegt.

Osnabrück, 11.05.16

(Ort, Datum)



(Unterschrift)

9. Summary

The ability to adapt to changing environments is a key feature of living cells which is usually mediated by signal transduction pathways. One of these pathways in *Saccharomyces cerevisiae* maintains the proper cell wall composition under cell wall remodeling and stress conditions which ensures cell shape and integrity. The pathway is hence commonly referred to as cell wall integrity (CWI) pathway. Five plasma membrane sensors detect surface stress and activate a conserved MAPK cascade through Rom2, Rho1 and Pkc1. Downstream of the cascade, Slr2 activates the transcription factors Rlm1 and SBF. These regulate the expression of genes which are involved in cell wall synthesis and cell cycle control, respectively. The sensors can be grouped into two protein families with Wsc1, Wsc2 and Wsc3 on the one hand and Mid2 and Mtl1 on the other hand. They all contain a highly mannosylated extracellular serine/threonine-rich region (STR), a single transmembrane domain and a cytoplasmic tail. Whereas Wsc-family sensors carry an additional cysteine-rich domain (CRD) headgroup, Mid2 and Mtl1 are N-glycosylated at an asparagine (Kock *et al.*, 2015).

A strain deleted in all five sensor genes is not viable and *WSC1*, *WSC2* and *MID2* are the main sensor genes to mediate the stress response. Wsc1 and Mid2 show non-overlapping spot-like and network-like localization patterns in the plasma membrane, respectively, whose formation is not governed by their transmembrane domains. Colocalization studies with marker proteins of the known yeast plasma membrane domains “membrane compartment occupied by Can1” (MCC), “membrane compartment occupied by Pma1” (MCP) and the “membrane compartment of the TOR2 complex” (MCT) revealed that Wsc1 forms a distinct plasma membrane domain which is here introduced as “membrane compartment occupied by Wsc1” (MCW). This microcompartment depends on the cysteine-rich domain (CRD) as sensors mutated in this headgroup accumulate in the vacuole. Blocking endocytosis either by an *end3* deletion or by mutation of the NPFDD endocytosis signal in the cytoplasmic tail of Wsc1 restores its signaling function but displays an altered pattern of membrane distribution, changing from spot-like in wild-type to network-like in the mutants. This indicated that clustering may protect the sensor from endocytosis. In addition, Wsc1 has amyloid-like properties suggesting a role in clustering. Accordingly, protein aggregation (clustering) is lost in a mutant of a predicted amyloid motif within the CRD, which also impairs Wsc1 signaling.

10. Zusammenfassung

Die Fähigkeit sich an verändernde Umweltbedingungen anzupassen ist eine wichtige Eigenschaft lebender Zellen und wird normalerweise von Signaltransduktionswegen vermittelt. Einer von diesen vermittelt die korrekte Zellwandzusammensetzung während der Neubildung von Zellwand und unter Stressbedingungen in *Saccharomyces cerevisiae*, um die richtige Zellform und -integrität zu gewährleisten. Dementsprechend wird der Signalweg als „Zellwandintegritätsweg“ (CWI) bezeichnet. Der Stress an der Zelloberfläche wird von fünf Plasmamembransensoren detektiert, die eine konservierte MAPK Kaskade mittels Rom2, Rho1 und Pkc1 aktivieren. Stromabwärts der Kaskade aktiviert Slr2 die Transkriptionsfaktoren Rlm1 und SBF, die ihrerseits die Expression von Zellwandsynthese- und Zellzyklusgenen regulieren. Die Sensoren werden in zwei Proteinfamilien zusammengefasst, die einerseits Wsc1, Wsc2 und Wsc3 und andererseits Mid2 und Mtl1 beinhalten. Sie alle weisen eine hochgradig mannosylierte, extrazelluläre Serin/Threonin-reiche Region, eine einzelne Transmembrandomäne und einen zytoplasmatischen Schwanz auf. Während die Sensoren der Wsc-Familie zusätzlich eine Kopfgruppe tragen, die als Cystein-reiche domäne (CRD) bezeichnet wird, werden Mid2 und Mtl1 an einem Asparagin N-glykosyliert. (Kock *et al.*, 2015).

Ein Stamm mit Deletionen in allen fünf Sensorgenen ist nicht lebensfähig und *WSC1*, *WSC2* und *MID2* sind die Hauptgene für die Vermittlung der Stressantwort. Wsc1 und Mid2 zeigen nicht-überlappende, punktförmige und netzwerkartige Lokalisierungsmuster in der Plasmamembran, die sich unabhängig von ihren jeweiligen Transmembrandomänen bilden. Kollokalisierungstudien mit Beispielproteinen der bereits beschriebenen Plasmamembrandomänen „Membrankompartiment von Can1“ (MCC), „Membrankompartiment von Pma1“ (MCP) und „Membrankompartiment des TOR2 Komplexes“ (MCT) zeigen, dass Wsc1 eine abgegrenzte Plasmamembrandomäne formt, die hier als „Membrankompartiment von Wsc1“ beschrieben wurde. Dieses Mikrokompartment ist von der Cystein-reichen Domäne abhängig, da Sensoren, die Mutationen in dieser Kopfgruppe tragen sich in der Vakuole anhäufen. Die Blockierung der Endozytose durch Deletion des *END3* Genes oder Mutation des NPFDD-Endozytosesignals im zytoplasmatischen Schwanz von Wsc1 stellt dessen Funktionalität wieder her, offenbart aber ein verändertes Membranlokalisierungsmuster von punktförmig im Wildtyp zu netzwerkartig in der Mutante. Dies deutet an, dass Clustering zum

Schutz des Sensors vor Endozytose dienen könnte. Zusätzlich zeigt Wsc1 Amyloid-ähnliche Eigenschaften, was auf eine Rolle für das Clustering hindeutet. Die Proteinaggregation (Clustering) und Signalweiterleitung geht nach Mutation eines vorhergesagten Amyloid-Motifs in der CRD ebenfalls verloren.

11. Curriculum vitae

Christian Kock

Date of birth: 18.10.1984

Nationality: German

Education

- 02/2012-05/2016 University of Osnabrück (Germany)
Faculty of Biology/Chemistry
Graduation
Dissertation: „Microcompartmentation of Cell Wall Integrity sensors in *Saccharomyces cerevisiae*“
Department: Genetics (Professor Dr. Jürgen Heinisch)
Presumed degree: Dr. rerum naturalium (PhD)
- 10/2009-12/2011 University of Osnabrück (Germany)
Faculty of Biology/Chemistry
M.Sc. Biology of Organisms
Master thesis: „Expressionsanalyse von 7 potenziellen Prolyl 4-Hydroxylasen des 75D1 Clusters von *Drosophila melanogaster*“
Department: Zoology / Developmental biology (Prof. Dr. Achim Paululat)
Degree: Master of Science
- 10/2006-09/2009 University of Osnabrück (Germany)
Faculty of Biology/Chemistry
B.Sc. Biology of Organisms
Bachelor thesis: „Ultrastruktur der Augen und Photorezeptorzellen von *Schmidtea mediterranea* (Plathelminthes, Rhabditophora, Tricladida)“
Department: Zoology / Developmental biology (apl. Prof. Dr. Günter Purschke)
Degree: Bachelor of Science
- 09/2005-08/2006 University of applied sciences Oldenburg/Ostfriesland/Wilhelmshaven
Emden (Germany)
Faculty of Biology/Chemistry
without degree
- 10/2004-06/2005 Military service in Goslar/Oldenburg (Germany)
- 08/1997-06/2004 Copernicus Gymnasium Lönigen (Germany)
Degree: Abitur / A levels

12. Publications

Kock, C., Arlt, H., Ungermann, C., and Heinisch, J.J. (2016)

Yeast cell wall integrity sensors form specific plasma membrane microdomains important for signaling.

Cell Microbiol, revision submitted, publication presumably in September 2016.

Kock, C., Dufrêne, Y.F., and Heinisch, J.J. (2015)

Up against the Wall: Is Yeast Cell Wall Integrity Ensured by Mechanosensing in Plasma Membrane Microdomains?

Appl Environ Microbiol 81: 806–811. doi: 10.1128/AEM.03273-14